Internal characterization of magnetic cores : a route for dimensioning and real time condition monitoring

Hilary Sorelle Nguedjang Kouakeuo

THESE de DOCTORAT DE
L'UNIVERSITE CLAUDE BERNARD LYON 1

Ecole Doctorale N° ED 160
ELECTRONIQUE ELECTROTECHNIQUE AUTOMATIQUE

Discipline : Génie électrique

Soutenue publiquement le 14/11/2022, par :
NGUEDJANG KOUAKEUO HILARY SORELLE

Internal characterization of magnetic cores: A route for dimensioning and real time condition monitoring

Devant le jury composé de :

Cavasila, Sophie	Professeur	Université de Lyon	Présidente
Lebouc, Afef	Directrice de recherche	CNRS Université de Grenoble	Rapporteure
Fotsin, Hilaire	Professeur	Université de Dschang	Rapporteur
Cheukem, André	Associate Professor	Université de Dschang	Examinateur
Daniel, Laurent	Professeur	Université Paris-Sarclay	Examinateur
Morel, Laurent	Maitre de Conference	Université de Lyon	Directeur de thèse
Tanyi, Emmanuel	Professeur	University of Buea	Directeur de thèse
Tsafack, Pierre	Associate Professor	University of Buea	Co-directeur de thèse
Ducharne, Benjamin	Maitre de Conférence	Université de Tohoku	Invité
Raulet, Marie-Ange	Maitre de Conférence	Université Lyon 1	Invité

DEDICATION

To my son Eythan Darryl

ACKNOWLEDGEMENTS

I wish to acknowledge the help provided by Prof. Laurent Morel for being my thesis director as also give me the continuous support during my Ph.D research. He relented no efforts to make sure everything is OK, for me to produce my best. His continuous encouragement, comments, and moral support helped me to hold on till the end of my PhD study.

My particular thanks go to my co-supervisor Prof. Tsafack Pierre,from Faculty of Engineering and Technology (FET), University of Buea for his priceless supervision, guidance, understanding and constructive and fatherly advice during my studying and living in Buea.

I would like to express my very great appreciation to my thesis co-director Prof Benjamin Ducharne for his valuable and constructive suggestions during the planning and development of my Ph.D. research work. His patience, motivation, enthusiasm, immense knowledge, and willingness to give his time so generously have been very much appreciated. My acquaintance and adaptation to the new environment of Lyon would not have been easier without his care and support to make me feel at home.

I am particularly grateful for the assistance, follow-up of Prof. Marie-Ange Raulet. Her dynamism, vision, sincerity, and motivation which deeply inspired me to carry out the research with resilience.

I am grateful to Prof. Tanyi Emmanuel, the dean of the Faculty of Engineering and Technology (FET), for all his tireless efforts in starting the postgraduate programme at FET that led to my Ph.D. admission.

This thesis would not have been accomplished without the financial support of Cooperation and Cultural Action Service (SCAC) of the French Embassy in Cameroon during my PhD studies

I am also thankful for the research facilities and support of the Ampere laboratory of University Lyon 1 and the Faculty of Engineering and Technology of the University of Buea, that permitted me to successfully conduct my experiments, present my results at an international conference, and publish my work in an international peer-reviewed journal.

I am profoundly indebted to the dual-opportunity to have access and work in both the Laboratory of Electrical Engineering and Ferroelectricity (LGEF), INSA Lyon and Ampere laboratory of University Lyon 1. The invaluable help and precious advice of the personnel in both laboratories with the experimental part of this thesis, fixing problems on my experimental setup as well as providing me the lab facilities and their interest shown in our many long and useful discussions.

My special thanks are extended to my senior colleagues and friends: Dr Yves Tene and Dr Valery Nkemeni for being as motivated and enthusiastic senior-interns with fun-loving spirit. Miss Ingrid Regine Ebongue Etoke for always cheering me up, encouraging and available all the time: my moral support and my french guru. I appreciate our team working session, discuss and lengthy exchange without barriers.

I am infinitely grateful to my family: Mr Nguedjang Jean-Robert and Mrs Tchakountio Noutossi Marie-Jeannette, my brothers and sisters for all their love, caring and supporting me spiritually throughout my life. Their indefectible encouragement and support have always galvanized me all through studies.

Last but not the least, an immense thanks to my lovely husband Djogue Christel Orellien for his tolerance, his assistance in organizing my responsibilities and his mentorship in social communication and stress management.

RÉSUMÉ

Un contrôle élaboré des équipements à composantes magnétiques requiert une connaissance précise des informations locales sur leur comportement magnétique. A cet effet, plusieurs approches allant de la modélisation, la simulation et la mise sur pied de divers capteurs ont été développées pour avoir une meilleure compréhension physique des interactions magnétiques qui ont lieu au sein d'un noyau magnétique. Mais alors, les données obtenues des résolutions numériques n'ont pas en contrepartie une validation expérimentale/pratique. En outre, tous les capteurs magnétiques qui ont été développés jusqu'ici ne permettent pas un monitoring in-situ en temps réel de ces équipements en fonctionnement. Cette incapacité est due à la taille géométrique des capteurs et limites liées à leur instrumentation. **Est-il donc possible de développer un système de capteurs magnétiques embarqués qui ne permettra pas juste de caractériser des composants magnétiques, mais qui ira plus loin en donnant la possibilité de contrôler en temps réel le comportement d'un noyau magnétique ?** Comme palliatif à la contrainte géométrique, tout au long de notre thèse, les capteurs ont été miniaturisés à l'aide de la technique des circuits imprimés. Nous avons donc fait bon usage des énormes progrès qui ont été fait dans le domaine électronique. Initialement, les pointes magnétiques de 1,5cm de hauteur ont été imprimées directement sur la tôle cible qui permet d'avoir une information sur son état magnétique lorsqu'il sera inséré dans le noyau magnétique des machines électriques. Cette technique de pointes magnétiques imprimées (PMI) ayant une épaisseur de 30µm nous permettra dorénavant d'avoir des signaux magnétiques de 1Hz à 200Hz ; d'où l'accès au information sur l'induction champ magnétique interne d'un noyau magnétique à partir des résultats expérimentaux. S'agissant de la mesure de l'intensité champ magnétique, la sonde à effet hall a été sollicité, mais par la suite remplacée par la technique de Magnétorésistances géantes(GMR). Cette dernière a été utilisée du fait de la possibilité de miniaturisation. Par ailleurs, nous avons élaboré une mini-plaquette 2en1 de 100µm d'épaisseur comportant la GMR et la PMI pour des mesures simultanées en 2D. Les résultats locaux ainsi obtenus et comparés à l'induction moyennée de la bobine encerclant révèlent l'état d'homogénéité dans une pile de tôle avec une erreur relative de 8%. Enfin, une évaluation numérique du comportement magnétique d'un noyau laminé par simulation éléments finis s'accorde aux résultats expérimentaux. Une erreur de 22% sur le paramètre des pertes hystérétique. Néanmoins, la variation des cycles d'hystérésis tout au long des différentes tôles de l'empilement est la même en simulation qu'en mesure ; d'où une validation des résultats obtenus auparavant par simulation. Cette étude contribue indéniablement à la conception d'un noyau magnétique

intelligent. Une garantie d'un monitoring en temps réel de l'état magnétique d'un matériau, du noyau magnétique d'une machine électrique point par point.

Termes clés : capteur induction magnétique, capteur non-invasif, mesure locale, technique pointes magnétiques, encre conductrice, technique d'impression, empilements de tôles magnétiques, magnétorésistance géante, simulation éléments finis, contrôle continu des noyaux magnétiques, distribution de champ magnétique.

ABSTRACT

A sophisticated control of equipment with magnetic components requires precise knowledge of local information on their magnetic behaviour. In this line, several approaches ranging from modelling, simulation and the setting up of various sensors have been developed to have a better physical understanding of the magnetic interactions that take place within a magnetic core. But then, the data obtained from the numerical resolutions do not have in return an experimental/practical validation. In addition, all the magnetic sensors that have been developed so far do not allow real-time in-situ monitoring of this equipment in operation. This inability is due to the geometric size of the sensors and limitations related to their instrumentation. **Is it therefore possible to develop a system of on-board magnetic sensors which will not only allow the characterization of magnetic components, but which will go further by giving the possibility of controlling the behaviour of a magnetic core in real time?** As a palliative to the geometric constraint, throughout our thesis, sensors have been miniaturized using the printed circuit technique. We have therefore made good use of the enormous progress that has been made in the electronic field. Initially, the 1.5cm height magnetic needle probes were printed directly on the target sheet which provides information on its magnetic state when inserted into the magnetic core of electrical machines. This technique of printed magnetic needle probe with a thickness of 30µm (PMNP) will now allow us to have magnetic signals from 1Hz to 200Hz; hence access to information on the induction of the internal magnetic field of a magnetic core from an experimental view point. With regards to the measurement of the magnetic field intensity, the hall sensor was used which was later on replaced by the technique of Giant Magnetoresistors (GMR). The latter chosen for its possibility to be miniature. Moreover, we have developed a 2in1 mini-wafer of 100µm thickness including GMR and PMI for simultaneous 2D measurements. The local results thus obtained and compared to the averaged induction of the encircling coil reveal the state of homogeneity in a sheet pile with a relative drift of 8%. Finally, a numerical evaluation of the magnetic behavior of a laminated core by finite element simulation agrees with the experimental results. Although, a drift of 22% on the hysteretic losses parameter evaluated from measured results and simulated results. Nevertheless, the variation of the hysteresis cycles throughout the various plates of the stack is the same in simulation as in measurement; hence a validation of the results obtained previously by simulation. This study undeniably contributes to the design of a smart magnetic core. A guarantee of real-time and point-wise monitoring of the magnetic state of a material, of the magnetic core of an electric machine.

Keywords: Magnetic core condition forecast, magnetic induction sensor, non-invasive sensor, local measurement, magnetic needle probe technique, conductive ink, printing technique, stack of magnetic steal sheets, giant magnetoresistance, finite element simulation, continuous control of magnetic cores, magnetic field distribution.

Table of Content

DEDICATION ii
ACKNOWLEDGEMENTS iii
RÉSUMÉ v
ABSTRACT vii
LIST OF FIGURES xii
LIST OF TABLES xv
LIST OF ABBREVIATIONS xvi
LIST OF SYMBOLS xvii
GENERAL INTRODUCTION 1
1.1 Background of Study 1
1.1.1 Optimization of energy conversion in electrical machines 1
1.1.2 Real time monitoring systems of the state of magnetic core 3
1.2 Problem Statement 3
1.3 Rationale of the study 4
1.4 Objectives and roadmap 6
1.4.1 General Objective 6
1.4.2 Specific objectives 6
1.5 Thesis organization 7
CHAPTER 1: 9
MAGNETIC CORE STATE CONDITION: MICRO-MAGNETISM, NON-DESTRUCTIVE TESTING 9
1.1 Magnetism 9
1.1.1 Magnetic field properties 10
1.1.2 Ferromagnetism at the Microscopic level 13
1.2 Condition monitoring 17
1.2.1 Magnetic core condition monitoring 18
1.2.2 Inter-laminar faults 19
1.2.3 MCCM Non- invasive schemes 21
1.3 Non-Destructive Testing Methods 23
1.3.1 Comparison of non-destructive testing methods 23
1.3.2 Eddy current testing (ECT) 24
1.4 Summary 31
CHAPTER 2: 33
PRINTED MAGNETIC NEEDLE PROBE 33

2.1 Concept of Magnetic Needle Probe 33
2.1.1 Principle of magnetic needle probe 34
2.1.2 Recommendations for optimal measurement 35
2.1.3 Modified versions of MNP 36
2.2 Printed Magnetic Needle Probe(PMNP) Technique 40
2.2.1 Principle of printed needle probe using printed electronics 40
2.2.2 Printing using mask 41
2.2.3 Printing using an inkjet printing machine 43
2.3 Validation of the PMNP 44
2.3.1 Experimental Set-up 45
2.3.2 Instrumented sheet Testing 47
2.3.3 Laminated magnetic core testing 47
2.4 Miniaturisation of B_H acquisition system coupled to magnetoresistance 49
2.4.1 Concept 49
2.4.2 Magnetoresistances 49
2.4.3 Experimental set-up 53
2.5 2-in-1 portable embedded B_H sensor 55
2.5.1 Concept 55
2.5.2 PMNP/GMR sensor design 56
2.5.3 Single sheet test 57
2.5.4 Local measurement in laminated core 58
2.6 Summary 59
CHAPTER 3: 60
SIMULATION AND NUMERICAL ANALYSIS OF INHOMOGENITY IN MAGNETIC FIELD DISTRIBUTION 60
3.1 Finite element modelling on Onelab interface 61
3.1.1 Geometric design 62
3.1.2 Meshing design 63
3.2 Jiles Atherthon modelling 64
3.3 Graphical distribution of magnetic field line 67
3.4 Post-processing 69
3.5 Summary 70
CHAPTER 4: 71
RESULTS AND DISCUSSIONS 71
4.1 Validation of PMNP 71
4.1.1 Comparison with other eddy current testing sensors 71
4.1.2 Laminated core sensing as per local flux distribution 74

4.2 PMNP + GMR lumped at a particular point 77
4.2.1 Single sheet testing 77
4.2.2 Laminated stack testing 78
4.3 Integrated PMNP + GMR sensor card 82
4.3.1 Single sheet testing 82
4.3.2 Laminated stack testing 83
4.4 Summary 85
CONCLUSIONS AND FUTURE WORKS 87
Limitations 88
Future works and perspective 88
Applications 89
RESUME ETENDU (EXTENDED SUMMARY) 90
REFERENCES 112
PUBLICATIONS 120

LIST OF FIGURES

Figure 1-1: Magnetic field lines created by a magnet 10

Figure 1-2 : Motion of an electron around the nucleus 11

Figure 1-3:magnetic moments within domains 14

Figure 1-4:Magnetism in a ferromagnetic material 14

Figure 1-5: insight on magnetic domain transition at bloch wall[40] (a) shows the side view on a Bloch wall (b) is a tilted view 14

Figure 1-6 : hysteresis cycle of a ferromagnetic material 15

Figure 1-7 : B_H curve of: (a) ideal material ;(b) soft magnetic material (c) hard magnetic material 16

Figure 1-8 :(a) 3-D view of a faulty transformer limb: interlaminar fault in red. (b) ideal eddy current flow in a laminated core. (c) impact of fault on eddy current flow 20

Figure 1-9 : Stator core melting caused by interlaminar insulation failure: Core fault in tooth wall 21

Figure 1-10 : A primary coil inducing eddy currents in a component 24

Figure 1-11: operator testing a mechanical spare part using an eddy current probe 25

Figure 1-12: different types of Eddy current testing probe 26

Figure 1-13 : Principle of eddy current testing (left) and distortion of eddy current due to crack, edge-effect, surface crack, and sub-surface void (right) 27

Figure 1-14: illustration of skin depth 28

Figure 1-15 :(a) External encircling-type coil for a ferrite bar inspection. (b) Eddy currents flow in the measuring system 29

Figure 1-16 : plane spiral coil 30

Figure 1-17 : Magnetic needle probe experimental lay out 31

Figure 2-1: magnetic needle probe concept 34

Figure 2-2: Principle of the two-needle-probe technique 35

Figure 2-3 : (a) Needle probe method; (b) Eddy-current distribution in a sample surface and edges 36

Figure 2-4: construction of needle probes 37

Figure 2-5 : Dual needle probe schematic 37

Figure 2-6 :The probes positioning and connection in the proposed modified MNP. 38

Figure 2-7 : The concept of capacitive coupling(a) top view, (b) cross-section view; A_C: area of the pad, d_S: thickness of insulating layer, V: measured voltage between pads 39

Figure 2-8 : Two sets of two dimensional flux density needle probe sensors. 39

Figure 2-9: Sketch of PMNP concept 40

Figure 2-10: various PMNP patterns tested 41

Figure 2-11: PMNPM printing process using masks 43

Figure 2-12: A-sonoplot printer; B- sensor printing process 44

Figure 2-13:3D Stacked design and photo of the experimental setup..... 46

Figure 2-14 :A) instrumented FE-Si sheet with sensors; B) classic needle probe sensor..... 47

Figure 2-15:A)Laminated magnetic core including PMNPM sensor. ;B) Zoomed view over the sensor area..... 48

Figure 2-16 :multilayer GMR, « Spin-valved » GMR..... 50

Figure 2-17:variation of GMR resistance according to the direction of external magnetic field 51

Figure 2-18: sensor design and shape 52

Figure 2-19: basic reference characteristic curve R(H) 53

Figure 2-20: 3D view of the entire set-up 53

Figure 2-21:a– sensor positioning on a sheet, b – The non-invasive sensor, c – The sensor embedded in a lamination stack. 54

Figure 2-22: Illustrative sketch of the backbone idea of 2-in-1 sensor..... 55

Figure 2-23:PMNP/GMR sensor design: (left) routing, (right) zoom on the disposition of GMRs 56

Figure 2-24:PMNP/GMR 2-in-1sensor; (a) view of the entire sensor; (b) zoom on the thickness of the sensor 57

Figure 2-25:characteristic curve of fabricated 2-in-1 sensor 57

Figure 2-26 : positioning of sensor for 2D measurement..... 58

Figure 2-27:a) laminated core ; b)embedded sensor in laminated core 58

Figure 3-1 : Geometrical design and meshing design of the electromagnet circuit. the right most picture is a zoom on magnetic core geometry..... 63

Figure 3-2 : meshing configuration of each space domain 64

Figure 3-3: Schematic illustration of Jiles-Atherton model parameters 66

Figure 3-4 : Superpositon of measured B_H signature of the material and hysteresis cycle from JA modelling..... 67

Figure 3-5 : graphical illustration of magnetic induction within a stack of 10 steel sheets..... 68

Figure 3-6: zoomed view on magnetic distribution of the first four laminations 69

Figure 4-1: Frequential B_H characteristic curves of RD-GO steel sheet as seen by 4 sensor(classic needle probe, 10 turns surrounding coil, search coil and PMNP) 72

Figure 4-2: Frequential B_H characteristic curves of TD-GO steel sheet as seen by 4 sensors(classic needle probe, 10 turns surrounding coil, search coil and PMNP) 72

Figure 4-3 : local measurement of B at each lamination vs tangent H-field as seen at the top of the stack(full lines) and at the bottom of the stack(dotted lines) 74

Figure 4-4 : : (a) Maximal induction field versus lamination position, (b) Hysteresis losses versus lamination position, (c) Coercivity versus lamination position, (d) Illustration of the lamination position; (top hall effect sensor measurement (**red**) and bottom hall effect sensor measurement (**blue**)) 75

Figure 4-5: reconstructed laminated hysteresis cycle and the overall hysteresis cycle as measured by 10 turns surrounding coil 76

Figure 4-6: B(H) hysteresis cycles at the center of the instrumented FeSi sheet..... 77

Figure 4-7 : Local hysteresis cycles within a ferromagnetic laminated core 79

Figure 4-8: local positon-dependent magnetic characteristic within a laminated magnetic core; (a)-The hysteresis cycle parameters , (b)– Evolution of the hysteresis area as a function of the lamination position, (c) – Evolution of the relative permeability as a function of the lamination position. 80

Figure 4-9 : Comparisons between the reconstructed laminated hysteresis cycles and the measured ones. 81

Figure 4-10 : PMNP + GMR sensor test of its features; (a) frequential test (b) amplitude detection test (c) 2-D measurement verification 83

Figure 4-11 : Comparisons of the Onelab® simulations and experimental results in local tests. 83

Figure 4-12 :Comparison measurements/simulations for the main hysteresis cycle indicators versus the magnetic sheet position. 84

LIST OF TABLES

Table 1-1: A summary of the three major types of magnetic behaviour..... 13

Table 1-2 : comparative evaluation[**3:excellent; 2:fair; 1:poor]** 23

Table 2-1 : Magnetic parameters of GO FeSi 45

Table 3-1 : features of commonly used theoretical magnetic hysteresis models 61

Table 3-2 : Jiles-Atherton (J-A) simulation parameters for the FeSi GO (RD) 66

Table 4-1: Precision of the PMNPM sensor compared to the conventional one (coil and search coil) under easy axis magnetic excitation situation. 73

Table 4-2:Precision of the PMNPM sensor compared to the conventional one (coil and search coil) under transverse magnetic excitation situation. 73

Table 4-3 : Quantitative evaluation of the simulation method (m = 10 is the laminations number). 85

LIST OF ABBREVIATIONS

AC/DC	Alternating Current/Direct Current
AMR	Anisotropic Magneto-Resistance
CAD	Computer Aided Design
CM	Condition Monitoring
CND	Contrôle Non-Destructif
EC	Eddy Current
ECT	Eddy Current Testing
FEM	Finite Element Method
FET	Faculty of Engineering and Technology
FD	Fault Diagnostics
GO	Grain Oriented
GO FeSi	Grain Oriented Silicon Iron
GMR	Giant Magneto-Resistance
ILF	Inter-Laminar Faults
J-A	Jiles-Atherton
MATLAB	Matrix Laboratory
MBN	Magnetic Barkhausen Noise
MCCM	Magnetic Core Condition Monitoring
MIP	Magnetic Incremental Permeability
MNP	Magnetic Needle Probe
MR	Magnetic Resistance
NDT	Non-Destructive Testing
NPT	Needle probe Testing
ONELAB	Open Numerical Evaluation Laboratory
PCB	Printed Circuit Board
PE	Printed Electronics
PMI	Pointes Magnétiques Imprimées
PMNP	Printed Magnetic Needle Probe
RD	Rolling Direction
RFID	Radio Frequency Identifier
SCAC	Service de Coopération et d'Action culturelle
SST	Single Sheet Tester
TD	Transverse Direction
TMR	Tunnel Magneto-Resistance

LIST OF SYMBOLS

abs	Absolute Value
H	Magnetic Field Intensity
B	Magnetic Field Density
μ	Magnetic Permeability
H_c	Coercive field
B_r	Remanent Field
m_i	Magnetic Moment of an Atom
μ_0	Magnetic Permeability in air
Γ	Alignment torque
$\mathcal{M}$	Magnetization Vector
∂v	Volume entity
∂m	Sum of atomic moments
χ	susceptibility
μ_r	relative magnetic permeability
P_T	Losses during Magnetization
δ	Skin depth
f	frequency
σ	Electrical conductivity
e	Electro-motive force (emf)
$\boldsymbol{\varphi}$	magnetic flux
V	Voltage
S	Sensitivity of the sensor
N	Number of turns of the coil
E	Electrical field
dS	change in cross sectional area
B_{mean}	average magnetic field density
T_C (°C)	Curie Temperature
J_s(T)	Saturation polarization
λ_s	magnetostriction at saturation
l	initial length of material
Δl	length variation of the material at saturation
R_{max}	Maximum Resistance
R_{min}	Minimum Resistance
M_s	saturation magnetization

c	reversibility coefficient of magnetization
k	average energy to break the pinning sites
α	interdomain coupling
a	domain walls density
M_{an}	Anhysteretic Magnetization
$<A>_{PMNPM}$	area of the hysteresis loop as seen by PMNP
$<A>_{S.Coil}$	area of the hysteresis loop as seen by Search Coil
$<A>_{Coil}$	area of the hysteresis loop as seen by encircling Coil
Error $_{S.Coil}$	measurement drift with respect to Search coil
Error $_{Coil}$	measurement drift with respect to encircling coil
$\emptyset_{tot}$	Total Magnetic flux
B_{tot}	Total Average Flux Density
S_{tot}	overall cross sectional area
B_i	Flux density in the i^{th} lamination
S_i	cross sectional area in the i^{th} lamination
$\emptyset_i$	Magnetic flux in the i^{th} lamination
H_{BOT}	magnetic field strength at the bottom of stack
H_{TOP}	magnetic field strength at the top of stack
H_{surf}	field strength at the surface of the material
M_{irr}	irreversible magnetization
M_{an}	anhysteretic magnetization
H_e	effective field strength
B_e	effective field density

GENERAL INTRODUCTION

1.1 Background of Study

Electrical energy at the centre of the industrial development is aimed at being of good quality at the level of end users. This has been a crucial matter to electrical researcher towards limiting the losses in an electrical power system; they are incurred when converting, transporting and using electrical energy. Referring to a standard power system configuration, we have as tags; electrical machines: transformers and rotational electrical machines which mainly represent key components in the production, transport and consumption of electrical energy. Inefficiency and failure of these electrical machines brings about consequences in the power system reliability. Transformers being present at all the stage of a power system, they contribute largely to power system losses; that is at range of 8-10% and 24-32% of the total during transmission and distribution stages respectively[1]. As a matter of fact, the electrical energy provider in Cameroon(ENEO) reported several damages of their transformers within the last five years[2]. This resulted in areas with total blackout for many days and a direct impact was felt on the economy, since many activities were on a hold. In addition, it is reported from statistics that, Western Europe had power systems' losses evaluated at 7.3% of the energy distribution[1]. These scenario are as result of defects in the transformer which also contribute in increasing losses in the transformer [3]and losses when converting from one voltage level to the other termed energy conversions losses. The latter cuts across the various types of electrical machines and consequently affects the reliability of the power system as well as its energy efficiency. A proper improvement of energy conversions in these machines and implementation of a real time monitoring systems gives way to limit these failures.

1.1.1 Optimization of energy conversion in electrical machines

All electrical machines such as transformers force-producing devices(relays)and continuous energy-conversion devices (electric machines) have a common part called electromagnets which plays a major role in electromagnetic conversions[4]–[6]. Energy conversion is assured by the electromagnet which is made up of a magnetic core around which wires are wounded.

Faradays law of electromagnetic induction governs this conversion by enabling the transfer of energy through the medium of the magnetic circuit. Magnetic losses are categorized into static and dynamic losses. They are incurred at this level due to domain wall motion, hysteresis and eddy current. To minimize these losses, researchers have developed new geometrical designs, materials, technologies, etc. Power losses due to eddy current can be achieved by reducing the intensity of eddy current flowing in the magnetic core.

As far as the geometrical improvements are concerned, the full block of ferromagnetic material constituting the magnetic core is sliced up to a stack of thin steel sheets of about 0.3mm thickness[7]–[9]. This configuration results to breaking the initial one block cross sectional area to multiple smaller cross-sectional area proper to each steel sheet. Thus reducing the amount of eddy current flowing in the core; thanks to the fact that eddy current intensity is smaller when the cross sectional area of the material through which magnetic field is flowing. More to that, this insulation layers found between successive steel lamination play a vital role in hindering perceptible eddy current. It can be concluded that the smaller the thickness of the laminations constituting the magnetic circuit, the lower the eddy current losses[10], [11].

Furthermore, researchers could reduce eddy current losses through material enhancements. In effect, the resistivity and doping concentration of the grain oriented ferromagnetic steel sheet are increased so as to facilitate the conduction in the easiest magnetization axis. In this axis, the vector magnetic field intensity **H** is collinear to that of magnetic field induction **B**. This leading to maximum transfer of magnetic energy; given that they are related by a parameter of proportionality known as permeability **μ**. Furthermore, macroscopic eddy current can be lowered three times lesser by integrating silicon in the constitution of steel sheets[12].

Technological-wise, new sensors were developed to contribute towards mastering and controlling the distribution of magnetic losses within a magnetic core. As described above, breaking up the magnetic core into thin laminations could highly reduce losses; but then there is no clear sight of how magnetic field lines propagate in the laminated core. That is why, researchers came up with some modelling programs with which they can reconstruct the magnetic lay out of the laminated core and have an insight of what is happening internally[12–17]. To improve the performance of electric machinery, the homogenization design method is applied to obtain the optimal topology of a structure in magnetic fields[19]. This is applied at the design level of magnetic core. It consists of solving the optimization problem defined by the total magnetic energy and the averaged vector potential of the design domain. Homogenized permeability values are thereafter obtained which helps in determining the optimal material distribution; thus an optimal microstructural shape is achieved. Even at that, it is still very

cumbersome to achieve the simulation of a single lamination as some assumptions are done on its point-wise magnetic behaviour. To increase the level of exactitude of the result gotten using the modelling, there is need for these latter assumptions to be verified experimentally. In the attempt experimentally have access to local measurements within the magnetic core, Krismanic et al. proposed a solution in his work[20]. He came up with a sensor made up of a 1 mm thick needle sensor and two 1.6 mm H-coils. This sensor is to be placed among the stack of lamination; from which its measurements will be used to infer on the behaviour of the laminated magnetic core.

1.1.2 Real time monitoring systems of the state of magnetic core

At the factory level, the fabrication of magnetic core brings in some source of defaults. When trimming steel sheets, raised edges termed as burrs are unfortunately present. The faulty incident exist when the sheets are being pressed to each other; that is the burrs create an electrical link between two successive sheets. This link give way to shorts circuits within the stack of steel sheets; we then talk of inter-laminar faults(ILFs) which reduces the overall energy conversion efficiency of the core and counteracts the gain obtained by laminating the core[3], [21]–[23]. When installed, electrical machines may encounter during their operation some defaults like ineffective cooling system, protection defaults windings and insulation defaults and many others. The two latter defaults represent 15% of contribution to machine malfunctioning[24];hence a keen follow up of them is undoubtfully of major interest to electrical machine users. Furthermore, statistics on transformers defaults reveals that 21% is found at the level of windings and magnetic core[25].With respect to magnetic core of machines, detecting theses faults as prompt as possible entails monitoring its behaviour whilst it is running. This brings forth a thematic known as Magnetic Core Condition Monitoring(MCCM) which helps to appreciate a decrease in conversion efficiency without much latency time[26]. The MCCM paradigm makes exploits input and output electrical signals of the device under control in order to derive the average quantities of the parameters concerned[27]. Although all improvements exposed above were done, there is still more to be done towards obtaining a lossless energy conversion system.

1.2 **Problem Statement**

The life span of an electrical machine is closely related to its capacity to handle /overcome recover from constraints. The follow up and proper knowledge of its functioning will gear us

towards a more efficient management of these device on a long run. Predictive and curative maintenance of these equipment demands having access to information on how healthy is their magnetic core. The latter is generally enclosed in a frame; thereby making the core difficult to access for potential diagnosis to be carried out, since unmounting this frame is not very trivial and turns out to be very costly. Since as there is no guarantee of proper functioning of the machine when recoupled. Also, Sanchez[28] reveals in his work that the Cigré group wished to study on various types of defaults affecting transformers on service, but were faced with difficulty of not obtaining/unavailability of significant data from power network analyst[29].

To date, there are no private companies in France and Cameroon implementing Non-Destructive Analysis methods in order to assess both the presence of possible defects, the physical properties of the part and to monitor the material health over time by leaving sensors permanently on/in the devices. That is: **<<in situ magnetic behavior monitoring of many electromagnetic devices such as electric transformers, AC/DC electric motors or even real time micro magnetic non-destructive testing of ferromagnetic steel components>>**.

These needs are relatively new, they arise from the need to ensure better monitoring of the materials constituting the finished parts, to optimize the costs and the lifespan of the equipment. The emergence of new materials such as carbon, glass and silica composites, in particular in high-tech industries, has led to an interest in their properties and their behaviour under different constraints / stresses. Only a few laboratories and technical centres on an international scale have showed interest in these methods and in the miniaturization and integration of sensors, but the work carried out turns out to be very academic and difficult to use implementing practically at industrial level.

1.3 **Rationale of the study**

Electrical machines are at the heart of all industries and are intensively used to almost close to their threshold of operation. Depending on their application they undergo different types of constraints. The damages caused by the electrical constraints are in majority hot spots; as a result of local overheating. The overheating is contributed by: induced eddy current which flow in the core and degradation of the internal insulation system. Basically, the flow of current in their magnetic core induces a magnetic field, which in turn induces eddy current; it constitutes the supplementary source of losses in the machines. So far many research works have been

conducted to reduce eddy current losses, but some limits have been identified to the various solution.

As reviewed in the background, the first attempt was to break the one block magnetic core to a stack of lamination. In a ferromagnetic laminated core, steel sheets are being covered by a coating layer ensures both the insolation and the adhesion of the laminations. This alternating structure (lamination, insulated layer …) however affect the propagation of magnetic field lines within the stack. When crossing the superposed two layers of insulation the magnetic lines slightly develop a hunch. Curvatures or undesired inclusions can also be sources of similar divergences. Unfortunately, it is impossible to insert in a non-intrusive way a classic magnetic measuring solution within the lamination stack to help identify these undesired phenomena.

Thereafter, the Second attempt in reducing these losses is to figure out in real what is going on inside these laminations. For the last few decades, researchers from all around the world have been working on this topic and using simulation tools to predict this behaviour [30], [31]. But, local experimental results have never been available to validate the behaviour of these simulations due to current sensor limitations. These models have always been validated by comparison to averaged results.

Furthermore, the third attempt of solution is the development of a hand-held sensors by Krismanic et al[20] for the analysis of local distribution of magnetic fields and losses. Although the total sensor thickness is less than 3 mm, positioning this sensor inside the 0.3 mm thickness laminations magnetic core constitutes significant challenges. Therefore, it is impossible to embed them permanently inside a lamination stack.

In sum, from the afore-mentioned limitations, we realize that current magnetic sensors and experimental setups are limited to cross-section averaged information or limited to surface measurements [32]. Also, the various approaches limit the magnetic core diagnostic to average quantities and makes it impossible to geo-localize eventual defects. The research presented here, intends to bridge this gap by printing the sensing method directly onto the magnetic layer within the stack.

All through this thesis, we will develop the printing technique as well as an experimental device from a laminated magnetic circuit. This will play the role of proof of concept and will validate the use of printed magnetic tips as a magnetic characterization tool. Combined with modelling, this new tool will, among other things, improve the understanding of magnetization phenomena.

1.4 Objectives and roadmap

1.4.1 General Objective

The aim of this thesis is to investigate and implement a non-intrusive system for real-time monitoring of a magnetic core using a printed magnetic probe method.

In this study, we developed a Printed Magnetic Needle Probe Method(PMNPM) which is a non-intrusive printed sensor capable of measuring the local magnetic field distribution and evolution with relatively good accuracy. The sensor can be placed inside a ferromagnetic lamination stack in a non-intrusive way. The sensor can transmit information about the lamination's magnetic behaviour throughout the electromagnetic device's life; thus having a real time monitoring system. In achieving this goal, some milestones were set in order to take into account various parameters in a progressive manner.

1.4.2 Specific objectives

This research was carried out in a step-wise manner with milestone as follow:

1. Access to local measurements of magnetic flux density through an Embedded printed magnetic needle probes sensor.
2. Non-invasive local magnetic hysteresis characterization of a ferromagnetic laminated core
3. Experimental illustration of the Inhomogeneous distribution of magnetic field within a laminated magnetic core which is dependent on the position and direction of sensor when measuring.
4. A match between Internal characterization of magnetic cores with respect to finite element simulations
5. real-time condition monitoring of a laminated magnetic core health through a point-wise control of its magnetic behaviour

To achieve these objectives , the following actions were taken

1. Building up an instrumented lamination: With the use of Printed electronics technique, the needle probe is printed on a steel sheet with a conductive ink.
2. Validating the feasibility of the printed sensor: Through experimental tests, results gotten with the printed sensor will be confronted to that obtain with classical magnetic measurement sensors namely: search coil, wound coil, needle probe. This is done with same experimental conditions

3. Develop a non-intrusive measurement system: Integrating Giant Magneto-Resistor(GMR) to the printed sensor in order to obtain a B_H measuring system on a single substrate
4. Simulation of the equivalent experimental model: result from simulation using fine elements methodology will be confronted to experimental result so as to validated the solution of the new sensor built.

1.5 Thesis organization

This thesis is grouped into 4 chapters, which includes the theoretical and experimental aspects of the development of a Printed Magnetic Needle Probe Method for the local characterization of magnetic core. More to that, a comparison of results obtained to that gotten from numerical simulation of the magnetic set-up.

Chapter one presents ferromagnetic behaviour and concept. An overt presentation of local magnetic characterisation basic concepts. A report on state-of-the-art technology for material characterisation methods in NDT is done; the most relevant: eddy current testing sensors. The concept of condition monitoring of magnetic material is also described.

Chapter two describes the concept of magnetic needle probe sensor underlying principles and technologies are discussed. Thereafter, the printed magnetic needle probe method (PMNPM) constitution, principles and design are described in details; the experimental setup developed for the validation of the PMNPM. The GMR sensor is described along with its corresponding experimental setup for the validation of our local non-intrusive hysteresis cycle characterization, **B(H)**.

Chapter three discusses the numerical simulation of the magnetic circuit under characterization. For this purpose, finite element analysis is employed using the open-source Onelab software suite. The selected mathematical model implemented by the Onelab Software program for simulating the material's behaviour is presented: that is the scheme used to mimic the specific experimental conditions so as to generate a gradient of magnetic induction through the laminated magnetic core. Not leaving out an insight on the post-processing treatment done using MATLAB software.

Chapter four is devoted to results and discussion. Firstly, we will confront measurement of classical magnetic sensors to the data gotten with PMNPM. Secondly, sorting individually the magnetic state of every lamination using the PMNPM and compare the sum of these local measurements to the average value obtained from a global wound coil. These comparisons serve as a validation of the PMNPM. Thirdly, we will monitor the local hysteresis cycle of every lamination and compare the experimental and simulated gradient of magnetic induction found through the laminated magnetic core.

Conclusions drawn from the research work and areas of potential investigations for further work are given at the end.

CHAPTER 1:

MAGNETIC CORE STATE CONDITION: MICRO-MAGNETISM, NON-DESTRUCTIVE TESTING

The notion “non-destructive testing (NDT)” is a set of methods which make it possible to characterize the state of integrity of structures or materials, without degrading them, either during production or during use or in the context of maintenance. This new way of material diagnosis was boosted with the fast growth in metallurgic industries, in aeronautics and nuclear plants. The complexity, fragility and sensibility of some equipments in these various domains bring forth some constraints when dealing with their maintenance. Constraints such as: the nature of the defect to be sorted out, the part to be inspected which could be rived, welded, rolled or of complex shape and the conditions under which the inspection needs to be carried out (during manufacture or in service). These defects are classified into 2 categories: defects on the surface, in-depth defects[33].

1.1 Magnetism

Magnetism is the force exerted by magnets when they attract or repel each other. André Marie Ampere explains this phenomenon through her discovery: the motion of electric charges is at the origin of magnetism[34]. Earlier before André ampere, Hans Christian Oersted had observed that a current carrying wire caused a deflection of a compass needle located near it; this scenario shows a direct relationship between electricity and magnetism. These two words combined gives electromagnetism; this term is brought to light thanks to Michael Faraday who showed that a moving magnet creates an electric current in wire placed nearby: thus electromagnetic induction. A magnet is actually a material having a north and a south pole and can creates a magnetic field; that is making the area around where it is found to possess a magnetic force. When field fillings are thrown in such an area, the fillings align themselves following the magnetic field lines as portrayed by figure 1-1.

Moreover, there exist various types of substances which are used to create magnetic field.

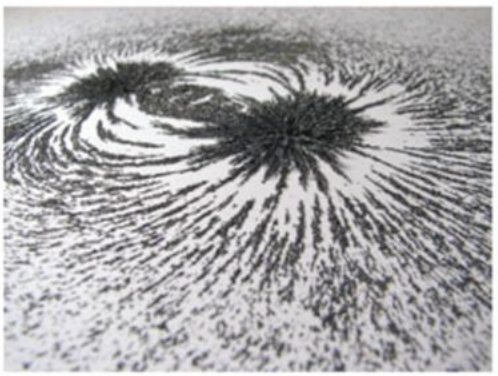

Figure 1-1: Magnetic field lines created by a magnet

Depending on their features we classify them in three major categories: permanent magnet, temporary magnet and electromagnets. The latter constitutes our area of interest throughout our work.

1.1.1 Magnetic field properties

The strength of a magnetic field describes the amount of magnetising force of the field termed magnetic field intensity noted H. From this magnetising force H, there is an induced magnetic force on a material found in the field which is quantified by variable B termed magnetic flux density. This induction is directly depending on the extend at which the substance reacts to the magnetic field in which it is found. This parameter is referred to as the permeability of the material (μ) which is the coefficient of proportionality between B and H; Thus the relationship

$$B=\mu H \qquad 1\text{-}1)$$

Where μ is the relative permeability.

Furthermore, the magnetic theory when seen at the level of electron, reveals that each material possesses permanently an intrinsic magnetic moment. The latter is proper to the nature of the atoms constituting the material. In effect as seen in figure 1-2, when electrons gravitate in orbit around the nucleus of an atom, they create a magnetic moment called orbital moment. Same during their gravitation, they do spin on themselves; this spinning create another magnetic moment called spin moment. These two moments constitute the total magnetic moment of the atom m_i. Application of an external magnetic field will turn to align all atomic moments to follow its direction. The amount of torque used for such alignment is evaluated through the expression:

$$\Gamma = \mu_0 . m . H \qquad 1\text{-}2)$$

Where m is the magnetic moment of the material(Am^2), H: is the magnetic field strength(Am) and μ_0 the permeability in air.

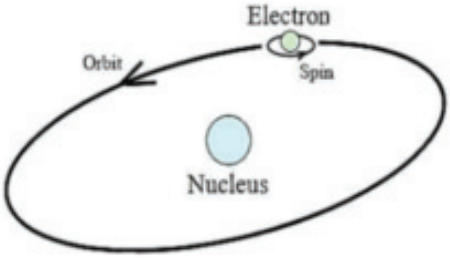

Figure 1-2 : Motion of an electron around the nucleus[35]

However, if the number of electrons spinning in a direction is equal to the number spinning in the opposite direction, the material in concern shows non-magnetic properties. Conversely, if more electrons spin in one direction than the other, then the material is a magnet.

Let's us consider an electromagnet, that is a smooth, homogeneous and isotropic material wounded with a copper conductor in a helicoidally manner. When the electromagnet is supplied with current, a magnetic field is created and the reaction of the piece of material in the midst of a magnetic field is perceived through the magnetization vector $\boldsymbol{\mathcal{M}}$ with S.I unit $A.m^{-1}$ and expressed as:

$$\mathcal{M} = \frac{\partial m}{\partial v} \qquad 1\text{-}3)$$

Where m is the sum of atomic magnetic moment and ∂v is the volume entity considered

Integrating the magnetization vector as part of the relationship between B and H, we have the following expression:

$$B = \mu_0 (H + \mathcal{M}) \qquad 1\text{-}4)$$

Factorising out H we have: $B = \mu_0 (1 + \frac{\mathcal{M}}{H}) H$ 1-5)

Another parameter which is proper to the type of material comes in to help correlate the magnetization vector according to magnetic field strength / excitation field; it is called susceptibility (χ) and is expressed as :

$$\chi = \frac{\mathcal{M}}{H} \quad 1\text{-}6)$$

Equation 6 then becomes : $B = \mu_0(1+\chi)H$ 1-7)

Comparing equation 8 by analogy to equation 2, we derive the following:

$$\mu = \mu_0(1+\chi) \quad 1\text{-}8)$$

and we know that: $\mu = \mu_0.\mu_r$;

thus, $\mu_r = (1+\chi)$

μ_r is a dimensionless scalar which is proper to each materials' properties as per their isotropic medium. From this, emanates a classification of material depending on how its responses to magnetic field. As shown in table 1-1, we have:

- ✓ Diamagnetic materials such as copper, zinc, gold, silver, lead [36] : these are materials whose atoms don not possess an intrinsic magnetic moment in absence of an external magnetic field. When placed in magnetic field, it causes electrons to spin, but the resultant magnetisation counteracts the source field[37]; we then talk of a repulsive effect. Their magnetic susceptibility being of very small and negative values implies having a relative permeability $\mu_r \leq 1$. a perfect diamagnetic material has its susceptibility to be -1; thus a supraconductor.
- ✓ Paramagnetic materials: they have a non- linear characteristic curves namely: aluminium, chromium and sodium. In effect, they possess permanent atomic magnetic moments which are oriented randomly in absence of external magnetic field; thereby not magnetized. Nevertheless, in presence of a magnetic field, some moments align with the source field; thus the material is magnetized. Their relative magnetic permeability is slightly greater than one, $\mu_r \geq 1$.
- ✓ Ferromagnetic materials: their susceptibility and permeability are of very high value of the range of 10 to 10^6. Materials like iron, nickel, cobalt and their alloys permanently present intrinsic magnetization in absence of external magnetic source. Actually, the atoms constituting these materials are arranged in a lattice and the atomic magnetic moments can interact to align parallel to each other. This behaviour is best understood through the domain theory in the microstructure of the material as presented by Weiss in 1907.

Table 1-1: A summary of the three major types of magnetic behaviour[35]

Type	Atomic / Magnetic Behaviour	
Dia-magnetism	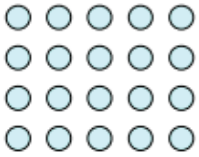 Atoms have no magnetic moment	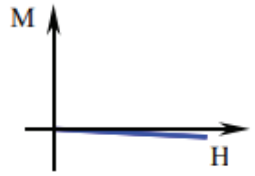
Para-magnetism	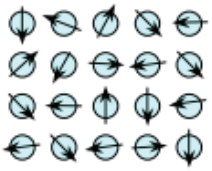 Atoms have randomly oriented magnetic moments	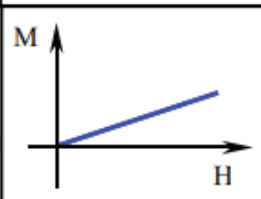
Ferro-magnetism	 Atoms have parallel aligned magnetic moments	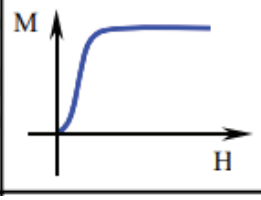

1.1.2 Ferromagnetism at the Microscopic level

The magnetic microstructure of ferromagnetic materials is basically made up of magnetic moments aligned within small macroscopic regions called domains (Weiss domain) and separated from each other by domain walls (Bloch walls)[38].

1.1.2.1 Magnetic domains

Magnetic domains are regions of ferromagnetic materials in which each is intrinsically magnetized to saturation as a result of the magnetic moment being parallel to each other. Each domain possesses a permanent magnetization. In the absence of external magnetic field, the moments of various domains have random orientation. This is an effect of the existence of magneto-static energy and magneto-crystalline structure of the material which hinders the global moment of the material to be at saturation. The magneto-crystalline energy favours moments of each domain to be aligned in its direction of easy magnetisation with respect to the structure of materials. Furthermore, magnetic interaction between moments give way to the creation of magnetic poles (negative and positive poles) within the material: this is referred to as magneto-static interaction. These three different interactions are at the origin of the formation of Weiss domain and Bloch walls as shown on figure 1-3. These latter are the junction between two successive domains with moment different orientations.

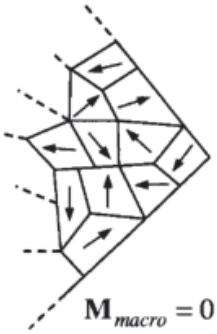

Figure 1-3:Magnetic moments within domains

However, in the presence of an external source of magnetic field, an energy boost will drive magnetic moments to align themselves following the direction of the external field. Nevertheless, not all the moment will be aligned simultaneously; the domains which magnetic moment do not have a big drift from the direction of the external field will be more favoured to align themselves first. The rest of the domain with higher drift will need to be subjected to higher amount energy for their orientation to align accordingly as perceived in the figure 1-4. The transition of a domain from one orientation to the other is done in a smooth manner and not abruptly[39] as illustrated by figure 1-5.

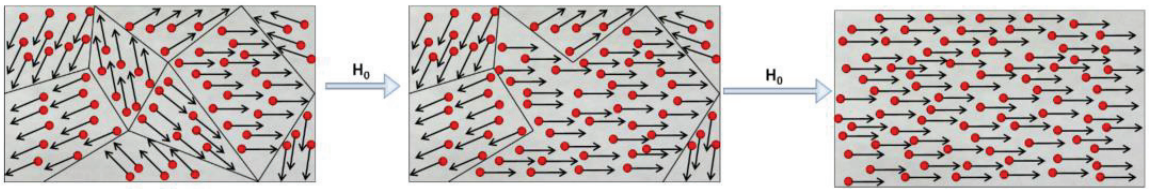

(a) In absence of H_0 (b) low magnetism (c) high magnetism

Figure 1-4:Magnetism in a ferromagnetic material[37]

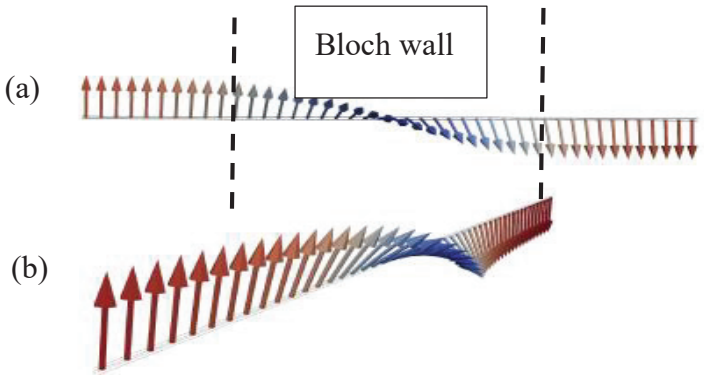

Figure 1-5: Insight on magnetic domain transition at bloch wall[40] (a) shows the side view on a Bloch wall (b) is a tilted view

The movement of the domain walls (reversible and irreversible) during the magnetization process, is characterized by the ease to overcome the spin–orbit coupling of the magneto-crystalline structure and the material imperfections, whether in the form of dislocations or impurity elements. Moreover, the magnetization response towards external excitation, is causal and non-linear. Thus, accounting for the magnetic hysteresis of the ferromagnetic materials.

1.1.2.2 Hysteresis mechanism

The term hysteresis describes a system whereby its state is dependent on its history. The characteristic curve of magnetization as a function of external magnetic field strength depends on previous state of the material in concern; it is referred to as Magnetic hysteresis. The corresponding B(H) curve doesn't exhibit bijective properties when dealing with ferromagnetic materials. The non-bijective nature implies obtaining a hysteretic loop as B_H curve in case the magnetic field excitation is an alternating signal. In effect, let's consider an electro-magnet, made up of a coil which is wound around a Ferro-magnetic material which has never been magnetized before. The magnetic behaviour of the material will be following the curve as shown in the figure 1-6.

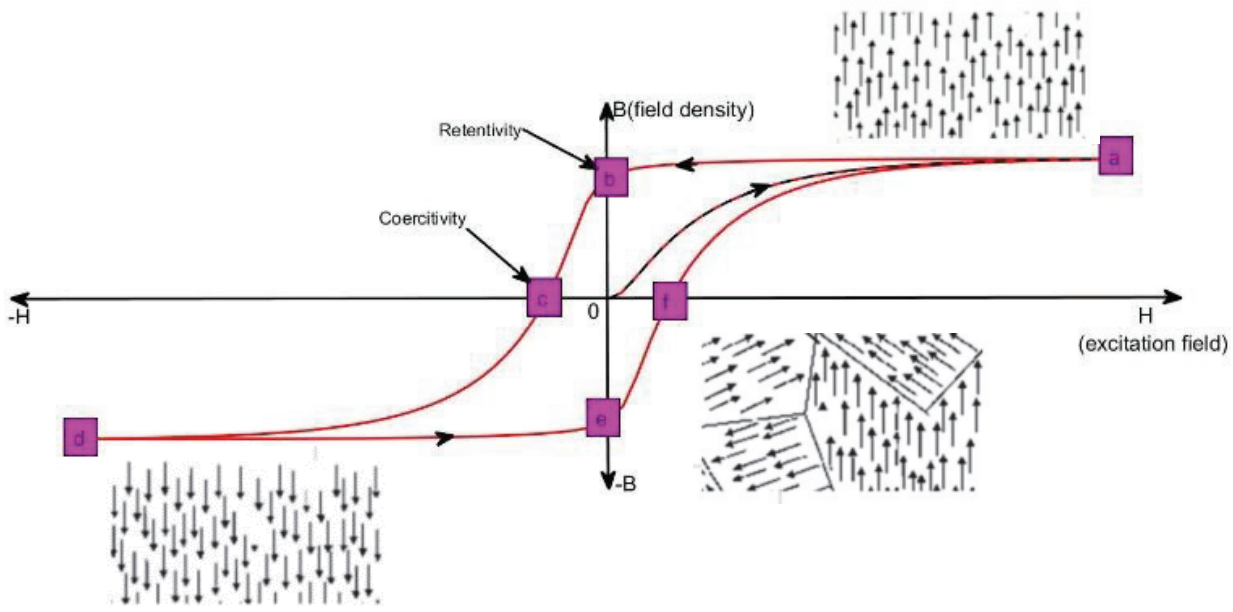

Figure 1-6 : Hysteresis cycle of a ferromagnetic material(adapted from[41])

When magnetized for the first time, the material response to an increasing positive excitation will follow the **first magnetization curve**; that is from the origin to point (a) as materialized by a dotted line on figure 1-6. The material will magnetize till **saturation** (point a): all the moment of the domain constituting the material are all align in the direction of the excitation

field; thus B is at his maximum. A subsequent decrease of the magnetizing force will cause a drop in the induced flux density following the path ab. If the external source is turned off at this stage (point b), there will be a remaining flux still circulating in the core; the value of this **residual flux** is noted $\mathbf{B_r}$. the latter is used to quantify the ability of the material to retain residual magnetism and is termed **retentivity**.

An increase of the magnetizing force in the negative direction, will imply the material losing magnetism as illustrated by the curve from point b to c. Point C is the point of **coercitivity** which denotes the state whereby the material has totally loosed magnetization; the corresponding value of the magnetic field strength is called **coercive force** noted **Hc.** Further increase of the magnetizing force still in the negative cycle will result to the material being magnetized in the opposite direction from the positive response. The material will hence response symmetrically as during the positive cycle.

The area covered by the hysteresis loop gives an insight on the quantity of losses(P_T) incurred during the magnetization process. It is derived through the equation:

$$P_T = \oint H.dB \quad (\mathrm{J/m^3}) \tag{1-9}$$

The area and form of the hysteresis loop depends also on the type of ferromagnetic material used as exposed through figure 1-7.

1.1.2.3 Types of ferromagnetic material

We distinguish two main category of magnetic material; namely: soft and hard magnetic materials. The hardness/softness of the material depends on the strength of the magnetic field needed to align magnetic moment of domains constituting the material.

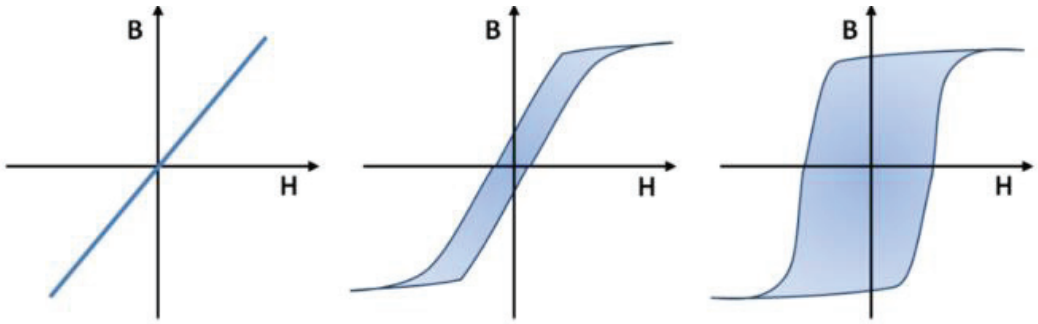

(a) (b) (c)

Figure 1-7 : B_H curve of: (a) ideal material ;(b) soft magnetic material (c) hard magnetic material[41]

- ✓ Soft magnets. They have a high susceptibility; thereby making them are responsive to low value to magnetizing field. Their B_H loop is of tiny-like shape given that it is less energetic to cancel their retentive ability ($H_C \geq 100$ A/m). its various features make them suitable for transformers and machines cores since as they can channel induced magnetic flux with less losses. The widely used iron alloy is Silicon-Iron(Fe-Si) material
- ✓ Hard magnets. These are ferromagnetic material that have a high retentivity, they retain their magnetization in the absence of an external source of magnetic field. Cancelling their residual flux demands much energy; that is a very high coercive force needed ($H_C \geq 10^4$ A/m). These properties make them good candidates for permanent magnets purposes and the coercitivity point is used as the threshold of degaussing field.

Soft magnets most especially FeSi is the material specimen concerned all through this thesis since as it is easy to manipulate in the lab and we are dealing with electrical machines core.

The Presence of flaws on a material, is perceived at the magnetic microstructure as disturbances in domain walls mobility and leads to noticeable shifts in the magnetic signature of the material generally observed on the magnetic hysteresis. The latter therefore plays a big role health control of materials.

1.2 Condition monitoring

In a hostile operating environment, under harsh and highly variable weather conditions, the difficulty and cost of maintenance and operation of electrical machines increase. Improvement of reliability of equipment, reduction of operation and maintenance costs of industrial equipment have triggered researchers to study more the domain of condition monitoring and fault detection. In same line, Shoudao et al assert in their script that: “condition monitoring (CM), fault diagnostics (FD), and operation control under electric power conversion system faults should be investigated to ensure reliable and safe operation of Wind Turbines (including grid and equipment) and to reduce the maintenance cost”[42]. So far strategies like Corrective Maintenance, also known as reactive maintenance consisting of curing already broken equipment; and Preventive Maintenance, which is regular maintenance carried out according to defined schedules, regardless of the condition of the equipment have been adopted by industrial operators to help cater for the proper functioning of their equipments. Nevertheless, there is an important demand for high degree of maintenance so as to provide a safe, cost-efficient, and reliable power output with acceptable equipment life. Thus a new paradigm called Predictive

Maintenance, which is based on constant monitoring of operating conditions of equipment and forecasting failures. The condition-based maintenance is part of the Predictive Maintenance.

The approach is based on the continuous diagnostic of physical or operational condition of materials making up equipment's during their usage. This is contrary to one sticking to statistical data and planned calendars programming maintenance activities. The continuous monitoring guaranties fault detection earlier as when it is still at its precursory stage, before there is any visible sign, and in its potential phase. Thus, the maintenance performed will always be better informed, necessary and timely, since the equipment will only be subject to maintenance when a breakdown is foreseen, which will reduce costs and labour time spent on maintenance[43]. Taking an example amongst many others, In the operation power generation systems, most of their faults occur in the generator and power converter, which account for 60% of all failures [44]. Actually, the main component of the energy generation system which is the generator stator core and base are permanently subject to damages, cracks, flaws and deformations at a long run. This is due to the position they occupy amongst the transmission of mechanical motion. Considering the difficulty and cost incurred for the maintenance of these parts, certain faults are being ignored; leading to a very high compromise of safe operation. Many works have been done by researchers categorising various faults encountered in an electrical machine and monitoring schemes that can help detect them. Depending on the location where a fault is likely to occur, we have: stator core faults, stator winding faults and rotor faults; the latter is just proper to rotatory machines. Our review is circumscribed to faults affecting ferromagnetic materials constituting magnetic core of these machines: that is magnetic core condition monitoring(MCCM)

1.2.1 Magnetic core condition monitoring

MCCM consists of a real-time inspection of the magnetic circuit performances to detect defects and anticipate drops in the electromagnetic converter efficiency. In effect, it goes beyond mere fault diagnostics to instantaneous monitoring related parameters and evaluating any deviations from the nominal values/trend. Given the laminated nature of the magnetic core, any fault to which it is subjected are described as interlaminar faults. As a matter of fact, they are ranked as the third main cause of transformer failures[45].

1.2.1.1 MCCM principle

MCCM provides a valuable reference for developing service quality evaluation methods and fault operation control systems to achieve high-performance and high-intelligence of electric

machines. MCCM consists of measuring electromagnetic parameters of the core that can indicate failure. Operators can thereby spot changes in the usual patterns in time to prevent a breakdown, save on reactive maintenance, and extend your asset's lifespan. MCCM sensors are called upon to be smart in providing real-time data. Real-time data allows managers to adjust preventive maintenance and contingency plans while providing greater reliability.

Three different steps constitute the process of carrying out MCCM:

- ✓ Designs inspection and testing based on the technical characterization of each magnetic core constituting the machine.
- ✓ Performs inspection and condition control services from real-time measurements of electromagnetic parameters.
- ✓ Assesses the condition of equipment in the operating context in which they operate, diagnosing abnormal situations and developing approaches for analysing and limiting damages

1.2.1.2 Advantages of MCCM

MCCM is advantageous not just in monitoring magnetic core, it also has an added value towards the overall functioning of the machine. It helps:

- ✓ Avoid major breakdowns and reduces downtime: optimization of maintenance
- ✓ Enables better asset management across its lifespan.
- ✓ Decreases costs, particularly with emergency maintenance.
- ✓ Provides the basis to develop predictive algorithms.

1.2.2 Inter-laminar faults

Basically, a fault in a sole lamination can't affect the entire magnetic core due to the double-side insulation of each lamination. This is due to the fact that eddy current flow is restricted within independent sheet as illustrated in figure 1-8b. So, for a fault to affect the core, there ought to be an interaction between two successive laminations. Generally, electrical-wise this fault is materialized by a short-circuit which has been created between two laminations. The appearance of this shorts are mainly caused by burrs and insulation failure. The latter ideally comes along with the wear and tear parameters of the material used for insulation and the wearing of the electrical devices at a long run. Nevertheless, there is cause-effect relationship between burrs and insulation failure. So, our interest is to understand the correlation between edge burrs and inter-laminar faults.

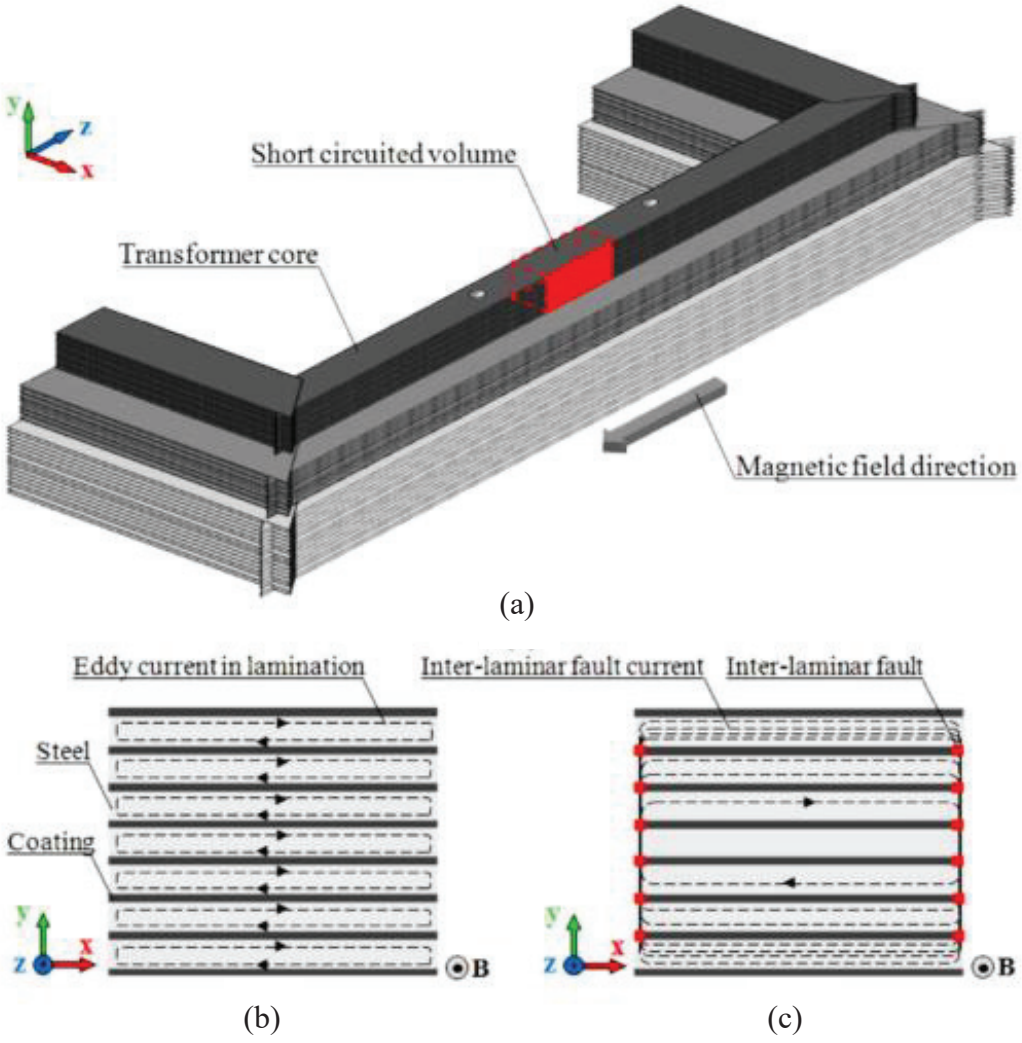

Figure 1-8 :(a) 3-D view of a faulty transformer limb: interlaminar fault in red. (b) ideal eddy current flow in a laminated core. (c) impact of fault on eddy current flow[21]

1.2.2.1 Burrs

The appearance of burrs in a magnetic core is traced as early as the basic components of magnetic core are produced. During the machining process, punching at trimming of electrical steel to desired dimension subjects the material to some plastic deformation. Although, in some cases the sheets go through the deburring process after fabrication. Unfortunately, during the rest of step of devices manufacturing and coupling process, burrs are still created. Burrs located at the edges of sheets are termed as edge burrs. They can easily establish an electrical contact between two adjacent laminations: an interlaminar fault is created. The recurrence of this electrical contact at many points affects critically the operation of the magnetic core as seen on figure 1-8a. Actually, once a close path is created from at least two points of short-circuit, eddy current flow will increase as exposed on figure 1-8c. The larger section of eddy current flow will therefore lead to more eddy current losses incurred[46].

1.2.2.2 Impact of interlaminar Fault

As aforementioned, multiple points of short-circuit in a magnetic core results to a high induced interlaminar eddy currents flow within the core. Taking into consideration the Joule's effect, there will be a corresponding local heating in the damaged area [47]; which can lead to core melting as illustrated in figure 1-9. If the generated heat is excessive and cannot be dissipated adequately, it can cause more interlaminar failures and may eventually cause burning or melting of the iron core and, thus, it raises the potential of a complete machine failure[22]. Localized heating due to the interlaminar fault currents can also damage the excitation winding insulation and lead to ground failure [48].

Figure 1-9 : Stator core melting caused by interlaminar insulation failure: Core fault in tooth wall [49]

1.2.3 MCCM Non- invasive schemes

Research work have been evolving for the past two decades towards achieving a hands-on real time control of core losses and magnetic core health. Various studies gravitate around evaluating the electrical performance of the core, then afterwards analysing them and inferring the condition of the core. Amongst various electrical quantities evaluated, we have:

- ✓ Insulation resistance measurement:

- ✓ current measurement,
- ✓ power measurement,
- ✓ capacitive measurement [46]
- ✓ external magnetic field measurement[50].

The above-mentioned parameters do not give the possibility to quantify spontaneously any inherent, abnormal condition of the magnetic core and identify the location of the area where the fault is located. Some few researchers push the research further gearing towards a real-time/ on-line evaluation of core condition:

- ✓ Lin et al worked on "Real-Time Monitoring of Iron-Core and Copper Losses of Transformers Under (Non)Sinusoidal Operation" [51]. Their approach was to use high accuracy current and voltage sensors coupled to voltmeters and ammeters to evaluate separately copper losses and iron-core losses.
- ✓ Hamezehbahmani recently came out with both phenomenological and experimental approaches aimed at following up the health condition of a core[26], [27]. They analysed the distribution of eddy current from which they could infer the corresponding mapping of loss amongst laminations of electrical steel with interlaminar fault.
- ✓ Lofti Et al studied the distribution and loss calculation of eddy current which can be used to detect multipoint grounded faults in magnetic cores[52].
- ✓ Fu et al monitored a transformer core through online estimation of core losses[48]. They based their evaluation on measuring instantaneous input voltage and excitation current. firstly, they characterize their device by obtaining the anhysteretic parameters by slowly demagnetizing the material with DC fields. From the non-linear magnetizing inductance model, they could derive the corresponding magnetizing current. With the two parameters, they dissociate core loss and eddy current losses and appreciate the latter's behaviour with varying degrees of interlaminar fault.

So far, main condition monitoring schemes structured by other researchers have been reviewed; For MCCM to hold, be consistent and reliable all through the systems life, there is essential condition that needs to be respected while choosing a measurement technique; **it should be non-invasive, non-destructive to the equipment under control, ;** thus non-destructive technique required for this purpose ;there is thereby need for us to choose ideally a technique that will permit us attaining our objectives.

1.3 Non-Destructive Testing Methods

1.3.1 Comparison of non-destructive testing methods

In this part we are evaluating Condition monitoring techniques with respect to predefined criteria. This will help select efficiently a technique we will duel on. In the literature, some comparatives analyses by other experts have already been carried out concerning non-destructive testing. Analysis done by an the modal shop is summarized in table 1-2. The company specialized in Non-destructing testing services compares the visual inspections technique, eddy current testing, magnetic particle inspection/liquid penetrant testing, ultrasonic testing and radiography testing.

Table 1-2 : Comparative evaluation(adapted from[53])[***3:excellent; 2:fair; 1:poor]***

Method	Visual inspection	Resonant acoustic	Magnetic penetrant	ultrasonic	Radiography	Eddy current
Defect/Issue						
Cracks	2	3	3	3	2	3
Material Properties	1	3	1	1	2	1
Missed operations	1	3	1	1	1	1
Structural intergrity	1	3	3	3	3	3
Product lot variation	1	2	3	3	3	2
Defect location						
Surface(external)	3	3	3	3	1	3
internal	1	3	1	3	3	1
Bonding/Welding	1	3	1	2	2	1
Speed/training/cost						
Throughput	3	3	2	3	1	2
Training/certification	3	3	1	1	1	1
Total Inspection costs	3	3	2	1	1	2
Automation Capacity						
Quantitative results	1	3	1	2	1	1
Ease of automation	2	3	2	1	1	2
Cost of automation	1	2	1	1	1	2
Total	**24**	**40**	**25**	**28**	**23**	**25**

Summing out the appreciation values based on each criterion, we have Resonant acoustic, magnetic penetrant and eddy current testing which top other techniques. That notwithstanding, one of our objectives were to optimizes energy conversion in magnetic core and to elucidate on magnetic distribution in the magnetic core and not just limiting ourselves to condition monitoring. With this, our choice goes for eddy current testing since as it makes uses eddy current which is one of the main properties describing the efficiency of energy conversion in electrical machines. Moreover, in a comparative analysis done by confronting Micromagnetic nondestructive testing Barkhausen noise vs other techniques namely MIP and ECT, it is revealed that "ECT is nowadays still very popular probably because of the experimental setup's simplicity"[54]. This implies that, ECT is a user-friendly and training an operator for the manipulation of these sensors won't be cumbersome. Thus a cost-effective method in technology and certification training.

1.3.2 Eddy current testing (ECT)

Eddy currents are created through a process called electromagnetic induction. If a ferromagnetic material is brought into the close proximity of a changing magnetic field(primary magnetic field), current will be induced in this material as illustrated in figure 1-10. These currents produce an another magnetic field (secondary magnetic field), but they are influenced by the nature of the material such as voids, cracks, changes in grain size, as well as physical distance between coil and material. These currents form an impedance on a second coil which is used to as a sensor.

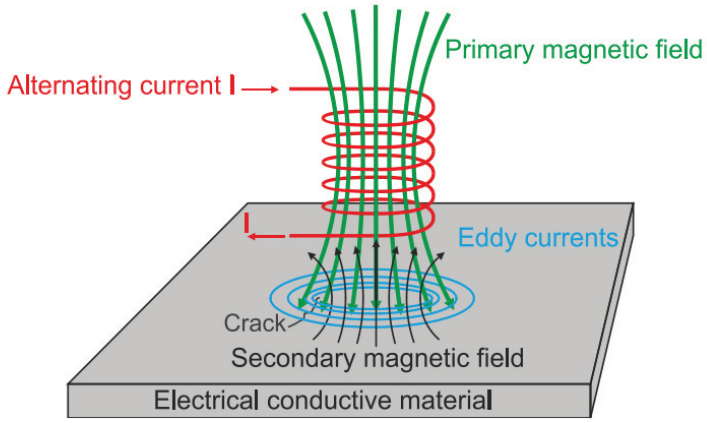

Figure 1-10 : A primary coil inducing eddy currents in a component[55]

In practice, as shown in figure 1-11, a probe is placed on the surface of the part to be inspected, and electronic equipment monitors the eddy current in the work piece through the same probe.

Figure 1-11: Operator testing a mechanical spare part using an eddy current probe[56]

The sensing circuit is a part of the sending coil. Eddy currents can be used for crack detection, material thickness measurements, coating thickness measurements, conductivity measurements for material identification, heat damage detection, case depth determination, heat treatment monitoring.

1.3.2.1 Eddy current testing sensors

During manufacturing stages of components made of alloys, heat treatment is given to ensure required levels of mechanical and physical properties and desired microstructures. Likewise, during service life of components, it is essential to ensure that there is no undesirable degradation in microstructures. EC technique is useful for assessing these two situations as it exploits measurement of changes in electrical conductivity and magnetic permeability. figure 1-12 shows some examples of eddy current sensors whereby: changes in microstructure, precipitate size and distribution, cold work, deformation, dislocation pile-up etc. alter the coil impedance or induced voltage in a pick-up coil. The magnitude and phase of induced voltage or impedance change are used for quantitative characterisation of microstructures and to estimate the volume fraction of various phases present. Usually, EC measurements for microstructure characterisation are location-based. In general, absolute probes are used and analysis is based on impedance plane signal interpretation. Reference standards with known electrical conductivity and magnetic permeability are used also for establishing calibration graph, apart from specimens heat treated to different ageing conditions through measurement of conductivity and permeability.

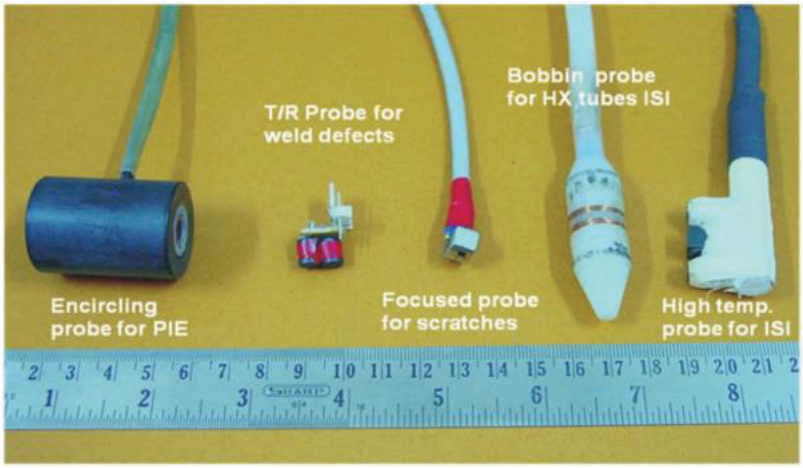

Figure 1-12: Different types of Eddy current testing probe[57]

1.3.2.2 Basic Principles

- ✓ eddy current

Eddy current also called in French "courants de Foucault" is named after the French researcher Jean Bernard Léon Foucault. He actually noticed that when a conductive material is placed in an area with changing magnetic field, current is induced in the thickness of the material without altering its properties. This current is thereby termed as eddy current. By analogy to Lentz Law, this induced current generates a counterpart magnetic field (secondary field) which turns to oppose the source field from which it was induced. figure 1-13a illustrates the electromagnetic induction as afore-explained with a varying current carrying coil which will create the primary magnetic field. Approaching a conductive material towards to this primary magnetic field will impact the value of the electromotive force(emf) of the coil. The emf represents a major parameter in ECT which will be exploited to inferred on the integrity of the conductive material (test piece). Any changes in the material be it on the geometry or a sudden crack causes a change in the counter-action of eddy current since as its pattern will no longer be smooth as shown in figure 1-13b; thus a reflection on the emf of the coil with change of value. In effect, Defects such as cracks, voids, inclusions, corrosion wall loss, microstructure degradation, localised stresses alter the local electrical conductivity σ, and magnetic permeability μ of the material and cause distortion of the eddy currents and change the coil impedance Z. The raw information gotten from the emf still needs to undergo post-processing for some numerical analysis to be done. The analysis is aimed at deriving the parameters best describing the nature of the faults from the measurements of the magnetic field.

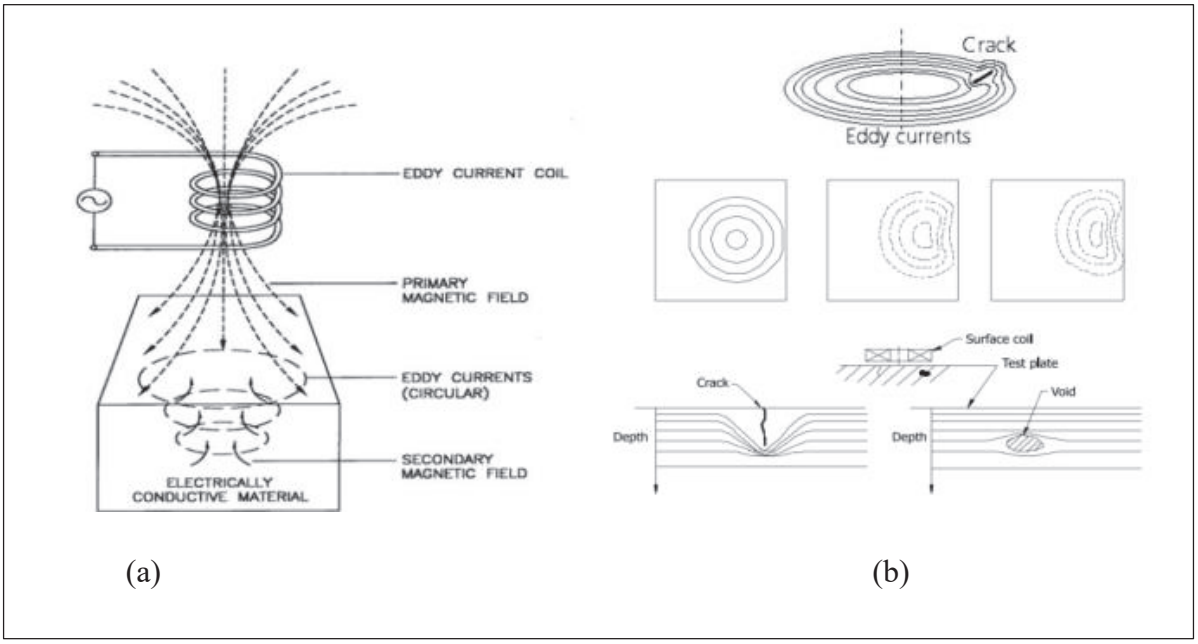

Figure 1-13 : Principle of eddy current testing (left) and distortion of eddy current due to crack, edge-effect, surface crack, and sub-surface void (right)[57].

✓ Skin effect/ skin depth

The flow of eddy currents in the test material is not uniform at different depths. The eddy currents are quite denser at the surface as compared to the deep inside, an effect referred to as skin effect [58]. The skin effect arises when the eddy currents flowing in the test object at any depth produce magnetic fields which oppose the primary field, thus reducing the net magnetic flux and causing a decrease in current flow as the depth increases as shown on figure 1-13a. Alternatively, eddy currents near the surface can be viewed as shielding the coil's magnetic field, thereby weakening the magnetic field at greater depths and reducing induced currents[59]. This effect is unavoidable and worth putting an interest on when dealing with ECT. It brings about an important parameter that quantifies depth of inspection of eddy current (EC) non-destructive testing which is termed Skin depth. Its expression is written as:

$$\delta = {1}\Big/{\sqrt{(\pi f \mu_0 \mu_r \sigma)}} \quad \text{(m)} \qquad \textit{1-10)}$$

Where: f is the primary field frequency(Hz), μ_0 is the magnetic permeability of free space, $44\pi 10^{-7}$H/m, μ is the relative magnetic permeability, dimensionless, and σ is electrical conductivity, mho/m. δ is the depth at which the surface eddy current density has fallen to 37%.

Figure 1-14 below exposes how materials with high conductivity turn to have a very short depth of penetration; whereas low conductivity austenitic stainless steel has deeper standard depth.

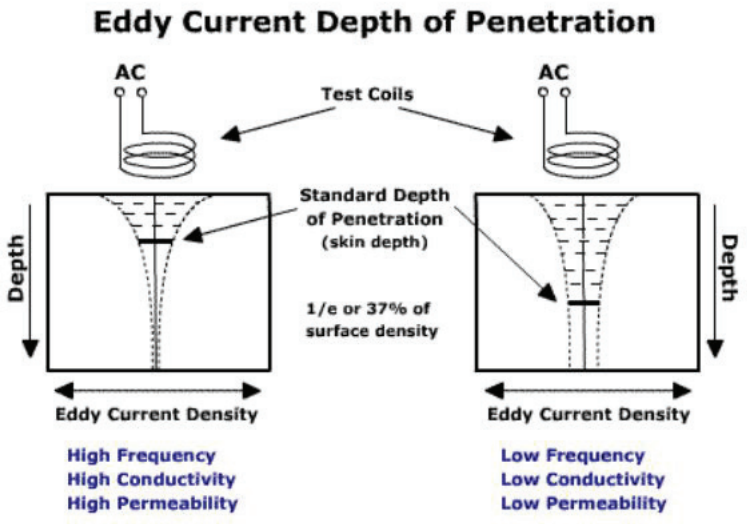

Figure 1-14: Illustration of skin depth[59]

Since the sensitivity of an eddy current inspection depends on the eddy current density at the defect location, it is important to know the strength of the eddy currents at this location. When attempting to locate flaws, a frequency is often selected which places the expected flaw depth within one standard depth of penetration. This helps to assure that the strength of the eddy currents will be sufficient to produce a flaw indication.

The added value brought by skin effect gives ECT techniques the capacity to control with no doubt surface defects and sub-surface defects if the frequency is chosen to fit detection to a specific depth. This is common to all eddy current testing method, most particularly search coil, local search coil and magnetic needle probe which constitute our area of interest.

1.3.2.3 Encircling coil

Encircling coil probes are induction based and are mostly made up of a few turns of copper wire usually wound around a ferrite core with or without shielding as seen on figure 1-15a. They are very cheap and accessible to all.

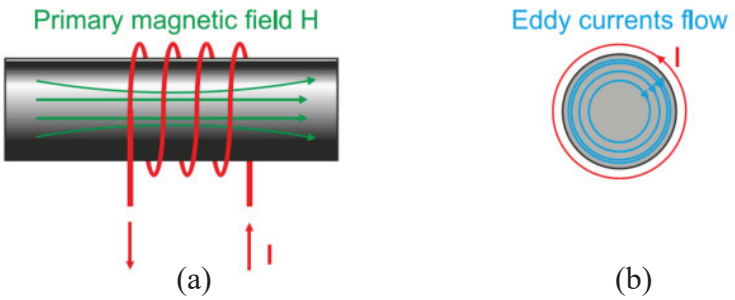

Figure 1-15 :(a) External encircling-type coil for a ferrite bar inspection. (b) Eddy currents flow in the measuring system[60]

Their functional principle is based on electromagnetic induction as afore-explained the resulting emf is expressed as follows:

$$e = -\frac{d\varphi(t)}{dt} \qquad 1\text{-}11)$$

Where **e** is the emf and $\boldsymbol{\varphi}$ the magnetic flux.

Eddy currents describe radial circumferences in an opposite direction of currents around the energized coil current, as shown in figure 1-15b. The time varying nature of the emf, makes this sensor not able to operate in a constant magnetic field. The response of encircling coils is highly affected by the presence of any parallel discontinuities to the axis of the tube or bar. The precision is ameliorated as the number on turns of the coils increases. The resulting voltage measured at the terminal of the sensor is mathematically expressed by:

$$V(f) = N.2\pi f.B(f) \qquad 1\text{-}12)$$

The sensitivity S of the sensor is evaluated as:

$$S = \frac{V}{B} = N.A.2\pi f \qquad 1\text{-}13)$$

The sensitivity is frequency dependent. It is thereby detrimental to work at relatively low frequency. Even though it is at low frequency that we have high depth of penetration. This dilemma can be overcome by increasing the number of turns and the diameter of the coils. In cases where there is space limitation and ergonomic needs, this solution won't be appropriate. Researchers then proposed a plane spiral coil figure 1-16 as done by Ravat et al., which was able to detect long cracks.

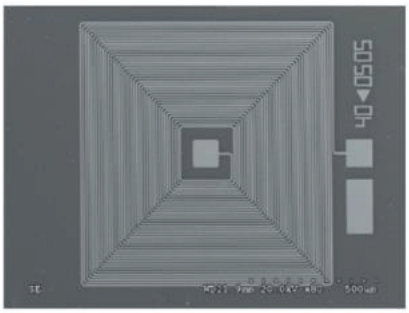

Figure 1-16 : Plane spiral coil [61]

Encircling coil have shown some points of shortcomings namely:

- ✓ Inspection of installed ferromagnetic components with the exception of tubes can't be inspected
- ✓ Difficulty to separate the influence of one desired variable in the combined presence (at the same location beneath the probe) of several other disturbing variables such as stress, microstructure, texture, anisotropy etc. that simultaneously change conductivity and permeability.
- ✓ Inability to identify circumferential location of a defect when encircling or bobbin coils are used.
- ✓ Difficulty in detection of a small defect under a large defect

Taking into consideration these limitations, a new sensing technique comes in play with localised information on the condition of a material.

1.3.2.4 Magnetic Needle probe technique

This consist of placing two needles in electric contact with surface of the specimen [62]. Based on the potential difference produced by eddy currents generated by ac magnetization, it is possible to measure the flux density in the area surrounded by points 1-2-3-4 as shown in figure 1-17. The voltage detected by the needle probes is equivalent to half the amplitude measured by a search coil (one turn) wound around the 1-2-3-4 area. This is the case if and only if we consider the flux distribution is homogenously distributed in the material. The equivalent faraday's law gives the following expression to obtain the voltage measured at the terminal of the probes,

$$e(t) = V(t) = -\frac{1}{2}N.A.\frac{dB_{mean(t)}}{dt} \qquad 1\text{-}14)$$

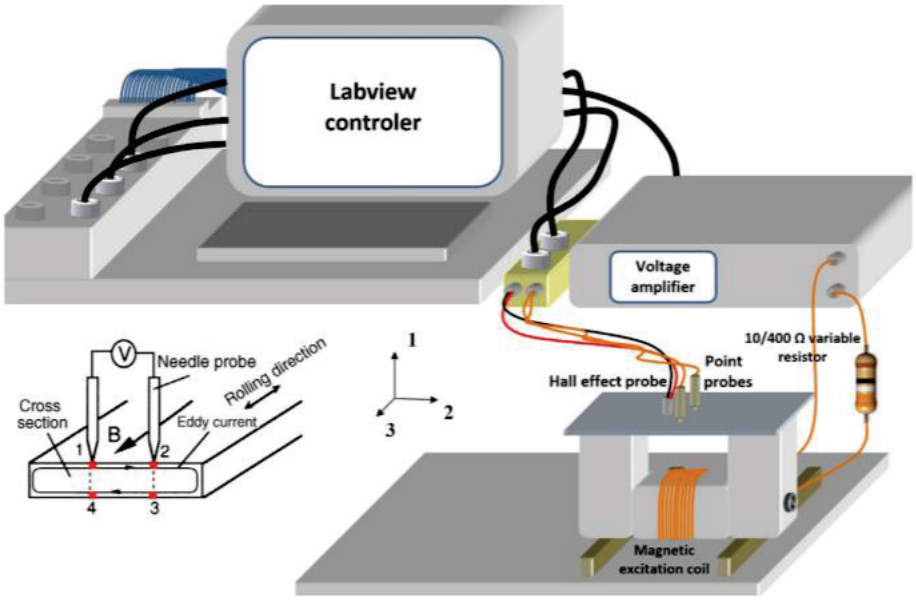

Figure 1-17 : Magnetic needle probe experimental lay out[54]

The measurements of localized flux density by the MNP upon signal processing makes it possible to establish an accurate and distinctive map of the treated part surface and subsurface integrity, be that for the outer (top) and inner (bottom) surfaces of the test material, as oppose to the overall average measurements by the encircling coil.

1.4 Summary

Every known material independent of its type, shape and composition has a unique magnetic signature in response to its physical properties. The onset and gradual propagation of anomalies in materials is a call for concern. A solution to this is to come up with localized magnetic measurement techniques. Herein, the adequacy of the magnetic measurement technique to faithfully evaluate the magnetizability within a circumscribed region of the material is requested. The utmost interest being to locally measure and compute/derive the magnetic signature of a magnetized material to its best possible accuracy. Hence, the quest of ***local magnetic characterisation*** of materials. As a matter of fact, magnetic hysteresis clearly exposes ferromagnetic materials' vulnerability on major defects causes such as mechanical stress and temperature. It is evaluated as function of the main magnetic properties like: permeability, coercivity and remanence, and hysteresis loss. Hence, a coupled "magnetic hysteresis – local non-invasive magnetic technique" could be an adequate alternative solution for micro-magnetic NDT characterisation and control of magnetic materials. Compared to the search coil technique long reported for its damaging effects and systematic measurement errors due to drilled holes

in the material [63], the MNP method equipped with a Hall effect probe forms a reliable NDT local magnetic sensor pair for in-depth investigation of the magnetic properties within a circumscribed region of a steel sheet. These are the plausible reasons why guide towards miniaturizing the MNP method to printed magnetic needle probe(PMNP)

CHAPTER 2:

PRINTED MAGNETIC NEEDLE PROBE

So far, NDT methods classified as micro-magnetic amongst which ECT, MIP and MBN are the commonly used. Their individual features already established some limitations in measurement. Combining them, gives more measurement span for diagnostics. In spite the combination strategy, there still exist some limitations in their measuring abilities. The sensor as shown in figure 1-12 are relatively bulky and bulky, and is clearly not intended to remain permanently on the elements to be inspected, or even on board moving systems. They are all affected by the influence of sensor design and orientation for directional stress sensitivity. On this ground, the Printed Magnetic needle probe sensor is developed and examined towards overcoming the afore-mentioned barriers. PMNP takes it blueprint from the MNP principle and is aimed at achieving the following characteristics: reliable test, reproductive measuring abilities, localisation of any defaults and non-invasive size. To evaluate its abilities and prove the concept, major steps are taken: the development of its theory according to physics, the design and characteristics tests.

2.1 Concept of Magnetic Needle Probe

MNP is based on exploiting the electromagnetic interaction within a section of a specimen when supplied a magnetic field. In effect, the magnetic flux density passing through the closed section considered directly describes the state of this section which result from the magnetic reaction at this point. This region is circumscribed by the point of contacts between the edges of the needles and the underneath cross-sectional area of the material under test as illustrated in figure 2.1. According to faraday's law, we observe a potential difference in between the two needles which is generated due to a variation of the flux density flowing within the material. An electrical set up is wired to the needles to permit the measurement of the resulting voltage quantity for processing and analysis. Werner is considered the father of this concept[64]. Stauffer Et al brought to light a sensor based on this principle in 1958[65]. The sensor as shown in figure 2.2 was made up of a chattock coil which played the role of magnetic potentiometer

and a pair of stylus probe which are all mounted on a single sheet lamination. Thereby a possible measurement of local flux density on an area coverage of 25.4 x 50.8 mm^2.Given that the values of voltage measured are in the order of mV, this method didn't captivate the interest of researchers. It is only 38 years later, with the advent of technological and instrumentation boom which made it possible to access and measure such small quantities. A team of researchers Yamaguchi[66], Senda[62], Ishida Et al thereby focalized on evaluating the accuracy, the span and theoretical analysis of the MNP sensing method. The outcome of these three analysis layed down the basic measurement protocol for an efficient use of the MNP technique.

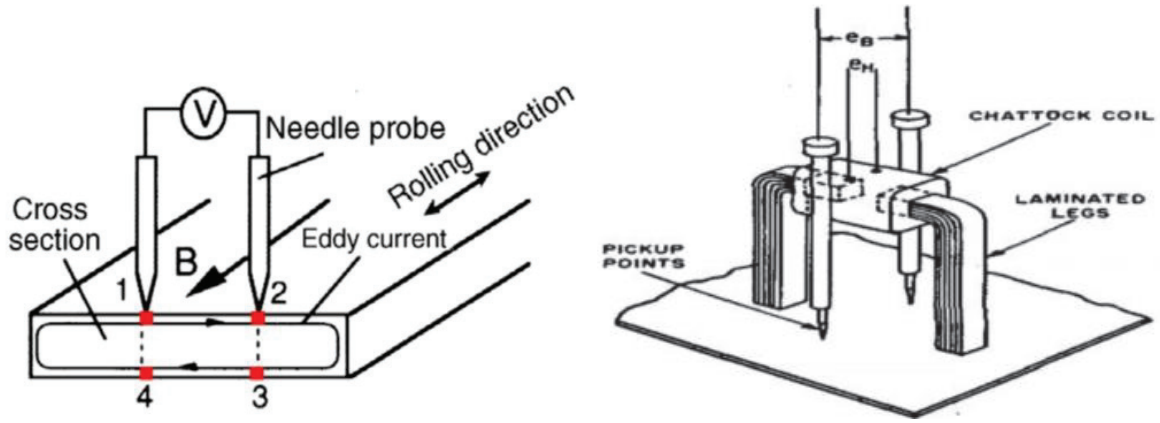

Figure 2-1: Magnetic needle probe concept[54],[67]

2.1.1 Principle of magnetic needle probe

The magnetic needle probe method consists of placing two needle probes perpendicularly to the surface of the specimen under study. The probes help measure the potential difference between the two points of contact with the sample. The measured voltage is simply the rate of change of the flux density within the sample. Figure 2-2 shows the cross sectional area span(S) encompassed by the needle probe.

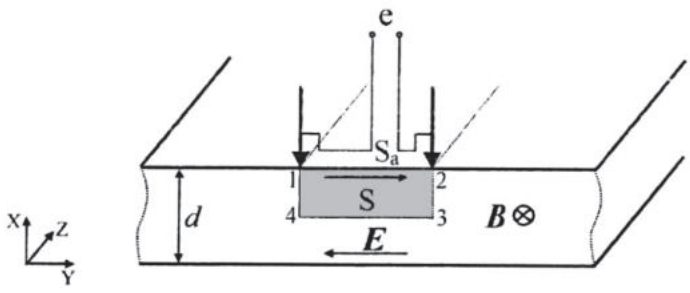

Figure 2-2: Principle of the two-needle-probe technique.[68]

This voltage expression is in compliance with Faraday-Maxwell's equation developed as followed:

$$\oint_C \mathrm{E.\,dl} = -\int_S \left(\frac{\partial \mathrm{B}}{\partial \mathrm{t}}\right) \mathrm{dS} = -\frac{\partial \phi}{\partial \mathrm{t}} \qquad 2\text{-}1)$$

$$\mathrm{V_{12}} + \mathrm{V_{23}} + \mathrm{V_{34}} + \mathrm{V_{41}} = -\int_S \left(\frac{\partial \mathrm{B}}{\partial \mathrm{t}}\right) \mathrm{dS} \qquad 2\text{-}2)$$

Assuming we have a symmetrical distribution of magnetic field flux with respect to horizontal axis passing through the centre of the material and parallel to the surface plane of the material; it implies V_{12}=V_{34} and V_{23}=V_{41}, hence:

$$\mathrm{V_{12}}+\mathrm{V_{41}} = -\frac{1}{2}\int_S \left(\frac{\partial B}{\partial t}\right) dS \leftrightarrow \mathrm{V_{12}} = -\frac{1}{2}\int_S \left(\frac{\partial B}{\partial t}\right) dS - \mathrm{V_{41}} \qquad 2\text{-}3)$$

V_{41} represents the induce voltage from the vertical components of the electric field. Given that, the spacing between the needles is supposed to be large enough compared to the sample thickness[69], the sample thickness can thereby be neglected [70]. This then implies having V_{41}=0.

Therefore, $$\boldsymbol{e = V_{12} = -\frac{1}{2}\int_S \left(\frac{\partial B}{\partial t}\right) dS} \qquad \textbf{2-4)}$$

Through analysis done by some researchers, the MNP technique shows slightly less accurate when compared to search coil. It results from errors due to non-uniformities of flux distribution, air flux induced voltage and influence of vertical electric field component which is assumed negligible in theory in the measurement[66], [71]. Also, the MNP method may yield systematic errors if the test sample shows asymmetry of in-plane eddy currents with respect to the central sample plane[72] .

2.1.2 Recommendations for optimal measurement

Basically, for an optimal and more accurate measurement of induced flux within the sample using MNP, and for the assumptions made above to be valid. there are some precautions recommended by some researchers when carrying out experimental test using MNP. Amongst which we have:

- ✓ -a 10mm spacing between the probes should be respected for an effective insight of the magnetic flux density in the specified region enclosed by the probe for a grain-oriented electrical steel sheet[66].
- ✓ -The probes spacing to specimen thickness ratio (1-2/d) must be significant[69]
- ✓ the admissible load on a needle probe tip is 300g. this is in order to minimize measuring error in the localized flux density of less than 1.7% when the yoke structure was symmetrical with respect to the sheet plane[71].
- ✓ The distance from the edges is also recommended to be higher than half of the specimen thickness (d/2) [74]. This is so as to avoid edge regions of electrical steel sheets where eddy current distribution is altered as shown in figure 2-3 [73]. It is caused by the intrusion of cutting stresses and strains.
- ✓ The leakage flux in the enclosed near-surface magnetized air must be negligible[71].

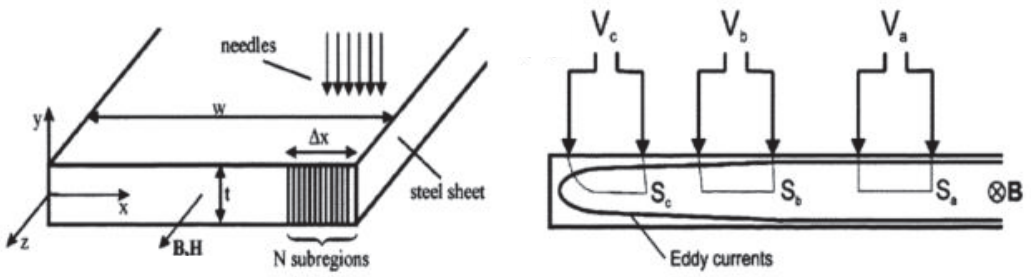

Figure 2-3 : (a) Needle probe method; (b) Eddy-current distribution in a sample surface and edges[74]

Over the years, the MNP method was subjected to amelioration, modernization, optimization and miniaturisation.

2.1.3 Modified versions of MNP

Taking into account the afore mentioned limitations, some modified/improved versions of MNP were proposed so as to attenuate or cancel the impact of the sources of error. We thereby identified the followings:

- ✓ the needles used in MNP were made up of brass and each mounted on a polystyrene rod as illustrated in figure 2-4. This design attempts the elimination of intrusive signals[75]. On placing the needles near search coil for comparative measurement, Wilkins Et al achieved a good agreement for all measurements

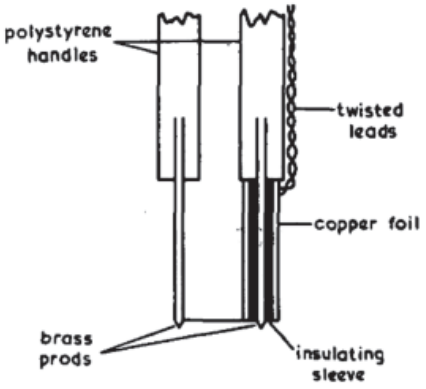

Figure 2-4: Construction of needle probes[75]

- ✓ In the quest of cancelling the error inquired from vertical component of the electric field and possibly that of the air flux induced voltage, Loisos and Moses proposed a dual MNP design [76]. As portrayed by figure 2-5, two pairs of classic MNP are placed at symmetrical locations on the top and bottom faces of a 0.5 mm thick laminated steel sheet. They achieved an error due to air flux to be less than ±0.0002% of the measured voltage. Inspite the remedy obtained by using the dual MNP setting, it is limited in application; it can only be used when there is access to the edge of sample in order to make the necessary wiring connections.

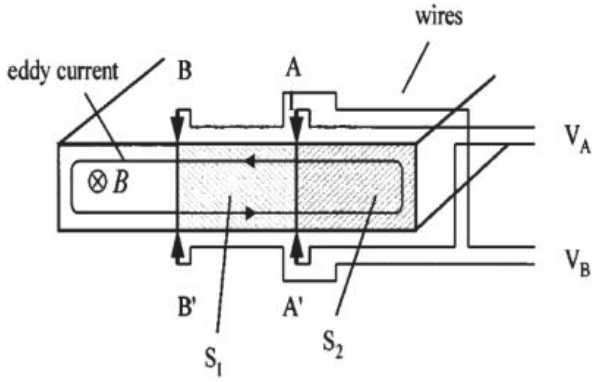

Figure 2-5 : Dual needle probe schematic[76]

- ✓ In an attempt to reconstruct the magnetic characteristics of materials with non-uniform magnetic field, Abdallh and Dupré [77] successfully developed a modified MNP method. The latter based on an anti-series connection of a set of two classic MNP sensors as illustrated in figure 2-6. The extra two needles compensate the air flux; thus the error introduced by the non-homogeneous air fields is cancelled. The proposed method does not however address the issue of vertical electric field in the measured voltage.

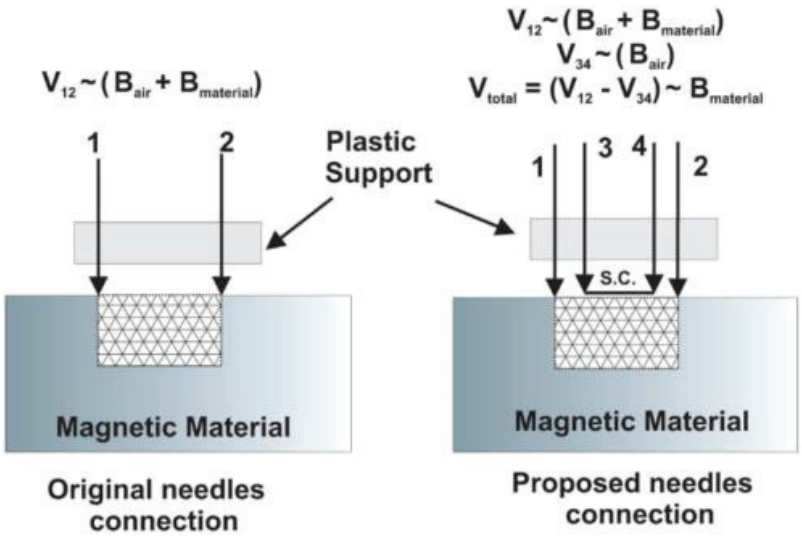

Figure 2-6 :The probes positioning and connection in the proposed modified MNP[77].

- ✓ Factors like coating removing and micro-damages on the surface of the materials due to sharp tips of needles prohibit the usage of NPT in measurement of *B* for some soft magnetic materials. In the same line, for good electrical contact, a force is usually applied on the needle by means of springs attached to the needles; when pressed against the sample the constant contribute to micro-damages. In order to limit cancel micro-damages caused by the used of classic MNP, A novel capacitive sensor was then suggested in [78] .It is a needle probe derive sensor in which the needle electrodes are substituted by capacitors of infinitesimally negligible capacitance as shown in figure 2-7. The conducting pads together with the laminated material form the capacitor plates separated by the insulation coating of the lamination, forming the dielectric material. However, a noticeable challenge in using this design is that the resultant reactance of the sensor (*XCs = 8.35 MO*) required a measurement device of much higher impedance for accuracy. Moreover, reactance is highly dependent of frequency; this leads measurement inaccuracy at high frequencies as this significantly decreases the impedance of the sensor

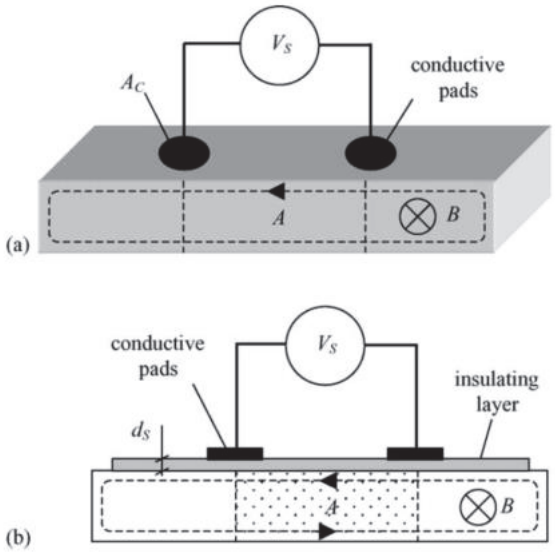

Figure 2-7 : The concept of capacitive coupling(a) top view, (b) cross-section view; A_C: area of the pad, d_S: thickness of insulating layer, V: measured voltage between pads[78]

- ✓ The capacitive MNP gave way to a miniature size of MNP which makes it a good candidate but an embedded measuring system. The capacitive nature of the probe is unfortunately the main throwback. As a remedy to this, Mazurek proposed thin films needle probe designs when studying the effects of burrs on a three phase transformer core as depicted in figure 2-8. He produced sensors of 4 mm thick aluminium plate, with an improvement of the 2 mm aluminium sheet still to be studied[79]. Such a printed MNP sensor drastically reduces the error due to the air flux.

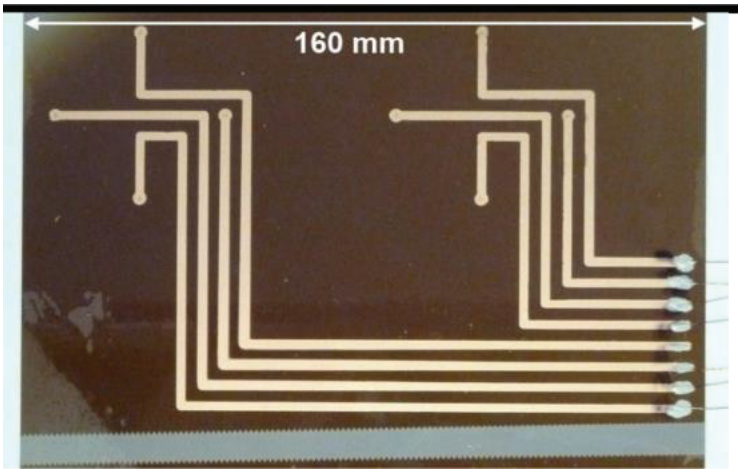

Figure 2-8 : Two sets of two dimensional flux density needle probe sensors.

The thin films needed probe presents more advantages than any other NDT sensor when it comes to acces local measurements in very tiny area in a non-invasive manner. This falls in

same line of our objectives, it will thereby constitute the springboard for our design aimed at reducing the thickness to the range of micrometers;

2.2 Printed Magnetic Needle Probe(PMNP) Technique

Classic magnetic needle commonly used in NDT made up of 2.5mm spring-loaded probes are incompatible for the purpose of in-line/ in-service monitoring of industrial processes. Mechanical parts can only be diagnosed when the production line is at halt, or the device stopped from running. The idea is to help enhance the applicability span of MNP method by reducing the needles to a printed conductive ink track. The relative small size of the sensor is appropriate for steady embedded system which will continuously relay information with no necessary interruption.

2.2.1 Principle of printed needle probe using printed electronics

The concept of PMNP is to draw conductive patterns on a substrate in such a way that, when in electrical contact with the material, it will be an equivalent to MNP testing. The features of Printed electronics(PE) which will be exploited in printing using a conductive ink. The most solicited ink is silver in which is highly used in printing circuit boards(PCB), RFIDs, etc[80]. So doing all the components constituting the MNP sensor (wires, spring and needles) will reduced a graphic print of ultra-thin thickness as sketched in figure 2-9. The flexibility, ultra-light weight, high ergonomic, robustness and low-cost nature of products derived from PE give an added value to PMNP.

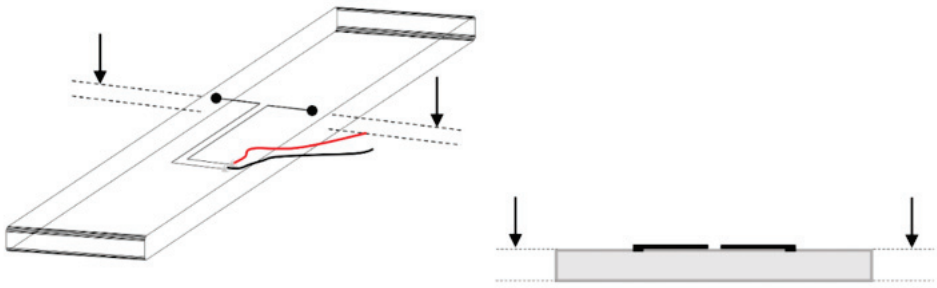

Figure 2-9: Sketch of PMNP concept

The figure above shows a rough illustration of the printed needle probes method. On the left hand side of this image one can observe the electric circuit design. The printed results of the two needles used in MNP are two black spots which ensure electric contact with the magnetic lamination. It is worth noticing that the flux leakage error voltage due to the loop formed by the surface of the specimen and the printed part connecting the needle probes to the measuring instrument, is extremely limited by this design. The right hand side of this image is a sensor/lamination cross section illustration. As a matter of electrical connection, the dielectric coating has been removed locally to allow the electric contact between the lamination and the conductive ink electric circuit. Two printing paradigm were employed to achieve an optimized version of PMNP; namely, manual printing and computer aided design (CAD) printing method

2.2.2 Printing using mask

Referring to the oldest technique of PCB printing, a mask is built from a self-adhesive stickers paper which is shaped to suit the desired the pattern we have chosen. The pattern was designed using Graphtec studio software which was directly loaded to the cutting plotter CE 6000-40 all developed and manufacture by Graphtec Corporation as shown if figure 2-10. The dimensions of the pattern were chosen so as to respect the recommendation for an optimal use of MNP and to fit the dimension of the substrate; that is, a 10mm spacing between the points of contact and path width of 1mm. Following a set of steps a PMNP is produced as illustrated in figure2-11.

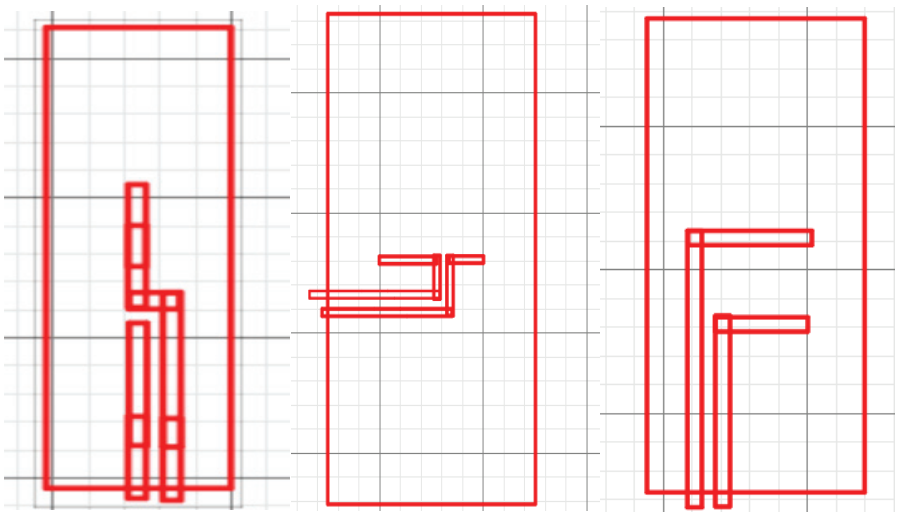

(a) (b) (c)

Figure 2-10: Various PMNP patterns tested

- ✓ the first step consists of preparing the specimen (STEP 1). That is the point of contact are spotted out while respecting MNP recommendation using a marker. The insulating

coating is delicately scrapped off so as avoid micro-damages on the substrate. The entire surface cleaned using ethanol to clear up any dirt or any residues which may be found on the surface of the substrate. An additional thin coat of cosmetic cortex is done on the part of the sample where the sensor will be printed. This is to be rest assured that they will be no electrical conductivity along the route of the sensor.

- ✓ The second step is all about adhering the mask on the steel sheet. This step needs to be with much care and attention. Any shakes of fingers may result to gumming the patch wrongly. The mask is to be positioned at the centre of sample and the scrapped contact should be in same line of sight with the edges of the routes as carved on the mask.
- ✓ As for step 3, the silver ink is coated on the surface of the sample using a soft fibre brush following the pattern on the mask. Excess paint dripping from the brush to the sides of the path will be trapped on the mask. The sensor is then set to dry on the steel sheet. it takes 10min to 30 min to completely dry up depending on the thickness and viscosity of conductive silver ink at room temperature.
- ✓ Once dried the mask is peal off gently leaving out just the routes of the sensor. Resistance check is carried out to make sure there is no discontinuity.
- ✓ Lastly, Copper patches are fixed at the terminals of the sensor and shielded wires soldered to the copper patches. The two cables are twisted on themselves limiting disturbances and unwanted signals to alter the signal measured.

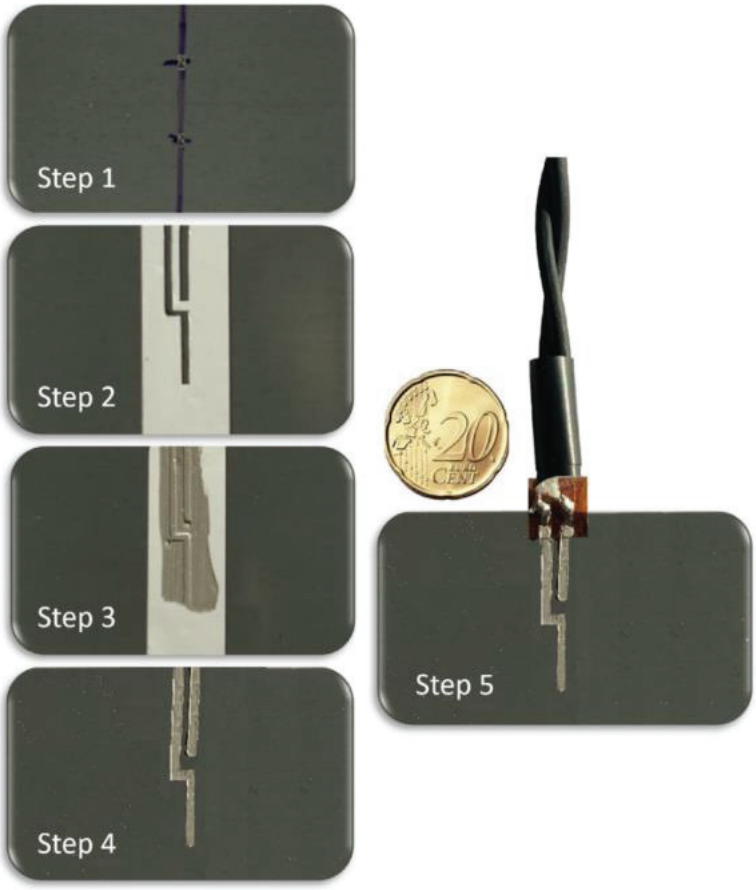

Figure 2-11: PMNPM printing process using masks.[81]

Passing the sensor in the Keyence LJ-V7000 profilometer, revealed a path thickness ranged from 24µm to 28µm. A less thick and smooth path profile was gotten using a more sophisticated method.

2.2.3 Printing using an inkjet printing machine

The inkjet machine used is a microplotter instrument developed by Sonoplot company which is equipped with an automatic fluid dispenser as shown in figure 2-12 . The various nozzles of the dispenser were of 30µm and 60µm opening. It is capable of printing following the X and Y directions. Pulses are send at a chosen frequency to a piezoelectric material attached to the dispenser. The vibration then expels silver fluid filled in the dispenser. Four interdependent parameters ought to be considered when printing: the viscosity of the fluid, the frequency of vibration, the voltage of pulses and the displacement speed of the mobile membrane holding the dispenser. These parameters will govern the smoothness and the thickness of the resulting routes. The sensor pattern is designed in Sonodraw software interface, appropriate settings done concerning the afore mentioned parameters and all saved.

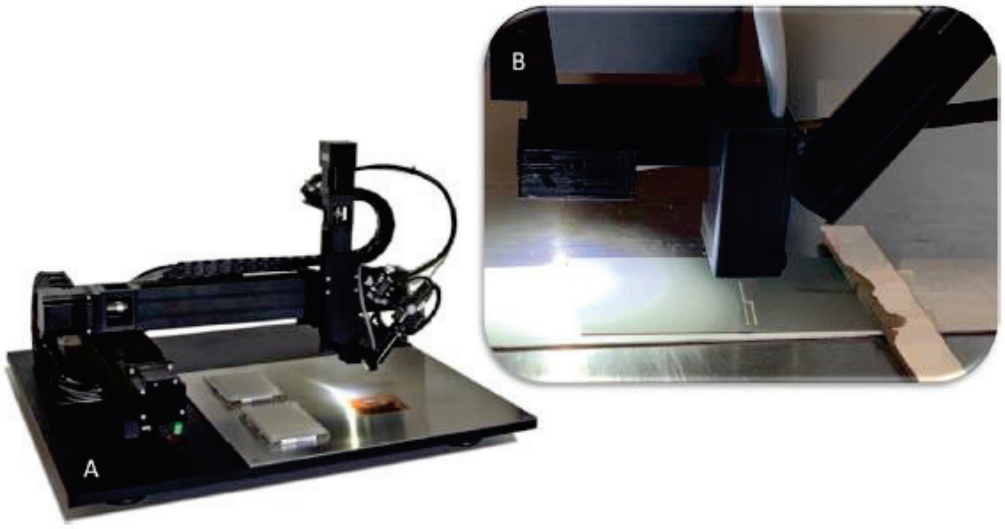

Figure 2-12: A-sonoplot printer; B- sensor printing process

The printing process begins by cleaning the dispenser. Thereafter the dispenser is dipped in the fluid bowl and loading will be done. Still depending on the viscosity of the fluid, the dispenser may be half full or one quarter full. Immediately the dispenser filling time is elapsed, the membrane goes directly to the position where it supposed to start printing so as to avoid the fluid to dry up and block the nozzle of the dispenser. The dispenser is supposed to fixed a little bit above the substrate to avoid the breaking of the dispenser made up of glass and not too far above if not the fluid will be sprayed out in a scattered manner. The time needed for such printing is 15mins and the sensor is placed to dry. Given the high viscosity of the silver ink we used, the 60µm dispenser was appropriate.

Passing the sensor in the Keyence LJ-V7000 profilometer, revealed a path thickness ranging from 20µm to 25µm.

The three patterns were tested, but pattern number a. needed less ink (shorter routes), the aperture between the patterns were narrower all along the pattern compared to the 2 pattern design. Thus making the possible effect of air flux negligible.

2.3 Validation of the PMNP

The idea of non-invasive MNP has been concretized. Given it is new version of MNP, its characterization and comparison with already existing ECT methods are of paramount importance. The outcome of the comparison will either confirm or infirm our claims. Furthermore, there is a necessity to reconstruct a set-up that mimics a laminated magnetic core

and imbed the sensor in the core so as to appreciate its behaviour, accuracy in local flux measurement and constraints it could be subjected to. These tests constitute preliminary checks before indulging in real-time monitoring case study.

2.3.1 Experimental Set-up

Preliminary investigations were carried out on a commonly used ferromagnetic material. The Grain Oriented(GO) laminated silicon steel was chosen for its historical application in transformers and inductors magnetic core. It falls under soft magnetic materials and is an iron alloy made up of 3%silicon content. With reference to its magnetic properties as listed in table 2-1; it is characterized by a low losses and high permeability as a result of the Thermal treatment(cold-process) it underwent. The grain orientation (GO) gives the material the capacity of been magnetized easily following the orientation of the grains, this direction is termed as rolling direction(RD) and its counterpart is termed as transverse direction (TD).

Table 2-1 : Magnetic parameters of GO FeSi

	composition	**Max. Relative permeability**	**Coercive field H_c(A/m)**	**Saturation polarization J_s(T)**	**Curie Temperature T_C (°C)**	**Saturation magnetostriction $\lambda_s=(\triangle I/I)_{J_S}$**
GO FeSi	$Fe_{97}Si_3$	15 – 80x10^3	4 -15	2.02	750	1- 3 x10^{-6}

where μr_{max}, Hc, Js, Tc, and λ_s are the relative permeability, coercivity, saturation polarization, the Curie temperature, and the magnetostriction coefficient, respectively. Here, l is the initial length and Δl is the length variation at saturation

The experimental components will be set up according to the prescriptions of single sheet tester standard as mention in the [IEC60404-3] [82] with some little modifications :

_ the use of a single yoke,

_ the yoke dimensions,

_ the primary winding is wound around the yoke instead of the tested specimens,

_ a stack of ten laminations replaces the single sheet of electrical steel for the stack tests.

The local measurements are assured by the PMNP sensor and a noise shielded radiometric Hall effect (SS94A from Honeywell) sensor which measure the magnetic field density and magnetic field strength respectively. They were placed on top, at the mid-way length and width of the

sample. This is so as to avoid the error caused by the magnetic field distortion near to the ends of the magnetizing winding [83]. Data of the surface magnetic field will be read at the terminals of the hall sensor. The wiring of different devices constituting the experimental bench is pictured out in figure 2-13. The source magnetic field used for exciting the magnetic circuit. This source is made up of a U-shaped yoke of cross sectional area 37x36mm^2 on which is wounded 500 turns of cupper coil. The magnetic yoke serving as a canal of distribution of magnetic field is made up Fe-Si GO laminations stacked and compressed together. The sample under test is placed on the U-shape yoke; thus closing the magnetic circuit. The dimension of the laminated steel sheet is 270mmx30mmx0.35 mm.

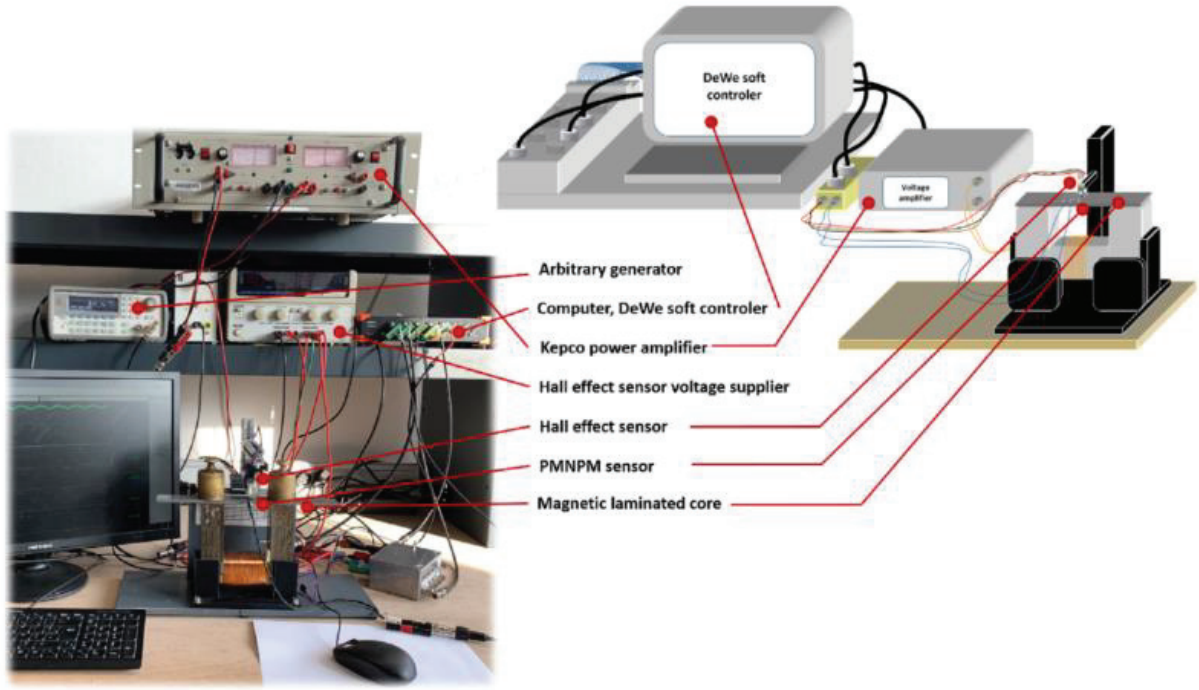

Figure 2-13:3D Stacked design and photo of the experimental setup.

The electrical supply of the excitation coil is assured by a power amplifier Kepco BOP 100-4 M whose input signal is provided by a frequency generator (Agilent 32220A). the power amplifier is set at imposed current configuration. Once the system is excited, the measured signals emanating from sensors acquired using a sophisticated data acquisition system. It is made up SIRIUSif 8 × CAN data acquisition interface operated upon using its software named DEWESoftX2 data acquisition software[84]. The data once collected are Post-processed using Matlab^{TM} software. Numerical differentiation and integration are done the data to recover the magnetic field induction flowing instantaneously in the sample at the local position. Drift error inquired during the mathematical operation is thereafter removed. The B_H curve can now be plotted. To make sure that we respect the criteria of reproducibility of our new sensor, the magnetic specimen is completely demagnetized in between a series of three tests under same

experimental conditions. That, is a 50 Hz triangular voltage signal which exponentially decreases are used to excite the coil to help the sample get rid of its remanent field. This can last for 2min. With all the apparatus set and wired, various experimental tests can now be carried out. Given that our primary objective in this study is to check on the feasibility of the new sensor, measurements are done at room temperature.

2.3.2 Instrumented sheet Testing

The main background idea here is to sort randomly an isolated magnetic lamination from a set steel sheet to be used in magnetic cores. The sorted sheet is instrumented with 4 different types of sensors; namely: a 10-turns surrounding coil, a centralized search coil, the classic MNP and the PMNP sensors as illustrated in figure 2-14. The search sensor being more invasive than the others was set few millimetres away from the sensors' set to limit induced residual stress effect due to the drilling of holes in the controlled sample. the local B-field responses as seen by the PMNP will be confronted to those obtained by three other sensors. The instrumented sheet is place on the yoke with two weight spacers of 0.5 Kg positioned on top of the sample at the two edge of the yoke as shown on figure 2-15. Thus limiting air gaps effect and ensuring reproductibility.

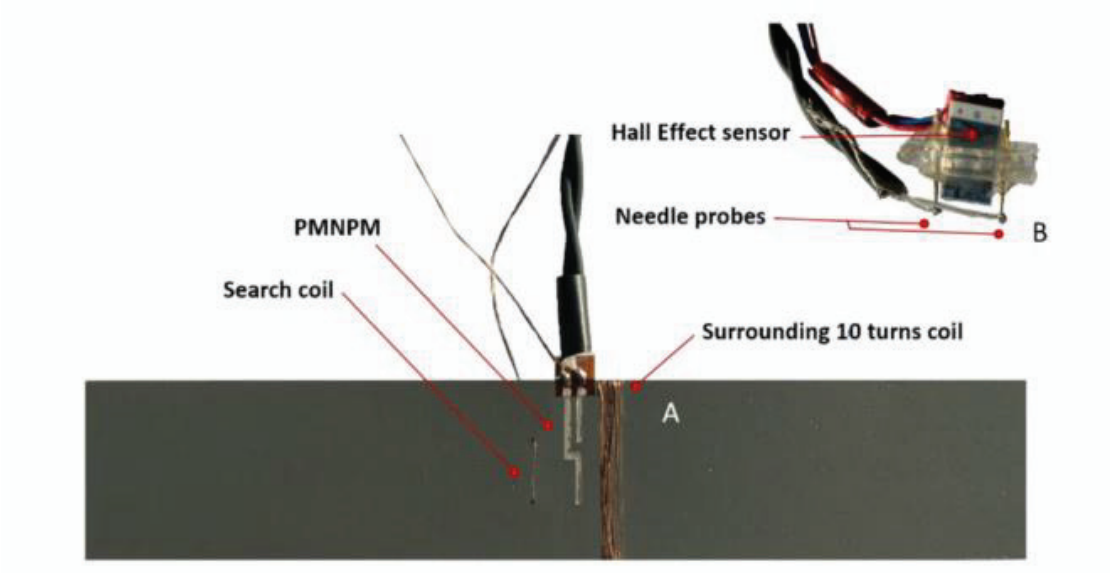

Figure 2-14 :A) Instrumented FE-Si sheet with sensors; B) classic needle probe sensor [81]

2.3.3 Laminated magnetic core testing

Our new sensor is claimed at been able to relay information on magnetic field density once embedded in laminated core of an electrical machine. At experimental laboratory level, a set of

16 magnetic laminations of each type (RD and TD) were used to reproduce a stack of insulated laminated sheets constituting a magnetic core. This experiment will go a long way to further validate the PMNP method as a homogenization method. The experimental protocol consists of moving the instrumented sheet with PMNP sensor across the entire stack. The lamination 1 is positioned directly in contact with the yoke of the single sheet tester, the lamination 16 is set at the opposite position of the magnetic core. The sheet is moved from the bottom position(first) to the top position(16^{th}) by occupying successively all intermediate positons within the stack. All the 16 laminations are placed on the single sheet tester yoke as shown in figure 2-15. The final step of the protocol is to wound a 10 turns coil around the packet of 16sheets. Data collected from the surrounding coil will be compared to the sum of induction as seen at all the position by PMNP. Top and Bottom surface magnetic field intensity are measured by two hall effect sensor; one place at the bottom and the other on the top of packet of sheets.

The use of H-sensor does not guarantee a simultaneously local measurements of magnetic field intensity at the same location where magnetic field density is measured. This is a result of the bulky geometric nature the hall sensor measuring 2.5cm height. Thus a quest for a miniature sensor able to be embedded in a laminated core and placed at the same point as PMNP sensor.

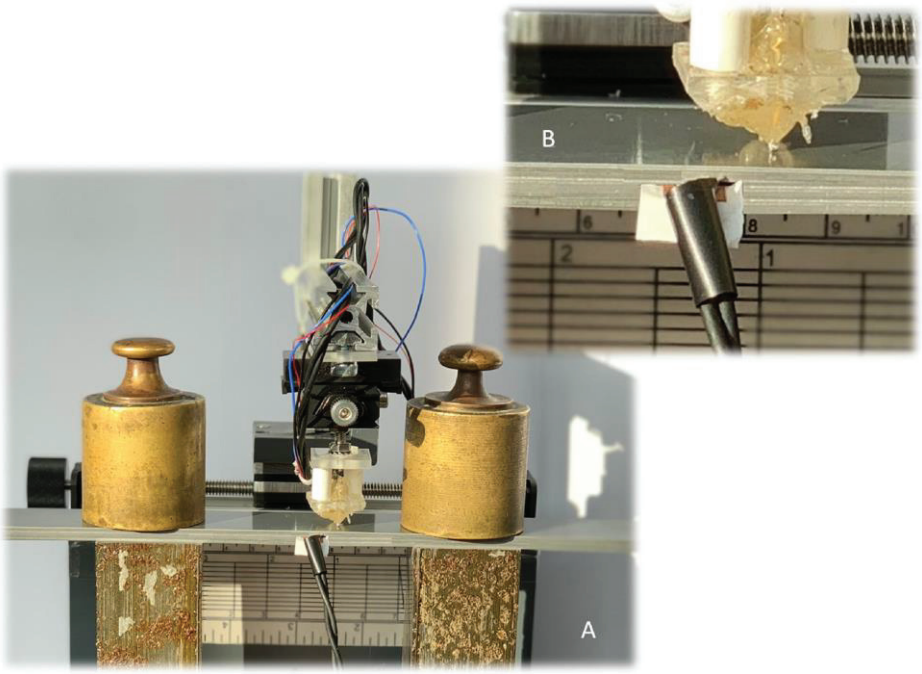

Figure 2-15:A)Laminated magnetic core including PMNPM sensor. ;B) Zoomed view over the sensor area.[81]

2.4 Miniaturisation of B_H acquisition system coupled to magnetoresistance

Miniaturised B_H measurement system is all about having a micro size sensors capable of accessing local magnetic field induction and intensity at a particular position.

2.4.1 Concept

Krismanic et all through their research had already prove this concept by building a hand-held sensor [20]. They combined the H_coils to needle probe at obtained a sensor with an overall thickness of 2.7mm. This was already astonishing for a start because it could enable deployment of non-invasive magnetic state sensor all through a laminated magnetic core. Thus guaranteeing the possibility of following up the material aging, detecting hot spots[18,19] and any anomalies in the magnetic behaviours. The hand-held sensor as proposed by krismanic Et al is faced with a problematic when embedding in a stack of laminations; that a wide air gaps will be created in-between lamination due to its thickness. This concept needs to be improved by achieving a combination of micro-thickness sensors for measuring B and H. The PMNP sensor is already available for measuring magnetic field induction. Concerning H- micro sensor, we going in for a Giant magneto- resistance (GMR) sensor which has the capacity of detecting few nanoteslas on a large frequency band[85], [86]. From the latest development in GMR sensor, one could acquire a GMR sensor of 270 µm thickness. The idea in this study, is to place the silicon substrate carrying the GMR next to PMNP contact points. Nevertheless for a more optimal measurement, there is a possibility of polishing the silicon substrate and obtain a thickness of approximately 10µm[87], [88] . Polishing will help reduce the incident air gap created by inserting the sensor within a stack of laminations. However proper attention and care need to done when manipulating this very thin sensor.

2.4.2 Magnetoresistances

2.4.2.1 Generalities

Magneto-resistivity is the capacity of a material to change its resistance in presence of a magnetic field. This attribute of magneto-resistive materials, their high sensitivity and accuracy makes them good candidates to be used as magnetic field transducers. Specific materials classified as anisotropic magneto-resistances(AMR) have a high magneto-resistivity which can

be used to monitor changes in magnetic field. The selection of the material is guided by its rate of change of their resistance(MR) of these specific materials is evaluated using the equation. It is evaluated as follows:

$$MR(\%)=\frac{R_{max}-R_{min}}{R_{min}} \qquad 2\text{-}5)$$

The AMR's magneto-resistive percentage is found around 1%-2%. Piling thin layers of these materials has been proved to enhance their magneto-resistivity; thus increasing their sensitivity. We thereby identify Giant magnetoresistance(GMR) and tunnel magnetoresistance(TMR) with a percentage of magneto-resistivity found to be 20%-60% and 60%-600% respectively[89]. Due to the less complex fabrication of GMR, we will focalize on GMR in this study for the monitoring of the local tangent magnetic excitation H(t) .

As far as GMR are concerned, as shown in figure 2-16 there exist two type of configuration which differ with the number of layers and their properties:

- ✓ a series of multiple thin layers ferromagnetic material. They are piled one on another with a non-magnetic material separating two successive ferromagnetic layer.
- ✓ "**Spin valved"** GMR: Two layers of ferromagnetic material separated by a conductive material. One is layer termed the "hard layer" is set in a fixed spin direction. The other layer "soft layer" is left free to follow the direction of the external source.

When the spin moment of the various layer constituting the GMR are aligned in the direction of the external source, the overall resistance is minimal[85], [86].

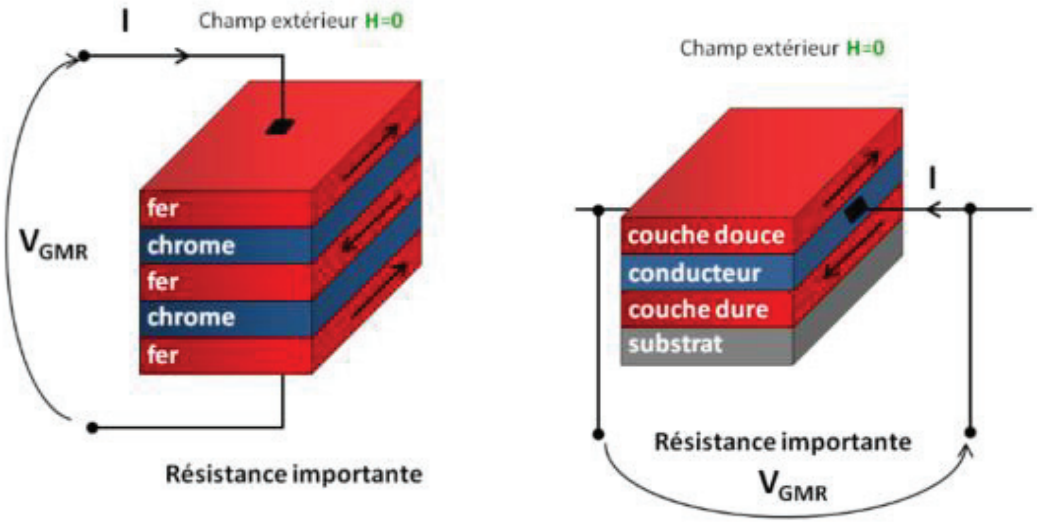

Figure 2-16 :Multilayer GMR, « Spin-valved » GMR[41]

2.4.2.2 GMR Design

In our design, we opted for the two-layer configuration given that, our aim is to achieve the thinnest GMR possible. The hard layer is set fixed in the direction of sensitivity . 90° away from the reference layer, the soft layer is positioned with a weak shape anisotropy. This is so to reduce some unwanted magnetic noise and assure a linear relationship between the GMR's resistance and the magnetic field excitation. As the free layer rotates, the resistance is directly proportional to the angle between the spin direction of the two layer as shown on figure 2-17. The blue arrow is reference layer's spin direction and the dark arrow that of the soft layer.

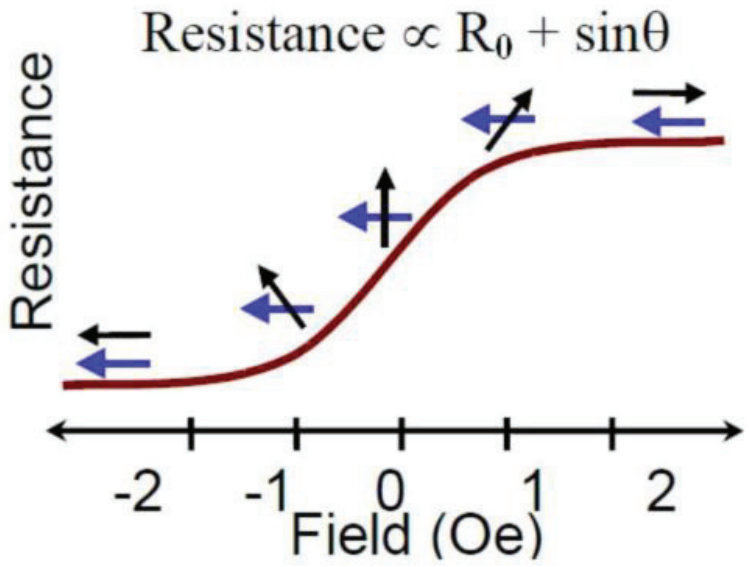

Figure 2-17:Variation of GMR resistance according to the direction of external magnetic field[89]

The structure is made up of :$Si/SiO_2(500)//Ta(3)/Co_{90}Fe_{10}(2.1)/Ni_{80}Fe_{20}(2.1)/Cu(2.9)/Co_{90}Fe_{10}(2)/Ru(0.85)/Co_{90}Fe_{10}(2)/Ir_{22}Mn_{78}(7.5)/Ru(0.4)/Ta(5)$(thicknesses in nanometres). Sputtering (Rotaris-Singulus) technics were used to deposit the GMR on an oxidizes silicon wafer. Standard lithography technics were employed to build up the GMRs coupled to the metallic path connecting them to points of metallic contacts. To ease the electrical interface of the GMR and signal treatment devices, the connection pads were made larger. As shown on figure 2-18, the GMR(blue rectangles) are placed horizontally, implying its direction of sensitivity is 90° away in the same plane. The red-hashed triangles illustrating the metallic contact sputtered of the substrate.

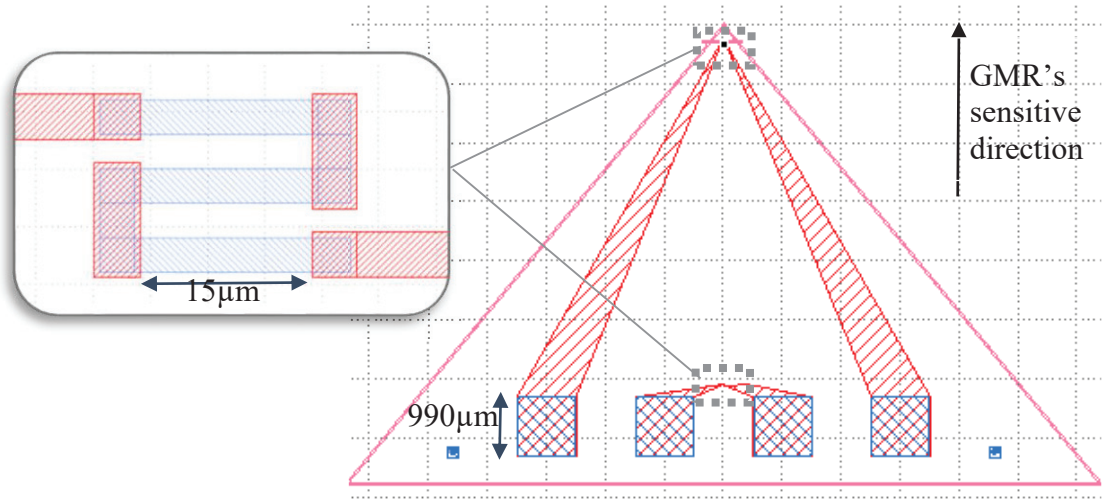

Figure 2-18: Sensor design and shape[90]

Once proper treatment done on the sensor, its response towards external applied field is appreciated. A Helmholtz coil of capacity ± 12000 A/m was used to create a magnetic field. The sensor was placed at the middle point of the coil and supplied with a DC current of 0.49mA. The resultant potential difference at the two terminals of the sensor was collected using 2 probes. Aa equilibrated resistor bridge used to interface the signal to the data acquisition device. The graph of figure 2-19 shows how the resistance of the sensor changes when placed in a magnetic field propagated flowing its direction of sensitivity. We can thereby understand the mobility of the free layer at different stages from the graph on figure 2-17. The noised spectral density and the threshold of detection were derived to be 0.7% and 50nT at 50Hz respectively[91]. With this good features, we could then proceed with no doubt to couple it to our PMNP sensor.

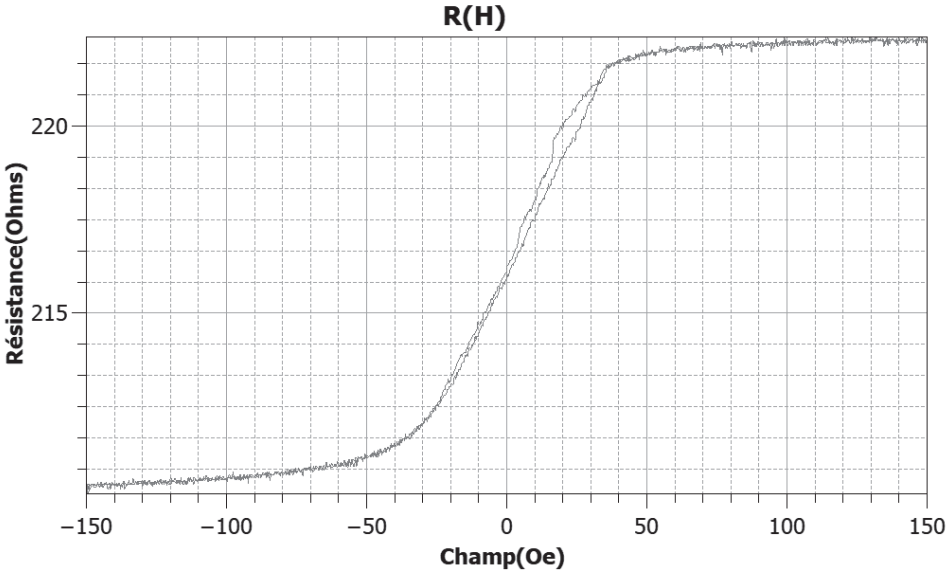

Figure 2-19: Basic reference characteristic curve R(H)

2.4.3 Experimental set-up

The experimental set-up is observed for two different regimes. The first is a sole evaluation of an instrumented sheet. The second, test in a laminated core scenario whereby, the instrumented sheet in placed within a stack of 10 steel sheets. However, the experimental set-up is the same for all the two tests as shown on figure 2-20. The devices remained unchanged as described in section 2.3.1. the samples were of same dimension and the demagnetization protocol (see section 2.3.1) respected.

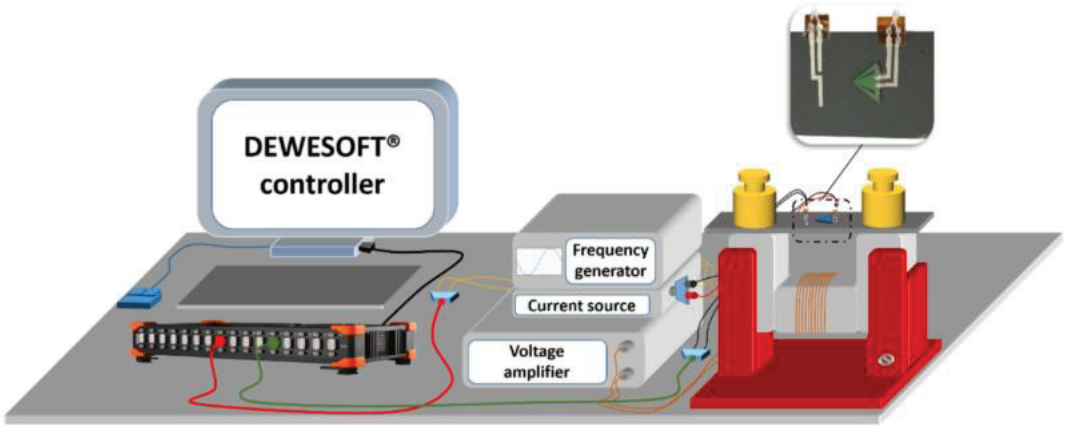

Figure 2-20: 3D view of the entire set-up[90]

2.4.3.1 Instrumented sheet Testing

A single GO steel sheet is instrumented with a PMNP and a GMR. The PMNP is printed following the mask printing protocol as described in section 2.2.2. The GMR is positioned just near the PMNP with some preliminary condition done. To avoid any unforeseen, short-circuit, a thin layer of an insulating gel (transparent nail cortex) was napped on the Si wafer side and borders of the GMR substrate while protecting the metallic pads. GMR is placed in such a way that its sensitive direction is same as the rolling direction of the lamination as shown in figure 2-21a. the tip edge of the isosceles-shaped substrates where the GMR is placed at the middle width of the sheet.

2.4.3.2 Laminated magnetic core testing

Test on a stack of lamination is realized to mimic an environment similar to that of laminated magnetic core as illustrated of figure 2-21c. Here, the instrumented lamination was successively moved from the first position up to the last one. The current amplitude in the excitation coil was set to ensure the reach of a saturated state in the bottom lamination (directly in contact with the yoke of the single sheet tester) and an unsaturated one for the top lamination (opposite position). Our idea here was to intentionally create a gradient of magnetic states through the laminated core and validate the accuracy of the non-invasive characterization method.

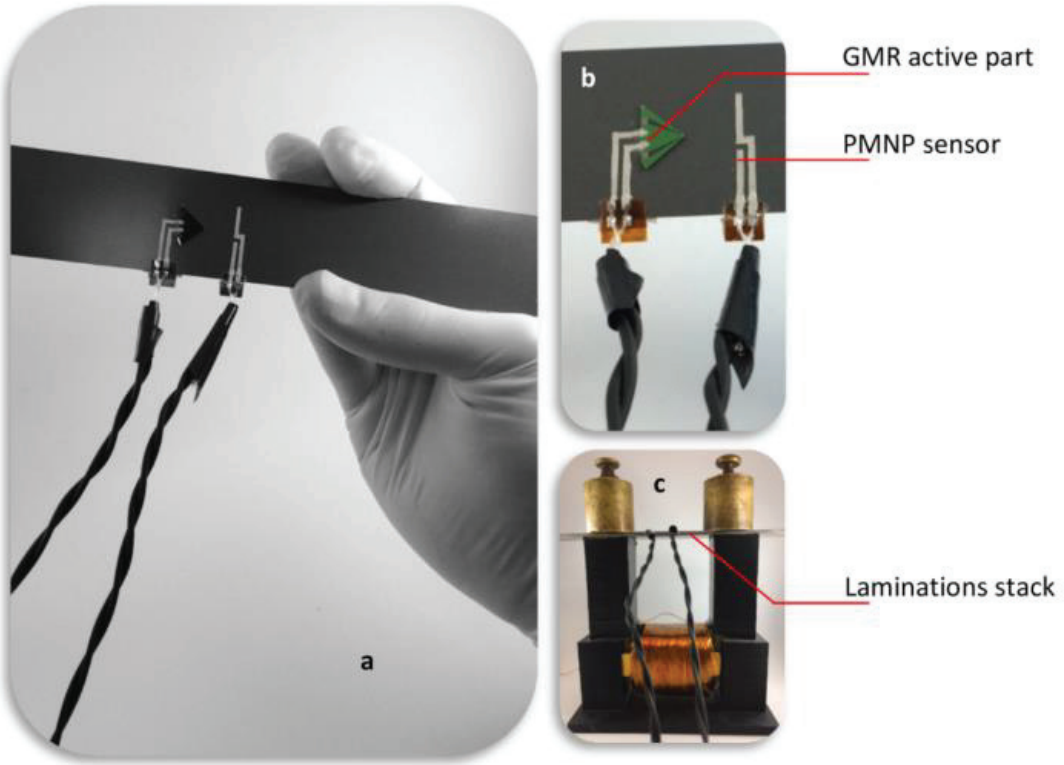

Figure 2-21:a– *Sensor positioning on a sheet, b – The non-invasive sensor, c – The sensor embedded in a lamination stack. [90]*

The resultant miniaturized sensor showed impressive outcomes. In spite the reductions done in terms of overall sensor size, the GMR sensor's thickness(270µm) is far greater than the admissible air gap in an electrical. Actually, inserting the GMR's substrate adds a significant gap between two successive laminations. In addition to this fact, the silver paint assuring the electrical link between the GMR and electrical cables of interfacing devices still increases the air gap by 100µm. thereby creating a small budge at the length-like edges. The 2-in- 1 embedded B_H is a proposed attempt to resolve this limitation.

2.5 **2-in-1 portable embedded B_H sensor**

2.5.1 Concept

The idea is all about having to print all the sensors on a single substrate. That being, the overall thickness of the sensor can be further reduced through polishing techniques during fabrication [88]. We aim at achieving a substrate thickness of less than 1nm. This is so to fall in terms of the condition of being the closest possible to the thickness coating found on laminations in a magnetic core as sketched out on figure 2-22. The feasibility of such a thickness for a start is not realistic due to the fragile nature of silicon at that thickness. Therefore, a thickness of tens of micrometres is much better for handling.

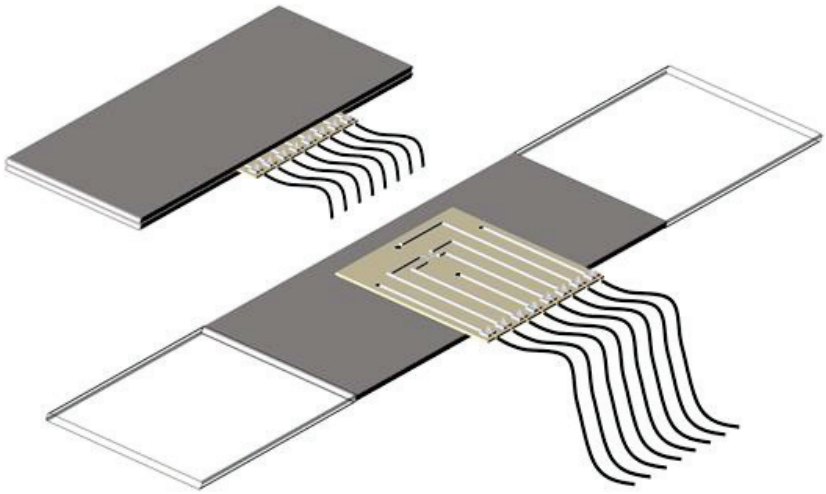

Figure 2-22: Illustrative sketch of the backbone idea of 2-in-1 sensor

2.5.2 PMNP/GMR sensor design

The pathing and disposition of two PMNP sensors and two GMRs are done following the design shown in figure 2-23. The leftmost design shows how the sensors are routed. The rightmost figure shows the disposition of two GMR's. the two magnetoresistances have their sensitivity direction 90° away in the vertical plane. As a result, the magnetic distribution with respect to the rolling ant transverse directions can be simultaneously monitored. Thus a possibility of bi-directional evaluation of magnetic field intensity and density guaranteed.

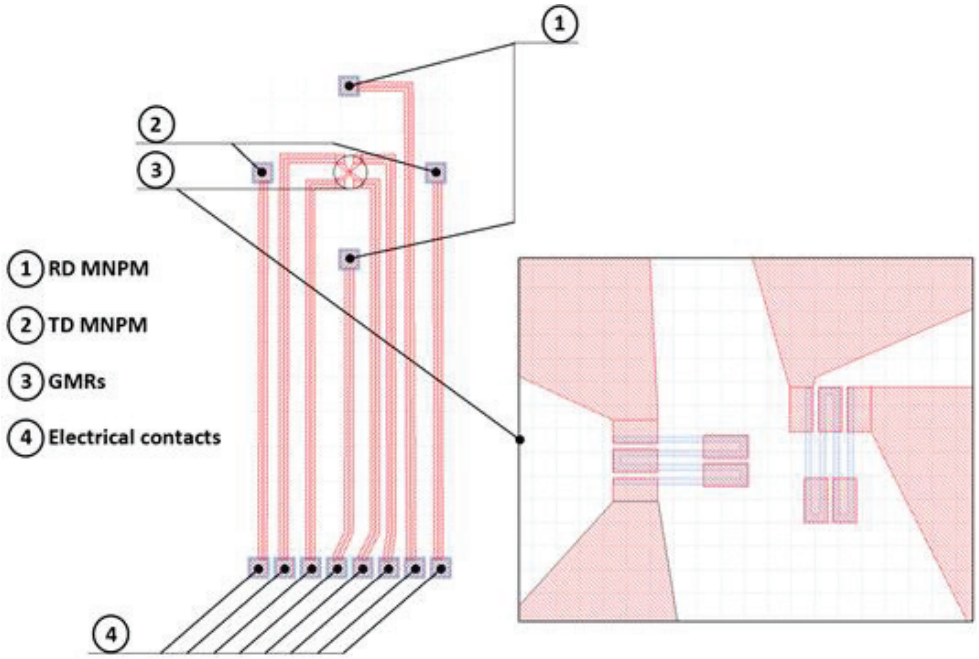

Figure 2-23:PMNP/GMR sensor design: (left) routing, (right) zoom on the disposition of GMRs

Following the above design, the Si/ SiO_2 (500)//Ta (3)/$Ni_{80}Fe_{20}$ (6.3)/$Co_{90}Fe_{10}$ (2.1)/Cu (2.9)/$Co_{90}Fe_{10}$ (2)/Ru (0.85)/$Co_{90}Fe_{10}$ (2)/$Ir_{22}Mn_{78}$ (7.5)/Ru (0.4)/Ta (5) (thicknesses in nanometers) GMRs were deposited by sputtering (Rotaris – Singulus) on 270 µm thick oxidized silicon wafers. Standard lithography technics were employed to build up the GMRs coupled to the metallic path connecting them to points of metallic contacts. The metallic contacts are made up of Ta/cu/Ta material with a thickness of 100nm. To ease the electrical interface of the GMR and signal treatment devices, the connection paths were extended to a PCB card on which electrical cables could be soldered. Moreover, the PMNP's points of contact with the sample under test are being applied a slight surplus at the 4 points of the PMNP. Further polishing of the substrate gave us a sensor thickness of 30µm. Figure 2-24 pictures out in real form the 2-in-1 sensor finally achieved.

(a) (b)

Figure 2-24:PMNP/GMR 2-in-1sensor; (a) view of the entire sensor; (b) zoom on the thickness of the sensor

Once fabricated, thermally treated and wired, the sensor undergoes a characterization test to evaluate its reference parameters. For this purpose, the Helmholtz coil and preliminary test as used in section 2.4 is used and followed. We thereby obtained the characteristic response to be as drawn on figure 2-25. The initial resistance of the GMR in the absence of magnetic excitation field is measure to be 630Ω.Contact resistances ≤ 0.5Ω when temperatures vary in the interval of 20°C-200°C and operating frequency range of 20Hz-1KHz. The good accuracy and precision as observed on the characteristic graph gives way to proceed to experimental tests

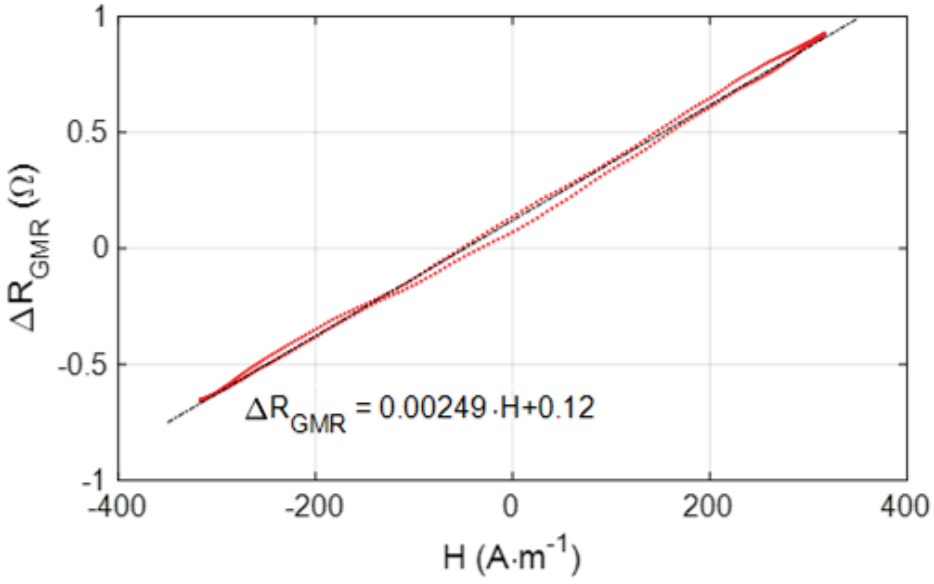

Figure 2-25:Characteristic curve of fabricated 2-in-1 sensor

2.5.3 Single sheet test

Experimental set-up seemly to IEC 60404-3 standard as described above in section 2.4 and 2.3 are followed. With the instrumented sheet, Frequency test and magnitude test to sort out the

operational frequencies and the threshold of magnitude detection were carried out. Also, the 2-D capability observed by placing the sensor 45° with respect to central length-line of the sheet in the surface plane as shown of figure 2-26.

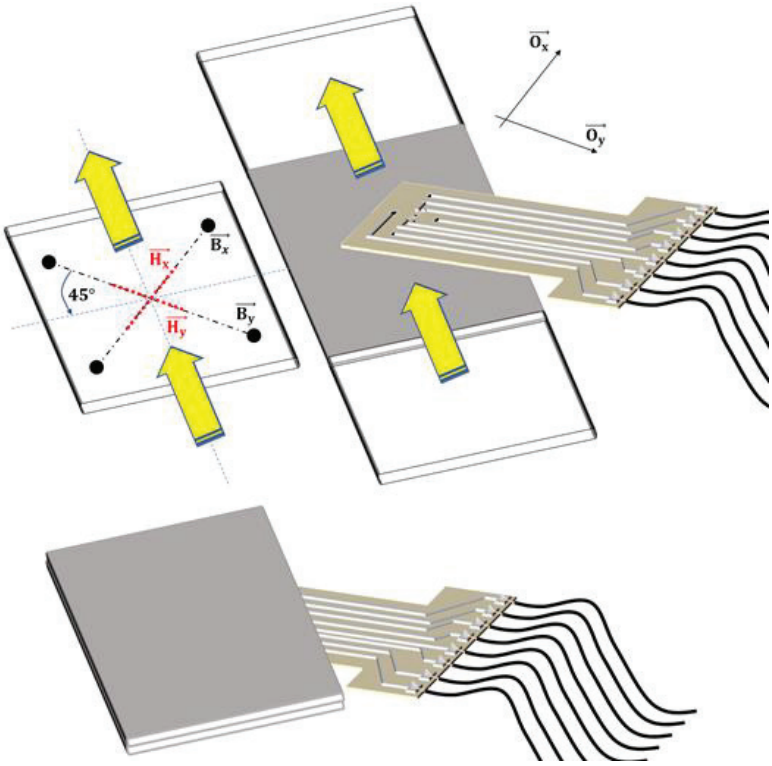

Figure 2-26 : Positioning of sensor for 2D measurement

2.5.4 Local measurement in laminated core

Experimental set-up seemly to IEC 60404-3 standard as described above in section 2.4 and 2.3 are followed. Inserting the sensor within a stack of sheets do not create significant air-gap as expose on figure 2-27b.

Figure 2-27:a) laminated core ; b)embedded sensor in laminated core

With all the experimentations done so far, the results obtained from the thinnest sensor will be compared to theoretical results. Numerical analysis tools" finite element modelling" and

software “ONELAB” will be used to solve the mathematical equations describing the electro-magnetism phenomenon in our work.

2.6 Summary

Being used as a magnetic sensor, the PMNP sensor equally takes advantage of its miniaturized geometry to further extend its scope of application to an embedded magnetic sensor inside a stack of laminations for homogenization testing/evaluation in magnetic cores. Core energy losses highly impede on the performance of electrical machines. Thus the elucubration of magnetic core losses via local magnetic investigations is of continuous attention in the electromagnetic field. However, the accuracy of such a study may request implicit experimental investigations of the local magnetic signatures from within a single lamination in a stack by a non-intrusive sensor, as oppose to conventional magnetic sensors limited to cross-sectional average or surface magnetic measurements. This sets the basis of the PMNP sensor concept. The sensor is built using mask and inkjet printing techniques. Latter on compared to other conventional sensor to validate and prove the new concept. For the experimental validation of homogenization methods, the PMNP is presented as the current most viable non-intrusive local magnetic induction sensor for the purpose. An equivalent magnetic core configuration was implemented in this chapter via a stack of 16 /10 (Fe-Si) grain-oriented laminated sheets mounted on the single strip tester (SST) design. Local magnetic signature of each lamination was measured turn by turn using the combination of PMNP and hall effect sensors. In the quest of more miniature measuring system, the local B_H was measured using the duo made-up of PMNP and GMR. The two latter were thereafter printed on the same substrate to constitute a compact and portable B-H sensoring system; thus a more simultaneous measurements assured.

CHAPTER 3:
SIMULATION AND NUMERICAL ANALYSIS OF INHOMOGENITY IN MAGNETIC FIELD DISTRIBUTION

The targeted materials for this research work are ferromagnetic materials. Increasing energy efficiency of materials is directly dependant on the magnetic properties of these materials in term of the power losses. For producing energy efficient machines, it is necessary to know actual magnetic properties of the used material. This can be obtained by measurements and for that purposes it is best to use measurement method defined by standard. In order to optimize the control system of machines based on non-destructive testing, local information on how the electro-magnetic interactions is a necessity. Experimentally, we achieved a non-intrusive embedded sensor for local measurements. Moreover, there is need to have a knowledge on how the choices of parameters can impact the overall functioning of the system[92]; without having to build numbers of prototypes which is very costly. Simulations tools are then used to model the experimental bench with various related parameters. From these models, numerical analysis of the mathematical expression of various physical phenomena is carried out to obtain solutions. Based on these analysis, Researchers can thereby predict a certain behaviour when some particular changes are being made[18]. There exist various modelling/simulation tools depending on their features: less cumbersome(user-friendly), solving time, exactitude level of solutions, the physical phenomenon under observation, accommodation graphical interface for more illustrative observation, just to name a few.

There exist two main categories of modelling approach to interprete material law: empirical approach, theoretical approach Empirical model is all about representing the non-linear behaviour of ferromagnetic materials from historical data[93]. As example, we have the Rayleigh model which unfortunately do not rely on theory but on observation; thus less appropriate for in-dept interpretation of micro-magnetic mechanisms[94]. As far as theoretical modelling is concerned, we have Jiles-atherthon, Preisach, Landu-Lifshitz and stoner-wohlfarth which are the commonly used hysteresis models. A feature-comparison of these 4 models as resumed in table 3-1 were done by Pradhu [95]and Raghunathan [96]. Equations from the various models are solved numerically using mostly iterative techniques;

Table 3-1 : Features of commonly used theoretical magnetic hysteresis models[97]

Model characteristics	**Stoner-Wolhfarth**	**Landau-Lifshitz**	**Preisach**	**JilesAtherton**
Mechanism	rotation	rotation	switching	motion
Interaction	yes	yes	no	yes
Anisotropy	any	uniaxial	any	Any
Scale	micro	atomic	micro	Meso
Pinning	yes	yes	not	yes
Wall energy	no	yes	no	no
Minor loops	yes	yes	yes	approximate
Anhysteretic	yes	yes	yes	yes
Parameters	3		3	5
Run-time	Average	Very large	average	Low

From the table above the Preisach and jiles-Atherton models show good features for our application. Nevertheless, when using preisach's model, the correct determination of parameters from simulation results implies fitting model parameters to experimental data and therefore, usually arbitrary in nature, and are time intensive[98].

Given that our main target is to be able to predict local distribution of magnetic field in a magnetic core in a short time process , we use the Jiles-atherthon theoretical hysteresis model. More-over, the rationale of our study revealed that numerical model of inhomogeneity in magnetic distribution were already done by researchers and eddy current losses in laminated core recently evaluated numerically by M. Taghizadeh et al[99],K. Bitsi et al[100] and E.Lamprecht[101] which had never been confronted experimentally. It is therefore beneficial and more logical for us to apply the same numerical method during their finding; that is FEM(Finite Element Method).

3.1 Finite element modelling on Onelab interface

Electromagnetic interactions develop themselves in an infinite vector space. There is thereby needs to curve out a finite vector space to better analyse these interactions: It constitutes the main of finite element modelling(FEM). The FEM sets boundary conditions of the finite space, creates a network of finite number of points called "elements" and derives the exact point-wise

algebraic properties of each vector of the system. The network of points is obtained by space discretization which is implemented by meshing the geometrical structure of the system under analysis. Each element has a particular response to the physical phenomenon to be observed; assembling each elements' response give the entire model describing the system. For the development of our ferromagnetic model, we used the open-source Onelab® software suite with in-built generic hysteretic mathematical models: linear, anhysteretic and Jiles-atherton formulation models[102]. Appropriate values of parameters gotten empirically from experimentation are keyed into the program and the simulation results processed and analysed. Throughout our thesis, detailed emphasis won't be laid on the theoretical modelling of ferromagnetic behaviour.

3.1.1 Geometric design

It is all about portioning the entire system in a geometrical shapes representing each component. The vector space is reducing to 2-dimension(x,y) considering the supposition done in deriving magnetic field density in chapter2: section 2.1.1 (the vertical component of electrical field with respect to the cross sectional plane of a lamination is considered negligible). The geometric shapes as illustrated on figure 3-1 is a halved representation of the electromagnetic circuit. This simplifies our model by taking advantage of the symmetry. The space domain under study is curved out by using the semi-arc of circle which accounts for infinity. The laminated core constituted of 10 GO FeSi sheet is represented with 10 rectangles (280mm x 0.3mm) representing the iron domain. Between two successive sheets, a rectangle(280x0.03mm) is placed to account for the insulation coating found on each sheet: that is the insulation domain. the induction coil represented by two rectangles in sky blue colour (2); the two rectangles represent the face view of excitation coil when it is cut follow the (x,y) plane.

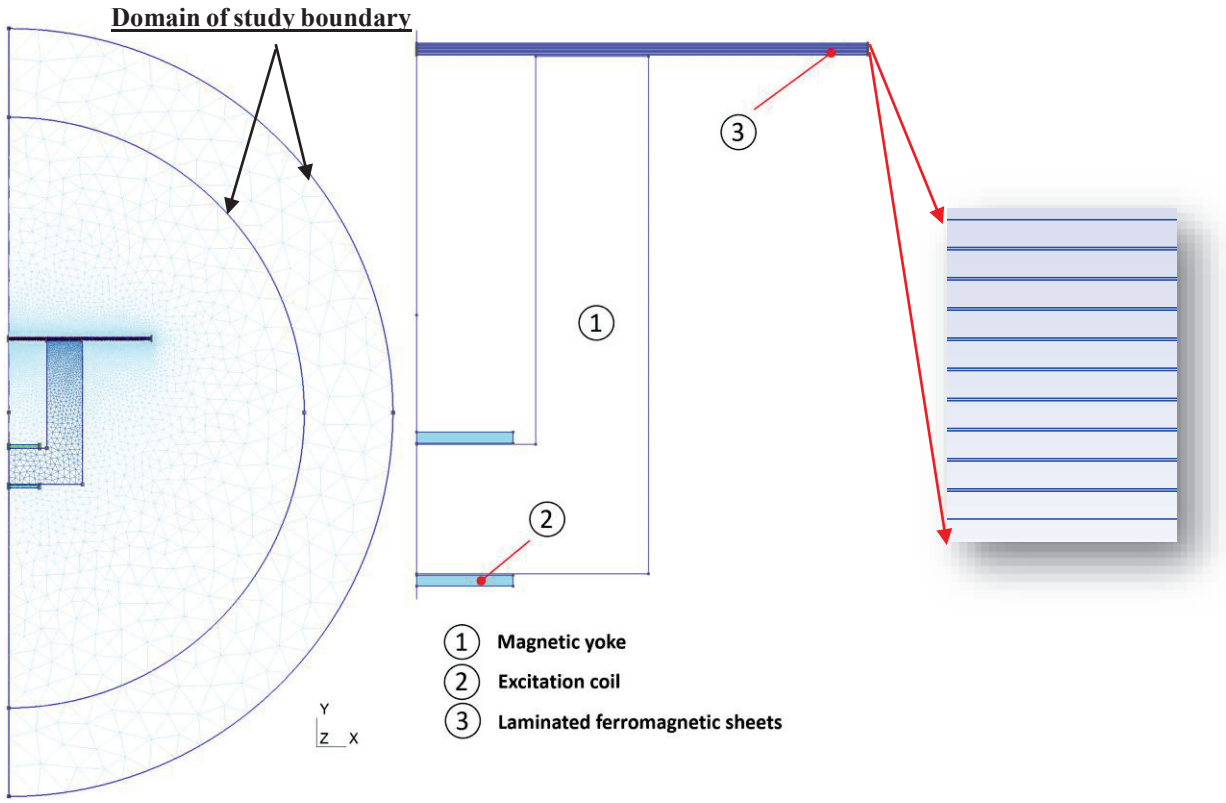

Figure 3-1 : Geometrical design and meshing design of the electromagnet circuit. the right most picture is a zoom on magnetic core geometry

3.1.2 Meshing design

It consists of dividing the geometrical environment into small cells of rectangular form or triangular forms which are called meshes. The vertex of each cells represents the point where an exact solution to the electro-magnetic problem can be found. Within the cells, solutions are obtained by polynomial interpolation of high/low order. Thus, each component of the geometric model is discretized. The higher the number of cells, the higher the precision of numerical calculation which brings along a longer processing time. An appropriate meshing is thereby a net compromise between the computation time and the level of precision needed. The discontinuity of electrical and magnetic fields between two component of different meshing design of the model, are accounted for by using electrical and magnetic potentials. Figure 3-2 illustrates the meshing design used for our magnetic set-up alongsidea zoomed view of the meshing style on 4 sheets . Each steal sheet of iron(FeSi) is represented by a domain having 4 discretization in the thickness plane using triangular meshes. Each insulating layer constitutes the insulation domain which has three discretization still using triangular meshes. Other domains constituting the system are meshed using splines.

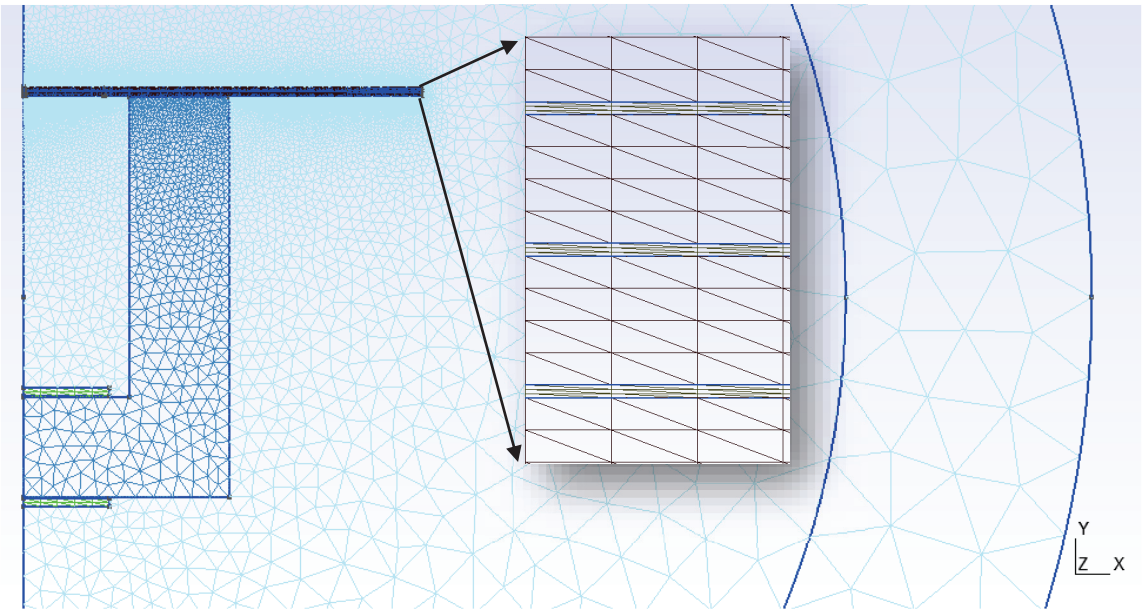

Figure 3-2 : Meshing configuration of each space domain

3.2 Jiles Atherthon modelling

The fundamental interpretation of hysteresis models by the theoretical methods of approach as referred by Jiles and Atherton[103], is either based on mathematical description of hysteresis of any physical nature. Principally, the inverse Jiles-Atherton model described in [104]was applied as material law in the ferromagnetic parts. The model's differential equation is expressed as:

$$\frac{dM}{dB} = \frac{(1-c)\frac{dM_{irr}}{dB_e} + \frac{c}{\mu_0}\frac{dM_{an}}{dB_e}}{1+\mu_0(1-c)(1-\alpha)\frac{dM_{irr}}{dB_e} + c(1-\alpha)\frac{dM_{an}}{dH_e}} \qquad 3\text{-}1$$

To numerical procedure involved in deriving M and H from B was used as described in [104] [105]. The procedure goes as follows:

- ✓ B(t) and H(t) are known from previous step
- ✓ For the time t+Δt ; we have B(t+Δt) and we derive H(t+Δt) by using the following equations

$$\Delta B = B(t + \Delta t) - B(t) \qquad 3\text{-}2$$

$$M(t) = \frac{B(t)}{\mu_0} - H(t) \qquad 3\text{-}3$$

The effective field strength by individual magnetic moment H_e is being derived by:

$$H_e = H + \alpha \mathcal{M} \qquad 3\text{-}4$$

The anhysteretic magnetization M_{an} is obtained using:

$$M_{an}(H_e) = M_{sat}\left[coth\left(\frac{H_e}{a}\right) - \left(\frac{a}{H_e}\right)\right] \qquad 3\text{-}5$$

$$\frac{dM_{an}}{dH_e} = \frac{M_{sat}}{a}\left[1 - coth^2\left(\frac{H_e}{a}\right) + \left(\frac{a}{H_e}\right)^2\right] \qquad 3\text{-}6$$

The irreversible component of magnetization is calculated as:

$$M_{irr}(t) = \frac{M(t) - M_{an}(t)}{(1-c)} \qquad 3\text{-}7$$

$$\frac{dM_{irr}}{dB_e} = \frac{M_{an} - M_{irr}}{\mu_0 k \delta} \qquad 3\text{-}8$$

With δ a directional parameter which takes the value +1 or -1 when $\frac{dB}{dt}$ is >0 or <0 respectively.

$\frac{dM}{dB}$ is calculated from equation 3-1 in which the values of $\frac{dM_{an}}{dH_e}$ and $\frac{dM_{irr}}{dB_e}$ obtained from equations 3-6 and 3-8 respectively are being substituted.

Thus :

$$M(t + \Delta t) = M(t) + \frac{dM}{dB} dB \qquad 3\text{-}9$$

then

$$H(t + \Delta t) = \frac{B(t+\Delta t)}{\mu_0} - M(t + \Delta t) \qquad 3\text{-}10$$

Where a is a parameter with dimensions of magnetic field which characterizes the general shape of the anhysteretic magnetization curve, M_s the saturation magnetization, c is the reversibility coefficient, k is the pinning coefficient and α is the mean field parameter representing inter-domain coupling The model parameters a, k, α and c can be determined from the experimental data belonging to the referent points of the measured hysteresis curve as shown in figure 3-3. The reversibility parameter c is determined experimentally by the ratio of the initial differential susceptibilities of the normal and anhysteretic magnetization curves. Similarly, the parameter k is directly related to the coercive field since it is affected by the time delay related to the rotation of the domain walls and hence, proportional to the domain walls pinning. The c, shows dependence on the parameter a as well, and are both influential in determining the permeability of the material.

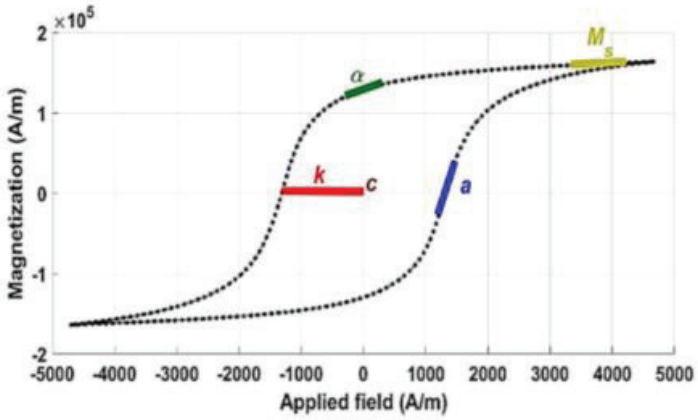

Figure 3-3: Schematic illustration of Jiles-Atherton model parameters[97]

According to the Jiles-Atherton theory of ferromagnetism, α quantifies the interdomain coupling, a the domain walls density with which one can alter the remanent magnetization and helps determine the permeability of the material, k the average energy to break the pinning sites which changes the coercive field, and c the magnetization reversibility [103]. The values used for our study which are proper to FeSi GO lamination are assembled in table 3-2. The resultant hysteresis cycle gotten from applying Jiles Atherton(JA) physical model is shown in figure 3-4 with an overlap of measured cycle.

Table 3-2 : Jiles-Atherton (J-A) simulation parameters for the FeSi GO (RD)

J-A Parameters	Typical value
a ($A.m^{-1}$)	4
Ms ($A.m^{-1}$)	1312000
k ($A.m^{-1}$)	40
c	0.01
α	$7.4\ 10^{-6}$

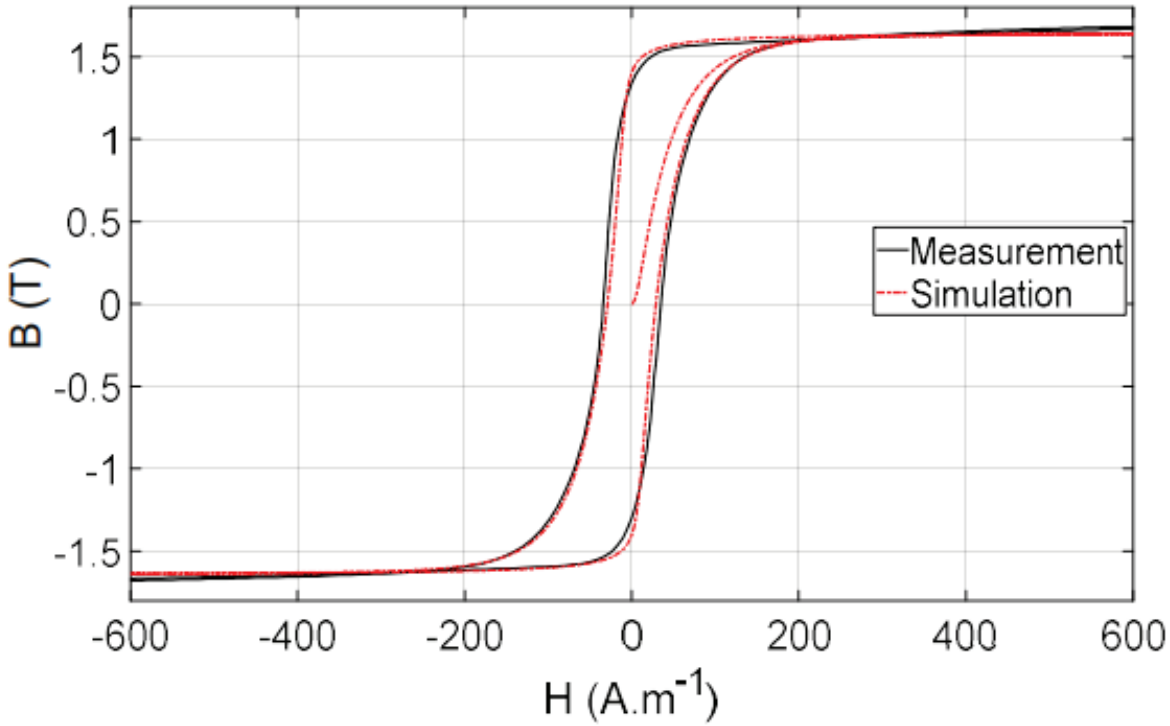

Figure 3-4 : Superpositon of measured B_H signature of the material and hysteresis cycle from JA modelling

3.3 **Graphical distribution of magnetic field line**

A homogeneous current density denoted $j_s(x, y, t)$ crosses the excitation coil. Eddy current sensing are done in both quasi-static and dynamic regimes Thus, we fixed an operating frequency of 50Hz. With a number of steps per period fixed at 300, we observed a spread of magnetic field as seen on figure 3-5 Here, the excitation field is same for all the simulation graphical display registerred. As the intensity of the exciting field keep increasing, the five different graphical distribution are captured at different time step. The magnetic field intensity as calculated on the surface of the first lamination(counting from bottom to top)) varies from 0 to 100 A/m annotated H_{surf}

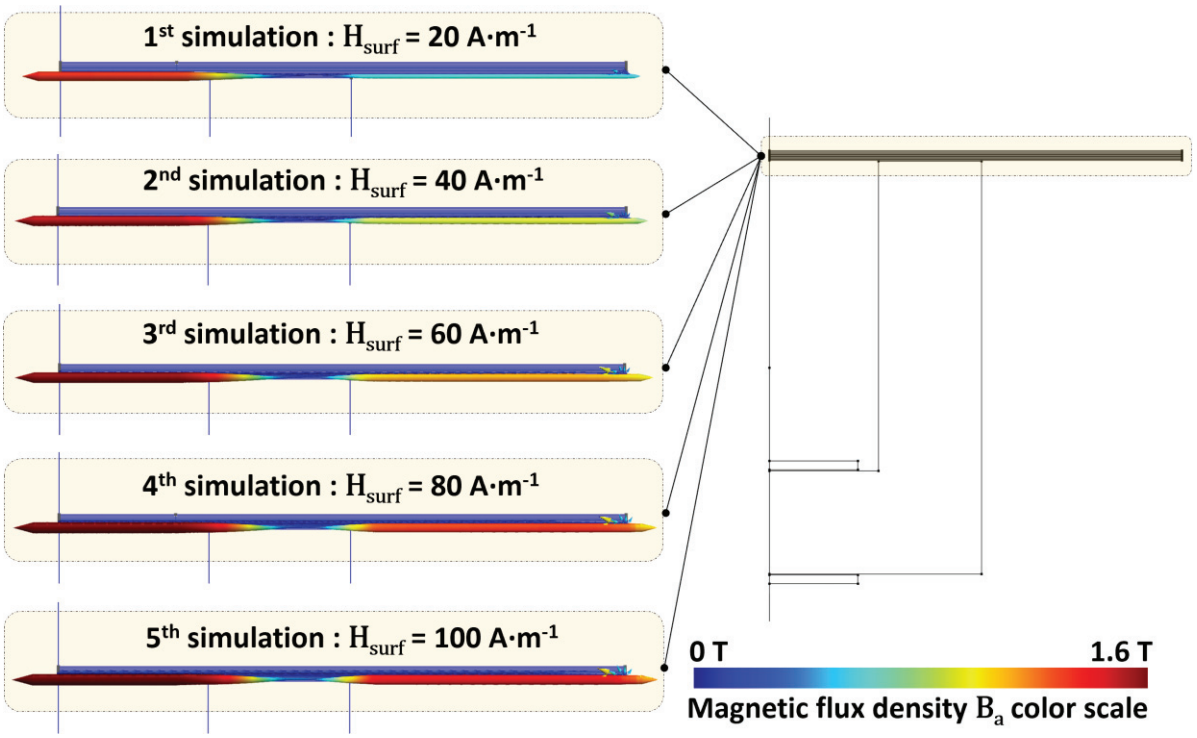

Figure 3-5 : Graphical illustration of magnetic induction within a stack of 10 steel sheets

The above figure exposes the general glance through of the graphical magnetic distribution in our electromagnetic system. An insight on how it progresses witching the thickness of a steel sheet is of interest. Figure 3-6 gives a detailed view on the propagation of magnetic flux density in the 4 first amination.

Observing the below figure, we notice that magnetic field do not propagate with the same intensity in all laminations. The strength of magnetic field induction weakens (changes from red to blue) as we progress to above laminations. The gradient in the deployment of magnetic field within the stack of steels show that magnetic field intensity is distributed inhomogeneously.

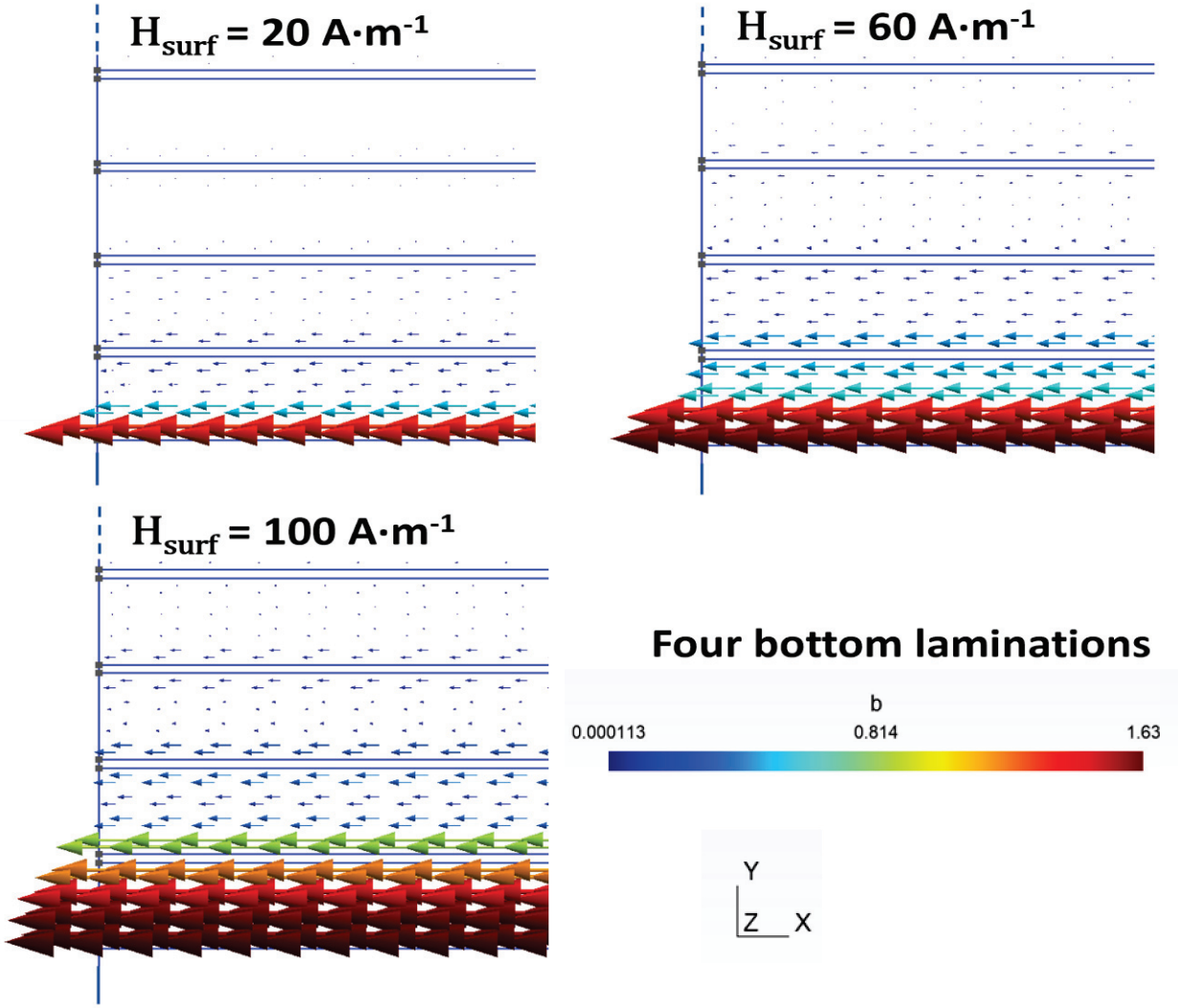

Figure 3-6: Zoomed view on magnetic distribution of the first four laminations

3.4 **Post-processing**

Calculated values of magnetic field intensity and magnetic field density are exported to MatlabTM for plotting. The hysteresis loop is obtained by plotting B against H. the B(H) loop possesses indicators that helps appreciate the intrinsic behaviour in the magnetic core. We distinguish the remanent field density and the coercive field intensity and the hysteresis loss which is area covered by the entire B(H) function. The area is numerically computed by integrating the B(H) function with respect to Hmax and Hmin

With all the verifications and preliminary tests done on the experimental benchmark and the finite element model, major tests were realized following the protocol described in this chapter. Data recorded, numerical results will be exploited through the observation of key parameter

and indicators all through various tests. Discussion and inferences done to evaluate if our claims are proved right or wrong. Conclusively if our objectives are attained.

3.5 Summary

The complexity of magnetic core geometries is an added disadvantage to the simulation of local magnetic behaviour in electromagnetic devices. We thereby model our electromagnetic-system using the FEM to which the JA model law of material was applied as implemented in the ONELAB environment. Simulation results of the magnetic flux density pattern within a stack of laminations is depicted in this chapter. However, the applicability of our simulation scheme in the investigation of local magnetic field patterns of a single lamination in a stack was attended to. The numerical solutions once gotten are processed using Matlab software. The derived magnetic distribution still pends validation from experimental measurements; it constitutes the subject matter in the next chapter.

CHAPTER 4:

RESULTS AND DISCUSSIONS

Having access spontaneously to local flux distribution within a laminated magnetic in a non-intrusive manner constitute the skeleton of our research so far. We claimed that the PMNP sensor we have manufacture open doors to get to the flux distribution line stream. As a new sensor format, there is need to do at the onset, a series of tests along with other sensing methods which have been acquire as standard. This constitutes our first set of experiments whose target is to do a relative comparison to existing standard test and validating the embedding/non-invasive feature of our sensor. the basic PMNP and GMR characterization sensors for B and H respectively, were so far distanced away; but was upgraded to a more lumped/concentrated positioning of the two sensors. The next set of experiment was then geared towards evaluating the accuracy of the miniature B_H sensing configuration. Furthermore, a 2-in-1 sensor combination of the PMNP and GMR sensor to achieve a seamless insertion within the magnetic core was designed. Thus, the set of results gotten from experiments using the 2-in-1 sensor were compared to simulated numerical results from finite element model.

4.1 Validation of PMNP

It is all about the experimental validation of the newly developed PMNP sensor as a local magnetic NDT method and an introductory tool to homogenization studies in a laminated core. The modified-SST experimental setup described in section 2.3.1 was used for both experimental validation procedures.

4.1.1 Comparison with other eddy current testing sensors

The PMNP sensor validation procedure is achieved via comparative analysis of the measurements from the sensors set earlier described section 2.3.2. The Rolling direction controlled (RD) GO magnetic lamination and the TD (traverse direction) controlled magnetic lamination were instrumented to investigate local magnetic flux density at various at different excitation frequencies ranging from 1 Hz to 200 Hz. Figures 4-1 and 4-2 are local B_H characterization curve for RD and TD GO FeSi sheets respectively. Just a single sheet of FeSi is used for these recorded data.

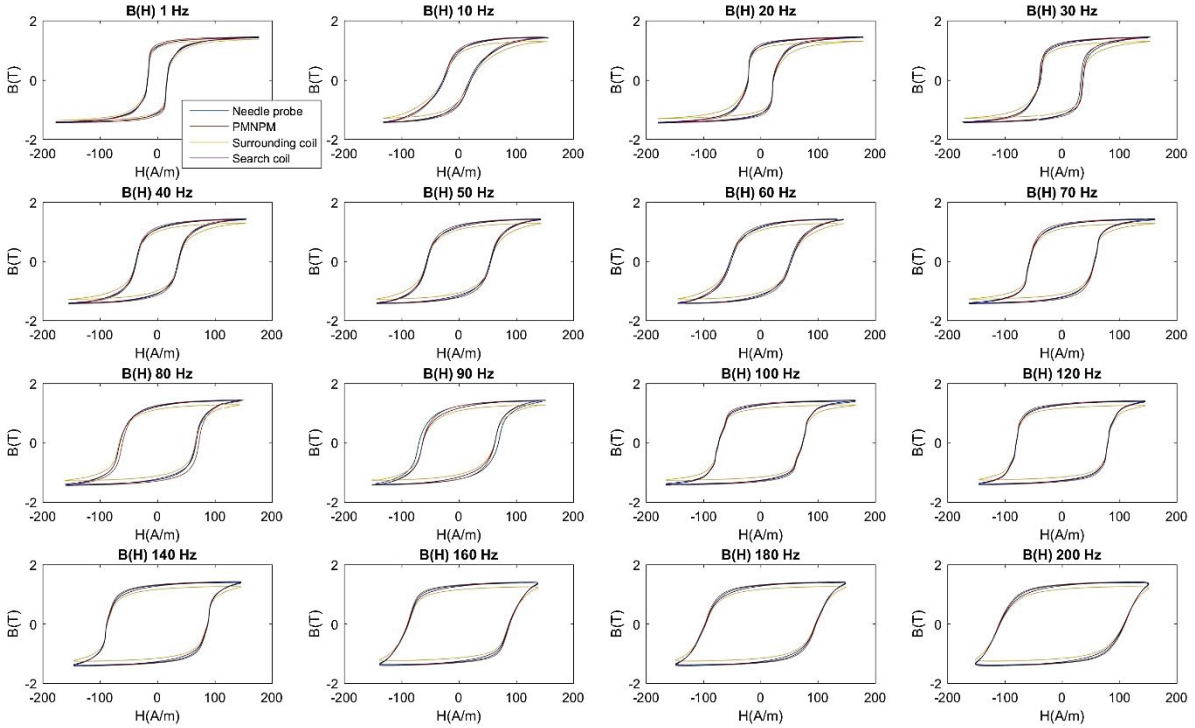

Figure 4-1: Frequential B_H characteristic curves of RD-GO steel sheet as seen by 4 sensor(classic needle probe, 10 turns surrounding coil, search coil and PMNP)

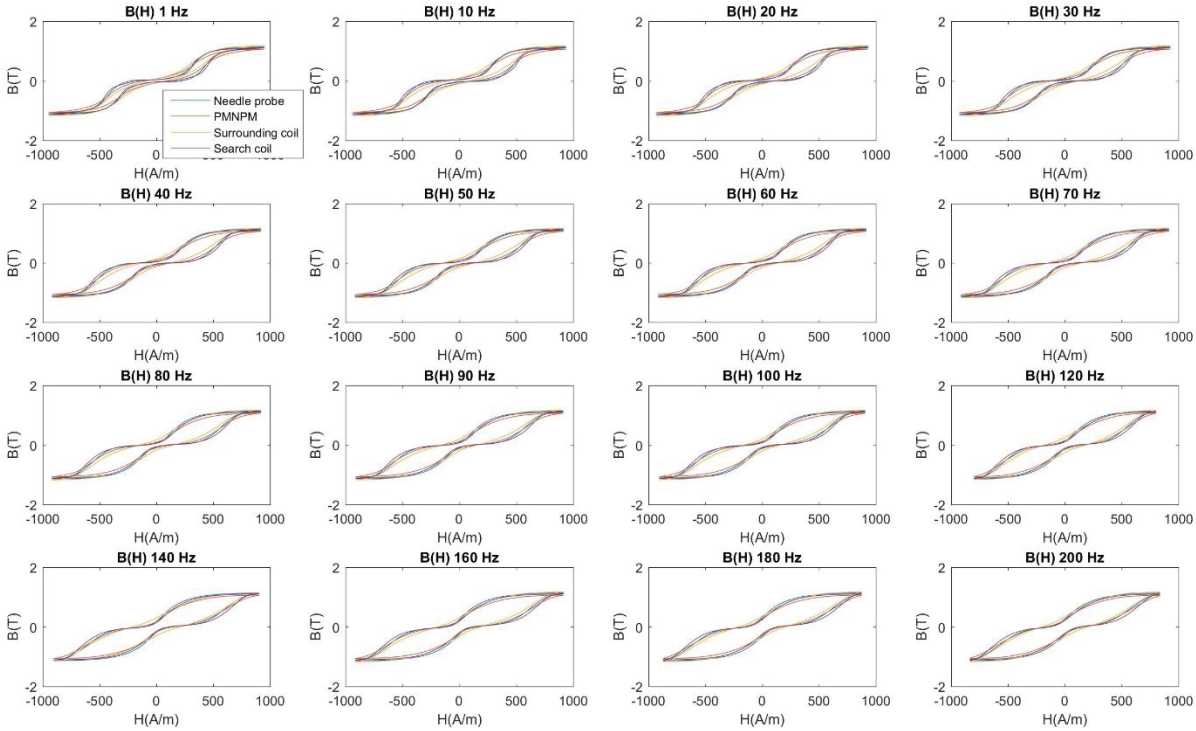

Figure 4-2: Frequential B_H characteristic curves of TD-GO steel sheet as seen by 4 sensors(classic needle probe, 10 turns surrounding coil, search coil and PMNP)

Visually observing the various curves of figure 4-1 and figure 4-2, one notes a slight amplitude mismatch of magnetic induction as seen by the surrounding coil. The roughness at the edges due to the trimming of sheets to appropriate dimension at the manufacturing industry or unexpected asymmetrical properties of the experimental set-up are possible causes of this mismatch. Although, this mismatch, there PMNP shows good accuracy with respect to MNP sensor and search coil no matter the frequency of operation.

For further comparative analysis, we computed the resultant hysteresis area of each loop at various frequency. From which, the search coil and surrounding coil were used as reference to evaluate the relative error in the PMNP measurements as shown in tables 4-1 and 4-2 respectively. The Error functions are calculated from the following equations:

$$\begin{cases} Error_{Coil}(\%) = 100.\left(1 - abs\left(\dfrac{< A >_{PMNPM}}{< A >_{Coil}}\right)\right) \\ Error_{S.coil}(\%) = 100.\left(1 - abs\left(\dfrac{< A >_{PMNPM}}{< A >_{S.Coil}}\right)\right) \end{cases} \qquad (4\text{-}1)$$

Table 4-1: Precision of the PMNPM sensor compared to the conventional one (coil and search coil) under easy axis magnetic excitation situation.

		1 Hz	20 Hz	40 Hz	60 Hz	80 Hz	100 Hz	140 Hz	180 Hz	200 Hz
Easy axis direction	Hysteresis Area PMNPM (J/m^3)	111,85	142,97	190,80	255,61	287,75	383,65	451,33	500,74	558,70
	Hysteresis Area coil (J/m^3)	113,19	140,87	183,96	242,92	263,51	351,63	403,16	447,10	494,82
	Hysteresis Area Search Coil (J/m^3)	114,99	146,01	196,03	262,95	287,04	382,61	445,58	495,54	549,38
	Error (%) coil comparison	1,19%	1,49%	3,71%	5,22%	9,20%	9,11%	11,95%	12,00%	12,91%
	Error (%) search coil comparison	2,81%	2,13%	2,74%	2,87%	0,24%	0,27%	1,27%	1,04%	1,67%

Table 4-2: Precision of the PMNPM sensor compared to the conventional one (coil and search coil) under transverse magnetic excitation situation.

		1 Hz	20 Hz	40 Hz	60 Hz	80 Hz	100 Hz	140 Hz	180 Hz	200 Hz
Transverse direction	Hysteresis Area PMNPM (J/m^3)	309,41	471,79	599,32	709,01	777,72	846,40	942,98	917,07	1048,69
	Hysteresis Area coil (J/m^3)	260,85	417,15	530,06	634,39	699,29	754,06	867,12	902,13	970,82
	Hysteresis Area Search Coil (J/m^3)	293,07	464,22	589,76	688,53	754,16	811,67	929,04	912,68	1019,53
	Error (%) coil comparison	18,62%	13,10%	13,07%	11,76%	11,22%	12,25%	8,75%	1,66%	8,02%
	Error (%) search coil comparison	5,28%	1,61%	1,59%	2,89%	3,03%	4,10%	1,48%	0,48%	2,78%

From the observation of both Table 4-1 and 4-2, one can conclude the PMNP sensor shows high accuracy with respect to search coil measurements. This is in both TD and RD GO steel sheet with an acceptable error range (<5%); be it at low frequency or at high frequency.

4.1.2 Laminated core sensing as per local flux distribution

Confronting the PMNP to other standard sensor, validates its capacity for local magnetic measurements. We can then go ahead to test the PMNP aimed at validating it as a potential experimental homogenization method. An equivalent laminated magnetic core was built from a stack of 16 magnetic laminations mounted on the previous experimental setup for homogenization analysis as displayed on figure 4-4(d). The measurement protocol as described in section 2.3.3 was followed and the data collected which were further exploited to plot the graphs of figure 4.3. That is, plotting the magnetic induction state measured locally for every lamination of the laminated magnetic core as a function of the tangent excitation field measured simultaneously on the laminations stack top and bottom. For more precise analysis, magnetic indicators were tracked all along the various set of data collected as seen on figure 4.4.

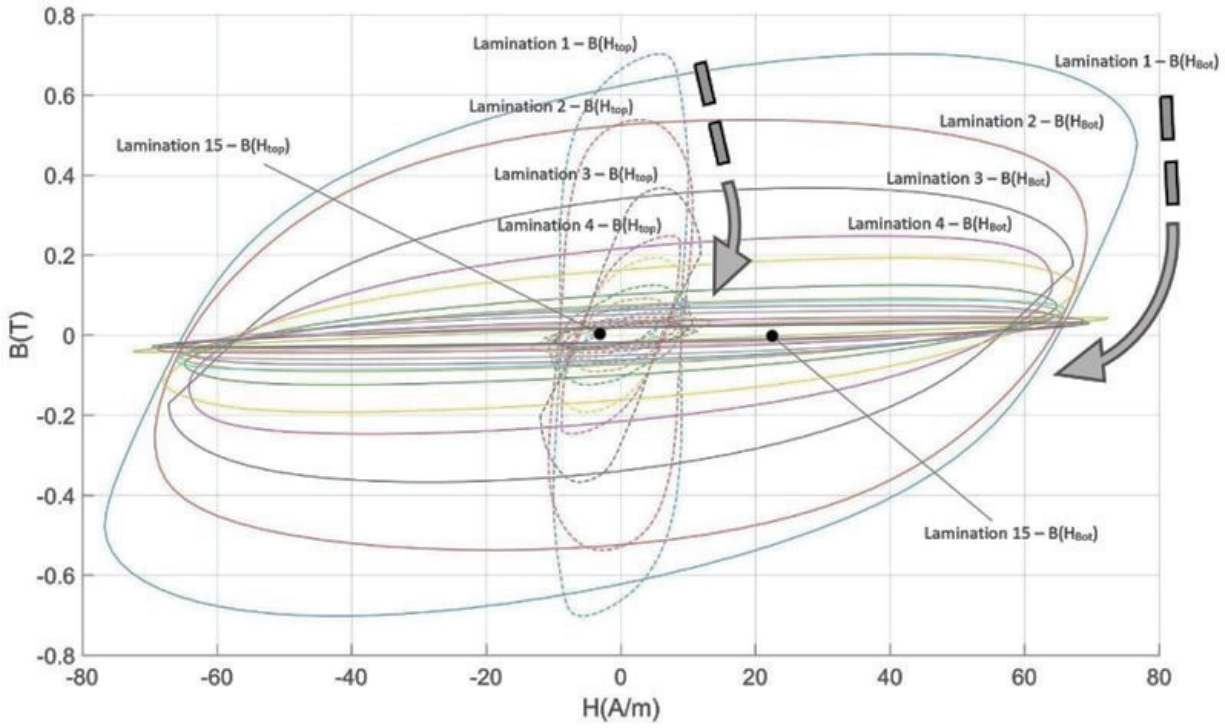

Figure 4-3 : Local measurement of B at each lamination vs tangent H-field as seen at the top of the stack(full lines) and at the bottom of the stack(dotted lines)

The maximum value of the magnetic excitation field is set intentionally weak to create a strong gradient of magnetic induction through the laminated magnetic core. Tracking down the behavior of magnetic hysteresis indicators, we observe as on figure 4-4(a) that the maximum value of the magnetic induction field decreases exponentially as the instrumented sheet is displaced farther away from the SST yoke's surface.

A similar trend can be observed for the evolution of the hysteresis losses on figure 4-4 (b). The absolute value of the coercive fields figure 4-4(c) are decreasing at a slow rate..

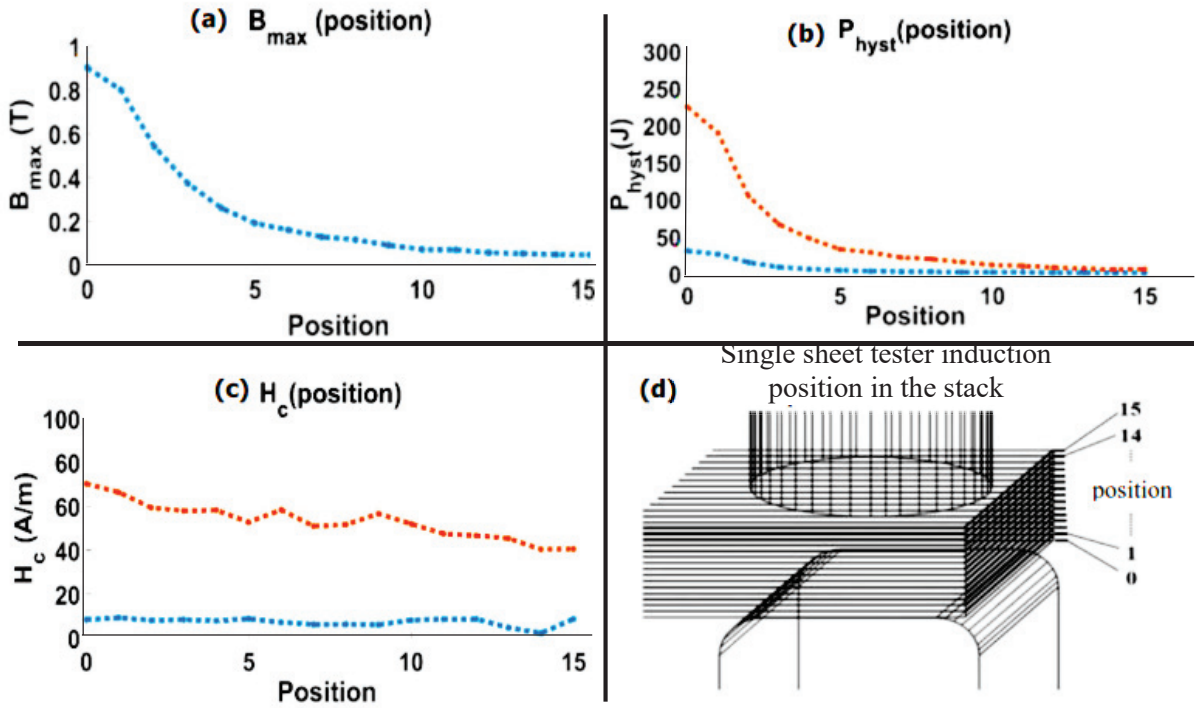

*Figure 4-4 : : (a) Maximal induction field versus lamination position, (b) Hysteresis losses versus lamination position, (c) Coercivity versus lamination position, (d) Illustration of the lamination position; (top hall effect sensor measurement (**red**) and bottom hall effect sensor measurement (**blue**))*

Furthermore, analysis was forged ahead towards reconstructing the overall hysteresis cycle of the magnetic core from the 16 local measurements and comparing it to the one obtained with the 10-turns surrounding coil positioned over the whole magnetic core. The average induction state is obtained through the conservation of the magnetic flux computed as follows:

$$\phi_{tot} = \sum_{i=1}^{16} \phi_i$$

$$B_{tot}.S_{tot} = \sum_{i=1}^{16} B_i.S_i \qquad S_{tot} = 16.S_i \qquad (4\text{-}2)$$

$$B_{tot} = \frac{1}{16} \sum_{i=1}^{16} B_i$$

At different intensity of excitation, the averaged cumulative values of the local magnetic induction field were computed following Eq. 4-2. This is aimed at obtaining the average

measurement in the overall stack of steels. The calculated values and measurements from the 10-turn surrounding coil were plotted against the top hall effect sensor measurement (dashed lines) and bottom hall effect sensor measurement (full lines); thus the graph in figure 4-5

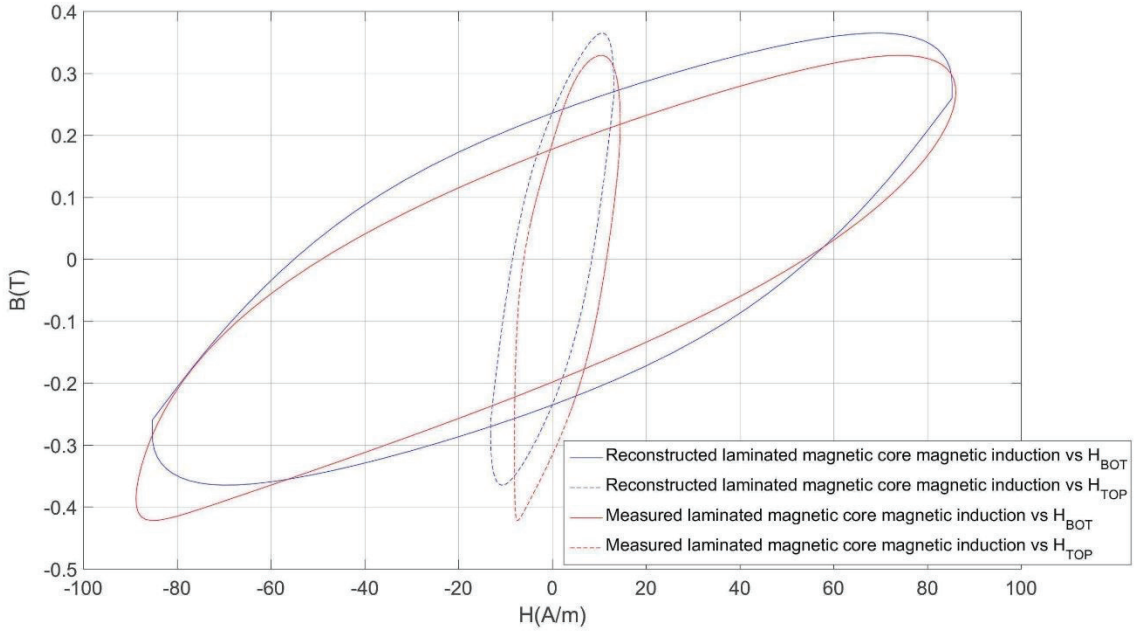

Figure 4-5: Reconstructed laminated hysteresis cycle and the overall hysteresis cycle as measured by 10 turns surrounding coil

These results provide evidence of feasibility in monitoring isolated magnetic lamination states through the laminated magnetic core. By comparing the surface areas between the measured and the overall average hysteresis cycles, the drift in measurement obtained with H_{BOT} is 13.5%, and just 2.1% for H_{TOP}.

Inference

In sum, we have been able to show that by using same excitation properties of the magnetic circuit, the voltage detected by the needle probes (MNP and PMNP) method is almost equivalent to values measured using a classic search coil (one turn) wound around the 1–2-3–4 area as seen in figure 2-1. Magnetic induction and hysteresis results have been obtained using the printed sensor in frequency ranges of 1 Hz to 200 Hz; Thus, the PMNP is a good candidate for in-depth flaw detection in material as well surface defect detection.

4.2 PMNP + GMR lumped at a particular point

In the previous experiment, the size of the hall effect sensor measuring the field intensity hinder us in achieving a local B_H measurement simultaneously at the same location. The Hall effect sensor is therefore replaced by a GMR sensor which will be placed next to the PMNP as described in section 2.4.2. a pre-characterisation of the dual sensors will be done to be rest assured it behaves as intended. This is needed before proceeding to its seamless embedment within a laminated core.

4.2.1 Single sheet testing

The pre-characterization curve (ref. figure 2-19) of the GMR sensor was used to determine its sensitivity (voltage to field conversion ratio); which is **0.7%/mT**. The distance between both the electrical contacts of the PMNP sensor and the tested lamination thickness were respectively 10 mm and 0.35 mm. They subsequently constitute key parameters for post-processing of data in order to derive the magnetic induction B. The same 3 wt% silicon GO steel sheet is used here. The dual sensors are placed at mid-length from the yoke legs where B and Hsurf vectors are supposed to be pointing in the RD and collinear. The instrumented sheet as shown in figure 2-21a was placed on SST yoke for a solo-sheet test. The magnetic excitation amplitude was gradually changed from 20 to 600 A/m. the preliminary material characteristic as measure by our dual sensor is displayed in figure 4-6.

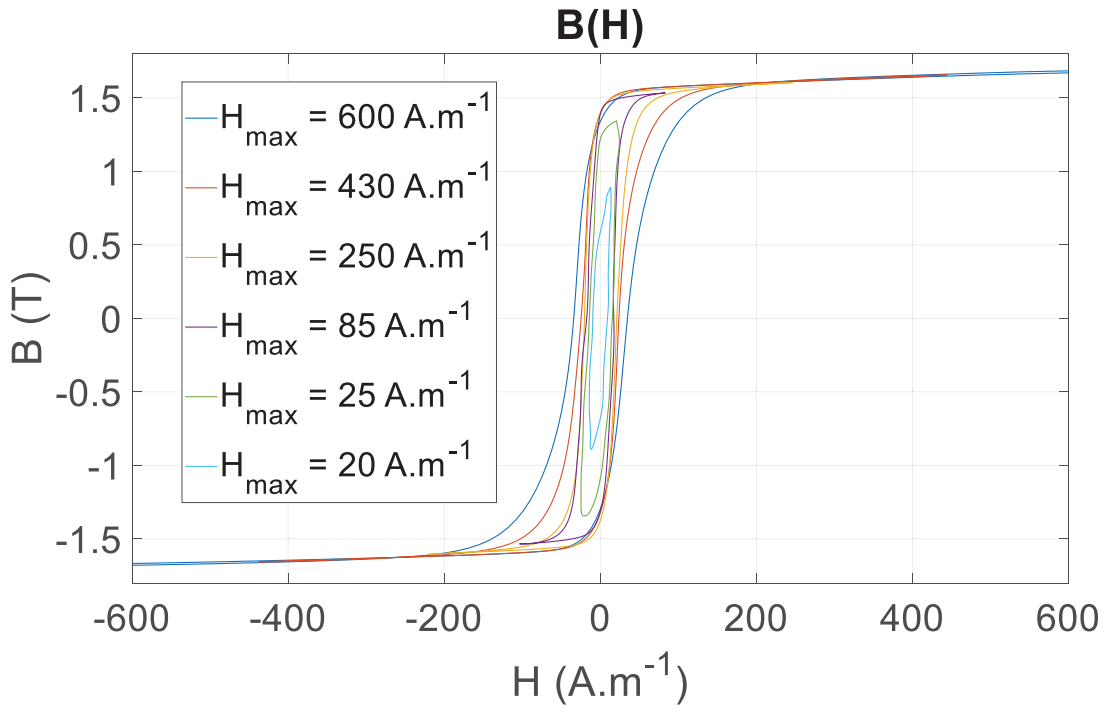

Figure 4-6: B(H) hysteresis cycles at the center of the instrumented FeSi sheet

We noticed that values of coercivity remain below 30 A/m and the value of induction at saturation approaching 1.8T. this implies there is a good tie with the manufacturer's information (ref. table 3-1) concerning the magnetic characteristic of steel sheet under test. The cohesion in the behaviours of magnetic indicators reveals at an effectiveness of the GMR sensor used in measuring the magnetic field intensity. We can therefore proceed to using it in a laminated core.

4.2.2 Laminated stack testing

Since from start, our main idea has been to know how magnetic field is distributed within a laminated core. In the quest for this information, we do not want to work with a totally saturated magnetic core. Rather, the stack of lamination will be excited in a way that, the lamination closer to the yoke of the SST will be set at saturation and the lamination farther away (on the top) should not reach saturation. That is to impose an environment where there is a gradient in the propagation of magnetic field; Thus a gateway to properly examine the features of our dual sensor configuration. The experiment was done following the protocol described in section 2.4.3.2 and data collected. Care was taken to always to place the sensors to follow the middle line of the yoke when displacing the instrument sheet from one position to the other. That is to ensure collinearity between the induction field and the lamination rolling direction. Data at each position were collected and processed to achieve the graphs of figure 4-7.

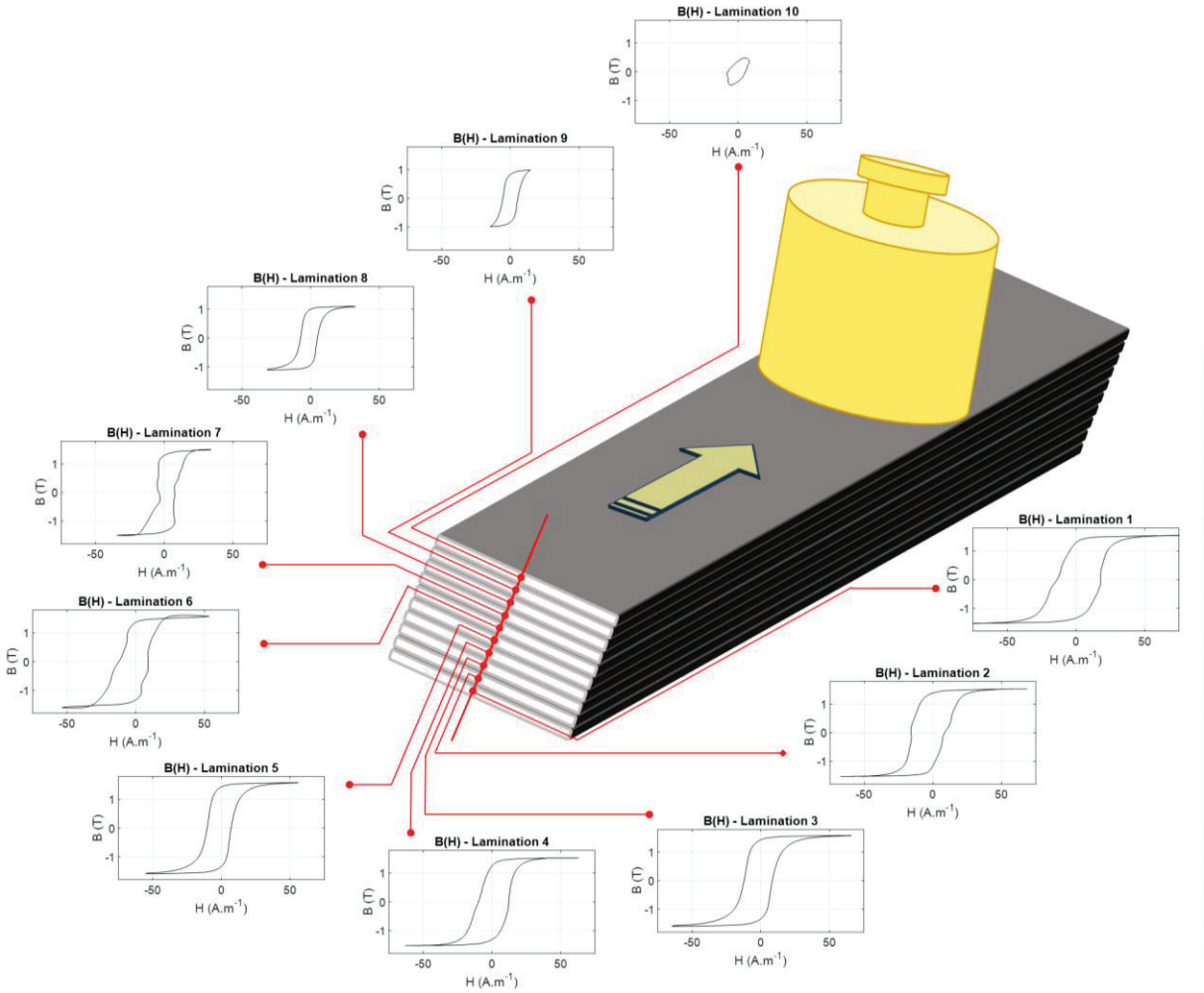

Figure 4-7 : Local hysteresis cycles within a ferromagnetic laminated core

Looking at the various loops, we spotted some asymmetries in the B_H curve of lamination 1,2,6,7 and 10. Undesired parasitic interference during the signals acquisition is probably at the origin of these distortion. Magnetic hysteresis indicators as spotted out on figure 4-8a are tracked as the experiment unfolds. From which the evolution of hysteresis losses and relative permeability as seen on figure 4-8(b) and figure 4-8(c) were analysed. The variations of the classic hysteresis characteristics plotted in figure 4-8 (quasi linear reduction of the hysteresis area and conservation of the relative permeability as a function of the lamination position) are consistent with our expectations and confirmed the inhomogeneity of the laminations magnetic state.

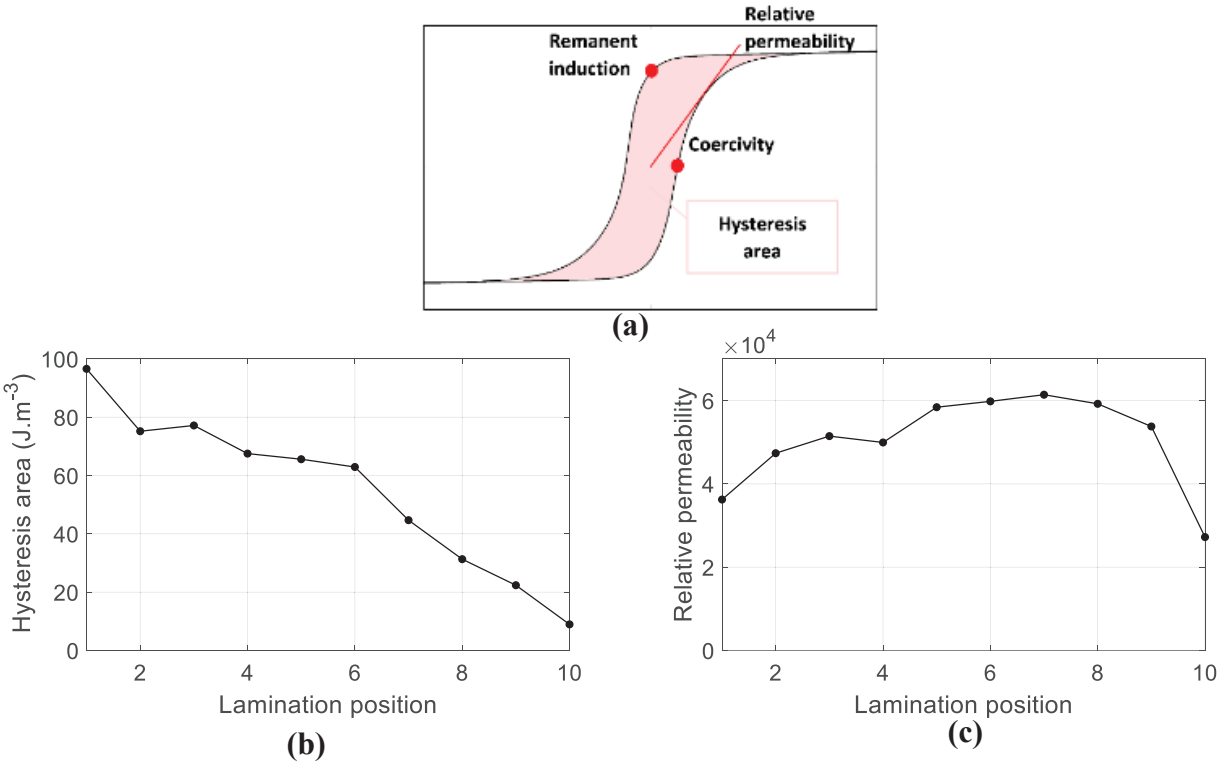

Figure 4-8: Local positon-dependent magnetic characteristic within a laminated magnetic core; (a)-The hysteresis cycle parameters , (b)– Evolution of the hysteresis area as a function of the lamination position, (c) – Evolution of the relative permeability as a function of the lamination position.

As a final validation step of the non-invasive characterization method, a 10 turns pick-up coil was wound all over the lamination stack. The electromotive force measured by this coil during the magnetization process was integrated and the drift corrected in post-processing just like we did for the PMNP sensor. This measurement returned the lamination stacks' average induction and was compared to the algebraic sum obtained considering the local measurements and the conservation of the magnetic flux by applying equation 3-2 and changing the number of laminations to 10 .

The total instantaneous magnetic field induction of overall stack of lamination and that of the 10 turns-surrounding coil were plotted against the magnetic field intensity as seen by the GMR and a hall sensor placed at the bottom of the stack: Thus the four graphs of figure 4-9.

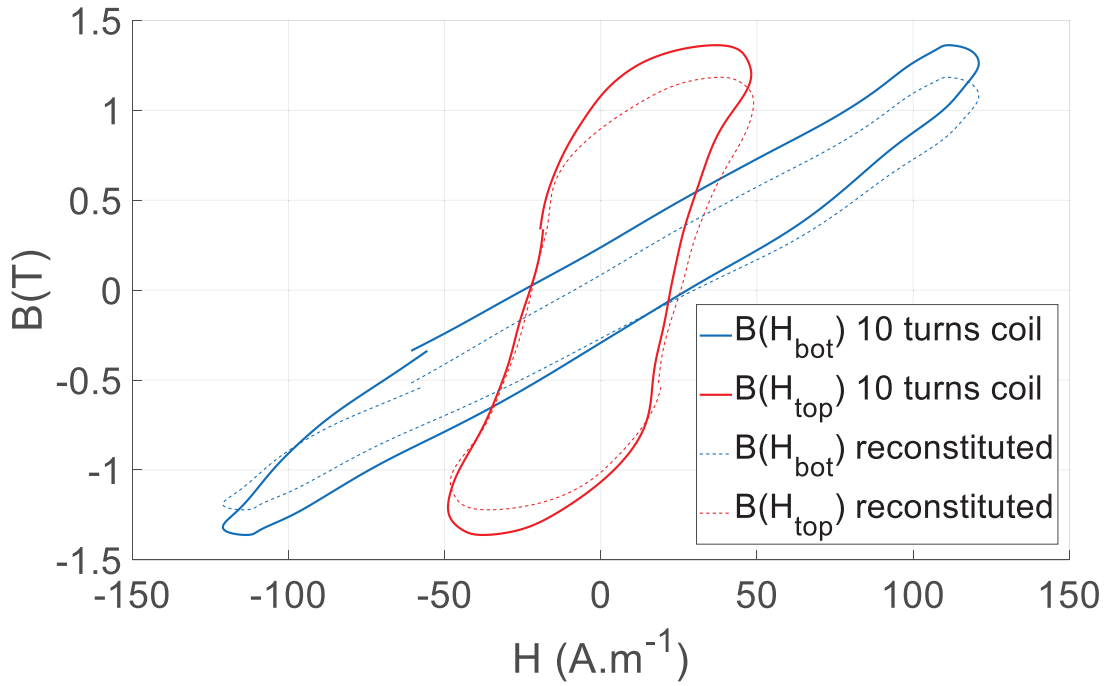

Figure 4-9 : Comparisons between the reconstructed laminated hysteresis cycles and the measured ones.

The shapes of the four graphs are same at a difference that the coil sees a little bit more magnetic induction. This mismatch is evaluated with the following formula:

$$Error(\%) = 100.abs\left(\frac{reconstituted(H(B)_{area}) - wound\ coil(H(B)_{area})}{wound\ coil(H(B)_{area})}\right) \quad (4\text{-}3)$$

The coherent and convergent results for both H_{BOT} and H_{TOP} reconstructed hysteresis cycles and experimental 10 turns coil cycles proves the validity of the non-intrusive sensors. Moreover, a 19 % and a 8 % error percentages (Eq. 5.4) in hysteresis loss can be calculated between the $H_{BOT}(B)$ and $H_{TOP}(B)$ hysteresis cycles respectively. These results therefore provide evidence for the feasibility of monitoring isolated magnetic lamination states through the ferromagnetic laminated core.

Inference

Unfortunately, due to the GMR substrate, the resulting sensor exhibits a still relatively large thickness of approximately 500 µm. However, a polishing stage was envisaged to reduce this thickness to less than 100 µm. The next set of experiments will be focalized on testing the non-invasive integrated PMNP + GMR sensor card. Its results will be compared to numerical results from finite element model for validation.

4.3 **Integrated PMNP + GMR sensor card**

Before indulging into the core of our experiment, there is need of doing a preliminary test of the card. That is the sensor patch is monitored at various frequencies and amplitudes.

4.3.1 Single sheet testing

A single ferromagnetic sheet was instrumented as described in section 2.5.3 and laid on the yoke. A frequency varying excitation signal ranging from 50Hz to 110Hz supplied to the exciting coil. The frequency generator voltage was adjusted for every measurement to maintain the excitation field maximum value as constant as possible. The material's response towards this excitation provides the data plotted on figure 4-10(a). Further analysis of the GMR+PMNP was done to evaluate the magnetic field strength range he can detect. The steel sheet instrumented with this card was subjected to magnetic field of varying strength (20 A/m to 140A/m) and the measurements of the card plotted as shown on figure 4-10(b). In addition, the 2D capability of the sensing solution was tested subsequently by positioning the sensor patch at 45° (figure2-26). As displayed in figure 4-10(c)., when the angle corrections were processed (projections), similar results were obtained in the x- and y-direction, which confirmed the 2D performance of the sensor card.

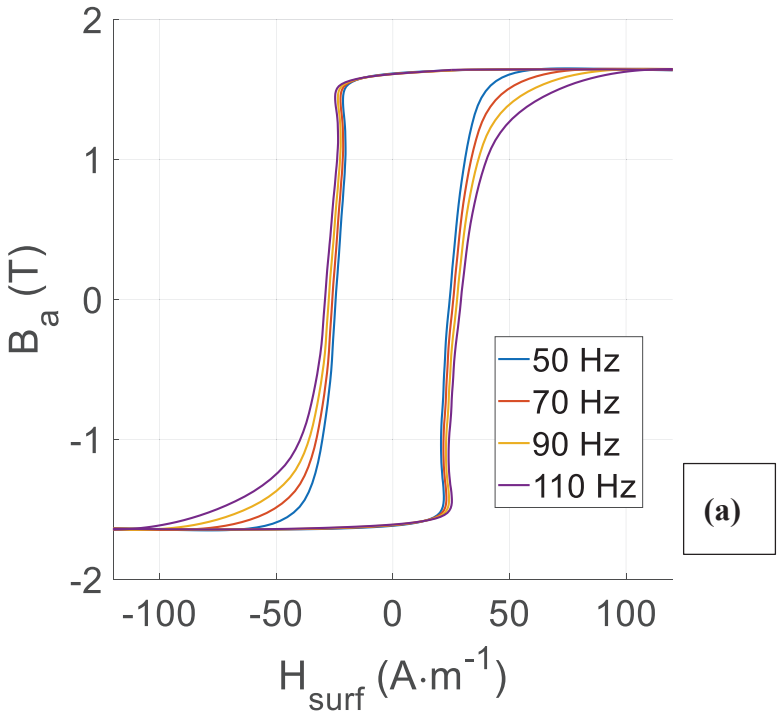

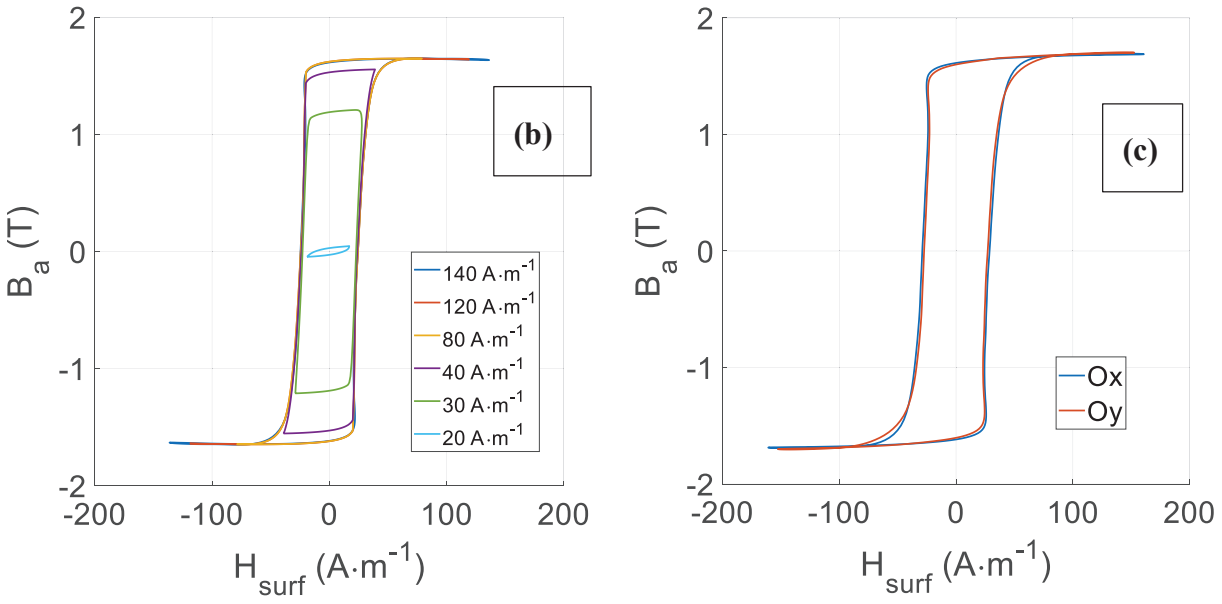

Figure 4-10 : PMNP + GMR sensor test of its features; (a) frequential test (b) amplitude detection test (c) 2-D measurement verification

4.3.2 Laminated stack testing

Still, the comparisons with the experimental observations were restrained to the X-axis . Various data recorded were measurements at the mid-length and at mid-width of the FeSi sheet.

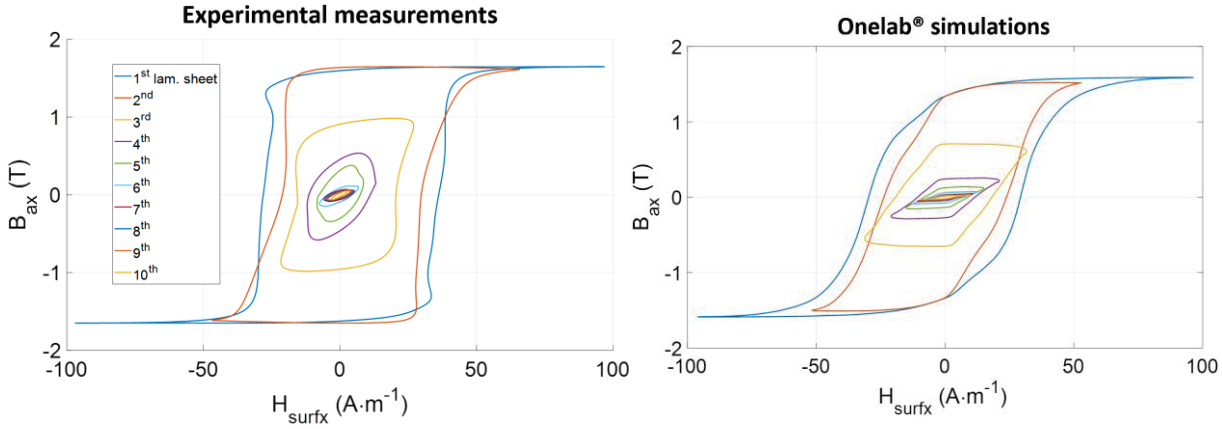

Figure 4-11 : Comparisons of the Onelab® simulations and experimental results in local tests.

At a glance, we notice that the resulting hysteresis cycles are not identical (probably because of an imperfect estimation of the J-A model parameters or to the simulation hypothesis).

Nevertheless, the evolution of the magnetic gradient in both cases have almost the same trend. we can infer therefore that the predictive capability of the simulation method is evident;

Moreover, a flexionis observed in the hysteresis cycles of the first, second, and third positions. Such behavior has already been noted in literature and associated with the dynamic losses during the magnetization process [106], [107].

Moreover, in-depth comparisons of the results were done with respect to the variation of a series of hysteresis cycle indicators as a function of the magnetic sheet position illustrated in figure 4-12. For a more quantitative evaluation, the uncertainty marker defined in Eq. 5.5 is applied to the five tested indicators to verify the global performance of the proposed simulation method. The results are presented in Table 4-3.

$$Error\ (\%) = \frac{1}{m} \cdot \sum_{i=1}^{m} \frac{\left|X_i^{sim} - X_i^{meas}\right|}{X_i^{meas}} \cdot 100\% \qquad (4\text{-}4)$$

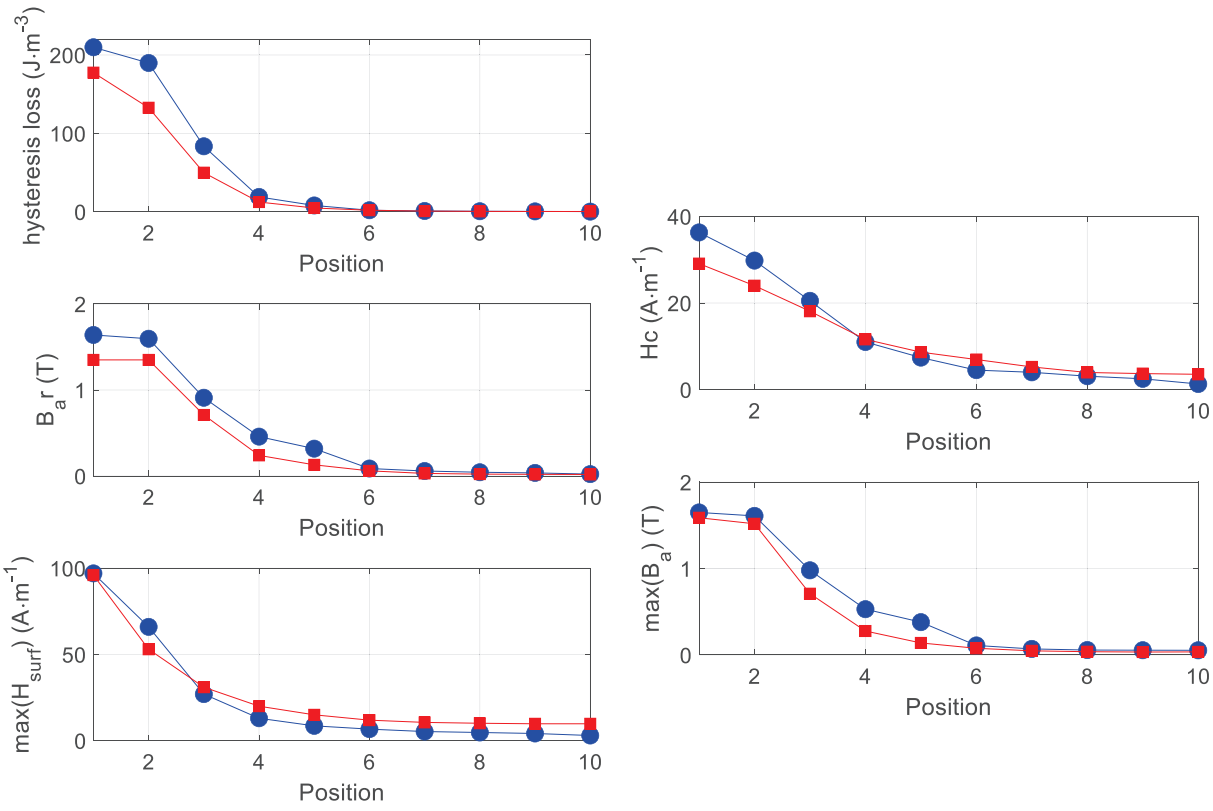

Figure 4-12 :Comparison measurements/simulations for the main hysteresis cycle indicators versus the magnetic sheet position.

Table 4-3 : Quantitative evaluation of the simulation method (m = 10 is the laminations number).

	Error (%)
Hysteresis loss	22
Hc	14.5
Br	32
max(B)	29.6
max(H_{surf})	32.7

Table 4-3 details the large errors between the simulation predictions and the experimental results. However, the Eq. 5-5 error definition is the average value of the relative error calculated on the ten sheet positions. Considerably lower error percentages could have been obtained by limiting those calculations to the bottom laminations at which the magnetic flux density is concentrated. The error is small for the first sheets (positions 1, 2, and 3). The measured magnetic quantities exhibit significant values for these positions and lead to a consequent ratio between the valuable signal and ambient noise. From laminations 4 upwards, the induction levels are in the same range as PMNP uncertainty. For these positions, the comparisons are inaccurate and considerably alter quantitative evaluation.

Inference

Accuracy was claimed to be improved and will be evaluated subsequently. Different paths can be followed to improve these results: from the simulation perspective, alternative vectorial hysteresis models have been described in scientific literature [108], [109]–[110]. Furthermore, the evaluation of the simulation parameters can be improved. Eventually, from the practicality perspective, the calibration of the GMR sensors and the signal treatment of PMNP can be improved.

4.4 Summary

This chapter is basically focused on the proof of PMNP concept, the accuracy evaluation of the various version of B_H measuring system namely: the PMNP and GMR lumped at a point and intergrated PMNP and GMR on a single patch. Results for proof of concept revealed a maximum error of 5% when compared to conventional sensors (search coil, needle probe sensor and encircling coil). Analysis of the quality and precision of the PMNP sensor at various frequencies ranging from 1Hz to 200Hz showed a good tie with results obtained using the 3

afore-mentioned conventional sensor; thus the PMNP is capable of sensing both surface and in-depth defects in material. Replacing the hall sensor with GMR attributed an added value of embedment of our B_H sensors of 500µm thickness within a stack of sheets. An error of 19% and 8% in hysteresis loss measurement when compared to a 10 turn overall coil measurements were portrayed for bottom and top measurement of the H field respectively. Furthermore, printing both PMNP and GMR sensor on the same patch of 30µm thickness reduced the possible air gap created when introducing the patch between two successive laminations. This setting gave the way forward for internal characterization and monitoring of core loss within a stack of 10 laminations in SST configuration. Comparison of magnetic distribution results to the numerical data gotten from the 2-D simulation of the finite element model of our electromagnetic system revealed a 22% drift. However, there was a good tie concerning the trend in the variation of magnetic parameters.

CONCLUSIONS AND FUTURE WORKS

The attractive features of the PMNP include ease of operation, high sensitivity to tight cracks, versatility, extremely high level of non-invasive potential, repeatability and reliability. Successful fabrication, implementation and testing for validity required a thorough selection of proper instrument and probes, optimisation test frequency and use of reference calibration standards. A slightly modified IEC 60404-3 standard and the search/surrounding coil measuring standard were used for characterization set-up and PMNP validation respectively. As per our objectives, we successfully achieved them through our experiments and verified the all except one stated at the beginning of our research; that is: "A match between Internal characterization of magnetic cores with respect to finite element simulations".

Initially, Non-invasive PMNP sensor was achieved by printing conductive ink directly to the laminate substrate. This method drastically reduces sensor volume and geometrical constraints. Magnetic induction and hysteresis results have been obtained using the printed sensor in frequency ranges of 1 Hz to 200 Hz, confirming this type of sensing can provide information on the internal magnetic behaviour of a magnetic lamination stack. Using a uniform magnetization model, the voltage detected by the needle probes method is almost equivalent to values measured using a classic search coil (one turn) wound around the 1–2-3–4 area as seen in figure 3-1. An average error of 0.89% is gotten when comparing the PMNPM is compared to coil measurements and search coil measurements. This initial test validates objectives 1 and 2 (ref. section 1.4)

Secondly, a whole non-invasive characterization method is proposed to measure the local hysteresis cycles through the laminated ferromagnetic core. PMNP sensor was used for the magnetic state characterization and miniaturized GMR for the magnetic field excitation. A lamination instrumented with these two sensor was set and moved successively to every position of the lamination pile. These results provide evidence for the feasibility of monitoring isolated magnetic lamination states through the ferromagnetic laminated core. When compared to surrounding coil conventional sensor, an 8% relative deviation with respect to the area of their hysteresis cycles. Due to the GMR substrate which is made of silicium, the resulting sensor exhibits a still relatively large thickness of approximately 270 µm. (objectives 1,2 and 3 validated)

Lastly, a polishing stage or thinning fabrication steps of the GMR was envisaged before its implementation. A 100-µm thick patch sensor (whose thickness can be reduced) combining MNPM and GMR sensors was proposed to provide in-plan magnetic characterization inside a ferromagnetic laminated sheet stack. The patch was tested first on a single ferromagnetic laminated sheet. A 2D measurement was done by comparing the two pairs of sensors in an experimental condition (sensor placed at an angle of 45°); the sensor provided same information in both directions. Next, stack tests were performed by positioning the sensor patch between every laminated sheet which revealed the inhomogeneous distribution of magnetic field within a magnetic core. Subsequently, comparisons with time-domain FEM simulations were proposed and used as validation for both the experimental and the simulation tools. An average relative error percentage ranging between 14.5% and 32.7% for the values of a series of hysteresis cycle indicators. This high level of error doesn't validate at a glance the hypothesis by which there is a match between measured and simulated results. Further improvements are of high need, towards achieving the measurement/simulation match; for instance: alternative vectorial hysteresis models, calibration of the GMR sensors and the signal treatment of PMNP can be improved.

Limitations

In spite the fact that, the proposed patch sensor provided accurate local measurements in all the performed tests, we noted the following limitations:

1) The PMNP electrical contacts were ensured from an additional layer of conductive ink processed in a further fabrication step. However, this solution is not optimal, and alternatives should be determined.

2) The fragility of the sensor patch was the most critical concern for high technology readiness level (TRL) developments. The thinned patch should be handled meticulously, especially during polish treatments. The use of flexible substrates is plausible but constitutes time-consuming developments beyond the scope of this project.

Future works and perspective

A flexible substrate is the long-term objective of this study. The following short-term prospects exist:

1) To test the sensor patch in a real-life situation. An instrumented power transformer was designed, including multiple sensor patches dispatched all over the transformer laminated magnetic core.

2) To evaluate the detection of ILFs or edge burrs with the sensor patch. A specific experimental setup including well-known defects should be designed for this purpose.

Applications

This technique can detect wall thinning, cracks, pitting, stress corrosion cracking, hydrogen embrittlement, carburization, denting and crud deposits etc. This technique finds a lot of applications in engineering industry including material sorting, determination of hardness, heat treatment adequacy assessment, material property determination, coating thickness measurements, and detection of defects in tubes, rods, bars, multilayer structures, discs, welds, blades and other regular as well as irregular geometries.

RESUME ETENDU (EXTENDED SUMMARY)

Introduction générale

L'énergie électrique, au centre du développement industriel, vise à être de bonne qualité au niveau des utilisateurs finaux. Il s'agit là d'une question cruciale pour les chercheurs en électricité, qui cherchent à limiter la quantité de pertes dans un système d'alimentation électrique, pertes qui se produisent lors de la conversion, du transport et de l'utilisation de l'énergie électrique. Si l'on se réfère à la configuration d'un système électrique standard, nous avons comme balises : les machines électriques statiques : transformateurs et machines électriques rotatives qui représentent principalement des composantes clées dans la production, le transport et la consommation d'énergie électrique. L'inefficacité et la défaillance de ces machines électriques ont des conséquences sur la fiabilité du système électrique. Le fournisseur d'énergie électrique du Cameroun (ENEO) a signalé de nombreuses explosions de ses transformateurs au cours des cinq dernières années. Les statistiques indiquent qu'en Europe occidentale, les pertes des systèmes électriques sont évaluées à 7,3 % de la distribution d'énergie. Une amélioration adéquate des conversions d'énergie dans ces machines et la mise en place d'un système de surveillance en temps réel permettra de limiter leur défaillance.

1.1 Contexte

1.1.1 Optimisation de la conversion d'énergie dans les machines électriques

Les machines électriques telles que les transformateurs, les moteurs, les alternateurs, les ventilateurs, etc., et les convertisseurs électromagnétiques rotatifs ont une partie commune appelée électroaimant qui joue un rôle majeur dans les conversions électromagnétiques. La conversion d'énergie est assurée par l'électroaimant qui est constitué d'un noyau magnétique autour duquel sont enroulés des fils. La loi actuelle de l'induction électromagnétique régit cette conversion en permettant le transfert d'énergie par l'intermédiaire du circuit magnétique. Les pertes magnétiques sont classées en pertes statiques et dynamiques.

Sur le plan technologique, de nouveaux capteurs ont été développés pour contribuer à limiter la maîtrise et le contrôle de la répartition des pertes magnétiques au sein d'un noyau magnétique.

Pour améliorer les performances des machines électriques, la méthode de conception par homogénéisation est appliquée pour obtenir la topologie optimale d'une structure dans les

champs magnétiques. Cette méthode est appliquée au niveau de la conception du noyau magnétique.

1.1.2 Systèmes de surveillance en temps réel de l'état du noyau magnétique

Au niveau de l'usine, la fabrication du noyau magnétique est source de défauts. Lors du découpage des tôles d'acier, des bords en relief appelés bavures sont malheureusement présents. L'incident défectueux se produit lorsque les tôles sont pressées l'une contre l'autre ; c'est-à-dire que les bavures créent une liaison électrique entre deux tôles successives. Cette liaison donne lieu à des courts-circuits au sein de l'empilement de tôles ; on parle alors de défauts inter-laminaires (ILFs) qui réduisent le rendement global de conversion d'énergie du noyau et contrecarrent le gain obtenu par le laminage du noyau. Lors de leur installation, les machines électriques peuvent rencontrer au cours de leur fonctionnement des défauts tels que l'inefficacité du système de refroidissement, des défauts de protection des enroulements et des défauts d'isolation et bien d'autres encore. Bien que des améliorations aient été réalisées, il reste encore beaucoup à faire pour obtenir un système de conversion d'énergie sans perte.

1.2 Énoncé du problème

La durée de vie d'une machine électrique est étroitement liée à sa capacité à gérer/se remettre des contraintes. Le suivi et la bonne connaissance de son fonctionnement nous orientent vers une gestion plus efficace de ces appareils sur le long terme. La maintenance prédictive et curative de ces équipements nécessite d'avoir accès à des informations sur la santé de leur noyau magnétique.

A ce jour, il n'existe pas en France ni au Cameroun d'entreprises privées mettant en œuvre des méthodes d'Analyse Non Destructive afin d'évaluer à la fois la présence d'éventuels défauts, les propriétés physiques de la pièce et le suivi de l’état de santé du matériau dans le temps en laissant des capteurs en permanence sur/dans les appareils.

1.3 Raison d'être de l'étude

Les machines électriques sont au cœur de toutes les industries et sont utilisées de manière intensive jusqu'à un seuil de fonctionnement presque proche. En fonction de leur application, elles subissent différents types de contraintes. Les dommages causés par les contraintes électriques sont en majorité des points chauds, résultat d'une surchauffe locale.

La première tentative a consisté à décomposer le noyau magnétique monobloc en une pile de tôles. Malheureusement, il est impossible d'insérer de manière non intrusive une solution de mesure magnétique classique au sein de l'empilement de tôles pour aider à identifier ces phénomènes indésirables.

La deuxième tentative pour réduire ces pertes est de comprendre en réalité ce qui se passe à l'intérieur de ces laminations. Les résultats expérimentaux locaux n'ont jamais été disponibles pour valider le comportement de ces simulations en raison des limitations des capteurs actuels.

La troisième tentative de solution est le développement d'un capteur portatif par Krismanic et al pour l'analyse de la distribution locale des champs magnétiques et des pertes.Nous nous rendons compte que les capteurs magnétiques et les montages expérimentaux actuels sont limités à des informations moyennées en section transversale ou limités à des mesures de surface.

Tout au long de cette thèse, nous développerons la technique d'impression ainsi qu'un dispositif expérimental à partir d'un circuit magnétique laminé. Celui-ci jouera le rôle de preuve de concept et validera l'utilisation de pointes magnétiques imprimées comme outil de caractérisation magnétique. Combiné à la modélisation, ce nouvel outil permettra, entre autres, d'améliorer la compréhension des phénomènes d'aimantation.

1.4 Objectifs et feuille de route

1.4.1 Objectif général

L'objectif de cette thèse est d'étudier et de mettre en œuvre un système non intrusif pour la surveillance en temps réel d'un noyau magnétique en utilisant une méthode de sonde magnétique imprimée.

1.4.2 Objectifs spécifiques

Cette recherche a été menée de manière progressive avec les étapes suivantes :

1. Accès à des mesures locales de l'intensité du flux magnétique par le biais d'un capteur imprimé embarqué de sondes à pointes magnétiques.

2. Caractérisation non invasive de l'hystérésis magnétique locale d'un noyau ferromagnétique laminé.

3. Illustration expérimentale de la distribution inhomogène du champ magnétique à l'intérieur d'un noyau magnétique laminé.

4. Correspondance entre la caractérisation interne des noyaux magnétiques et les simulations par éléments finis.

5. Surveillance en temps réel de l'état de santé d'un noyau magnétique feuilleté par un contrôle ponctuel de son comportement magnétique.

Pour atteindre ces objectifs, les actions suivantes ont été entreprises

1. Construction d'un laminé instrumenté.
2. Validation de la faisabilité du capteur imprimé.
3. Développement d'un système de mesure non-intrusif.
4. Simulation du modèle expérimental équivalent

1.5 Organisation de la thèse

Cette thèse est regroupée en 4 chapitres

Le chapitre un présente le comportement et le concept ferromagnétique.

Le deuxième chapitre décrit le concept de capteur à pointes magnétiques, dont les principes et les technologies sous-jacents sont discutés.

Le chapitre trois aborde l'aspect simulation numérique du travail .

Le chapitre quatre est consacré aux résultats et à la discussion.

Les conclusions tirées de ce travail de recherche et les domaines d'investigation potentiels pour des travaux ultérieurs sont donnés à la fin.

CHAPITRE 1 :

ETAT D'UN NOYAU MAGNETIQUE : MICRO-MAGNETISME, EVALUATION NON-DESTRUCTIVE

La notion de "contrôle non destructif (CND)" est un ensemble de méthodes qui permettent de caractériser l'état d'intégrité de structures ou de matériaux, sans les dégrader, que ce soit en cours de production, d'utilisation ou dans le cadre de la maintenance.

1.1 Le magnétisme

Le magnétisme est la force exercée par les aimants lorsqu'ils s'attirent ou se repoussent.]. L'électromagnétisme est le terme est mis en évidence grâce à Michael Faraday qui a montré qu'un aimant en mouvement crée un courant électrique dans un fil placé à proximité : c'est l'induction électromagnétique.

Les électro-aimants constituent notre centre d'intérêt tout au long de notre travail.

Cette section présente donc les propriétés du champ magnétique, le champ magnétique au niveau microscopique. Elle décrit aussi le phénomène de domaine magnétique et le mécanisme de l'hystérésis magnétique.

1.2 Surveillance de l'état

Dans un environnement d'exploitation hostile, dans des conditions climatiques difficiles et très variables, la difficulté et le coût de la maintenance et de l'exploitation des machines électriques augmentent. L'amélioration de la fiabilité des équipements, la réduction des coûts d'exploitation et de maintenance des équipements industriels ont incité les chercheurs à étudier davantage le domaine de la surveillance des conditions et de la détection des défauts. Néanmoins, il existe une demande importante pour un degré élevé de maintenance afin de fournir une production d'énergie sûre, rentable et fiable avec une durée de vie acceptable des équipements. D'où l'apparition d'un nouveau paradigme appelé maintenance prédictive, qui repose sur la surveillance constante des conditions de fonctionnement des équipements et la prévision des défaillances. La maintenance conditionnelle fait partie de la maintenance prédictive.

L'approche est basée sur le diagnostic continu de l'état physique ou opérationnel des matériaux composant les équipements pendant leur utilisation. Elle est contraire à celle qui s'en tient aux données statistiques et aux calendriers planifiés programmant les activités de maintenance

En fait, le composant principal du système de production d'énergie, à savoir le noyau et la base du stator du générateur, est en permanence sujet à des dommages, des fissures, des défauts et des déformations à long terme. Ceci est dû à la position qu'ils occupent dans la transmission du mouvement mécanique. Compte tenu de la difficulté et du coût de la maintenance de ces pièces, certains défauts sont ignorés, ce qui compromet fortement la sécurité de fonctionnement. Notre étude est centrée sur les défauts affectant les matériaux ferromagnétiques constituant le noyau magnétique de ces machines : c'est le « *magnetic core condition monitoring (MCCM) ».*

De ce fait, dans les sous-sections suivantes, nous allons parler du principe du MCCM et de ces avantages. Nous avons également abordé les différents défauts/ bavures inter-laminaires et les différents stratégies abordées lors de l'application du MCCM.

Jusqu'à présent, les principaux schémas de surveillance des conditions structurés par d'autres chercheurs ont été examinés ; pour que la MCCM tienne, soit cohérente et fiable tout au long de la vie des systèmes, il y a une condition essentielle qui doit être respectée lors du choix d'une technique de mesure ; elle doit être non invasive, non destructive pour l'équipement sous contrôle, ; donc une technique non destructive est requise à cette fin ; il est donc nécessaire pour nous de choisir idéalement une technique qui nous permettra d'atteindre nos objectifs.

1.3 Méthodes de contrôle non destructif

Dans cette partie, nous évaluons les techniques de maintenance conditionnelle par rapport à des critères prédéfinis. Cela nous aidera à sélectionner efficacement une technique sur laquelle nous nous battrons en duel. En outre, une présentation de l'essai par courants de Foucault abrégé en anglais(ECT) est faite ; en abordant les différents capteurs de contrôle par courant de Foucault et plus particulièrement la technique de la sonde à pointe magnétique, de leur principe de fonctionnement de base et de l'effet de peau.

Chaque matériau connu, indépendamment de son type, de sa forme et de sa composition, possède une signature magnétique unique en réponse à ses propriétés physiques. L'apparition et la propagation progressive d'anomalies dans les matériaux est un sujet de préoccupation. Une solution à ce problème consiste à mettre au point des techniques de mesure magnétique localisée. Par conséquent, un couplage "hystérésis magnétique - technique magnétique locale"

pourrait être une solution alternative adéquate pour la caractérisation et le contrôle non destructif , micro-magnétique des matériaux magnétiques.

CHAPITRE 2 :

CAPTEUR POINTE MAGNETIQUE IMPRIMEE

Jusqu'à présent, les méthodes de CND classées comme micro-magnétiques parmi lesquelles ECT, MIP et MBN sont les plus utilisées. Leurs caractéristiques individuelles ont déjà établi certaines limites dans la mesure. En les combinant, on obtient une plus grande portée de mesure pour les diagnostics. Malgré la stratégie de combinaison, il existe toujours certaines limites dans leurs capacités de mesure. Le capteur pointe magnétique imprimé en abrégé en anglais(PMNP) est développé et examiné afin de surmonter les obstacles susmentionnés. La PMNP s'inspire du principe de la MNP et vise à atteindre les caractéristiques suivantes : test fiable, capacités de mesure reproductibles, localisation de tout défaut et taille non invasive. Ce chapitre est donc axé sur l'évaluation de ses capacités et prouver le concept. Pour ce fait, des étapes majeures sont franchies : le développement de sa théorie selon la physique, la conception et les tests de caractéristiques.

2.1 Concept de la sonde à pointes magnétiques

Ici, nous allons présenter le concept de la sonde pointe magnétique, son principe de fonctionnement, les recommandations pour une mesure optimale et les différentes versions de sondes jusqu'ici implémentées

La MNP est basée sur l'exploitation de l'interaction électromagnétique à l'intérieur d'une section d'un spécimen lorsqu'il est soumis à un champ magnétique. En effet, la densité du flux magnétique traversant la section fermée considérée décrit directement l'état de cette section qui résulte de la réaction magnétique en ce point. La méthode de la sonde magnétique à pointe consiste à placer deux sondes à pointes magnétiques perpendiculairement à la surface du spécimen étudié. Les sondes permettent de mesurer la différence de potentiel entre les deux points de contact avec l'échantillon.

Fondamentalement, pour une mesure optimale et plus précise du flux induit dans l'échantillon à l'aide de la MNP, et pour que les hypothèses formulées ci-dessus soient valables, certaines précautions sont recommandées par certains chercheurs lors de la réalisation de tests expérimentaux à l'aide de la MNP. Parmi celles-ci, nous avons :

- -un espacement de 10mm entre les sondes doit être respecté pour un aperçu efficace de la densité du flux magnétique dans la région spécifiée entourée par la sonde pour une tôle d'acier électrique à grains orientés [66].
- -Le rapport entre l'espacement des sondes et l'épaisseur de l'échantillon (1-2/d) doit être significatif [69].
- La charge admissible sur la pointe d'une sonde à pointe est de 300g.
- Il est également recommandé que la distance des bords soit supérieure à la moitié de l'épaisseur de l'éprouvette.
- Le flux de fuite dans l'air magnétisé proche de la surface doit être négligeable [71].

Compte tenu des limitations mentionnées ci-dessus, des versions modifiées/améliorées de la MNP ont été proposées afin d'atténuer ou d'annuler l'impact des sources d'erreur. Nous avons ainsi identifié les points suivants :

- Les pointes utilisées dans la MNP étaient constituées de laiton et montées chacune sur une tige de polystyrène. Cette conception permet d'éliminer les signaux intrusifs [75]. En plaçant les pointes près de la bobine de recherche pour une mesure comparative, Wilkins et al ont obtenu un bon accord pour toutes les mesures.
- La sonde nécessaire pour les films minces présente plus d'avantages que tout autre capteur CND lorsqu'il s'agit d'accéder à des mesures locales dans des zones très minuscules de manière non invasive. Ceci s'inscrit dans la même ligne que nos objectifs, et constituera donc le tremplin pour notre conception visant à réduire l'épaisseur à la gamme des micromètres ;

2.2 Technique de la sonde à pointes magnétique imprimée (PMNP)

Les pointes magnétiques classiques couramment utilisées en CND, composées de sondes à ressort de 1,5 mm, sont incompatibles avec la surveillance en ligne/en service des processus industriels. L'idée est de contribuer à améliorer le champ d'application de la méthode MNP en réduisant les pointes à une piste d'encre conductrice imprimée. La taille relativement petite du capteur est appropriée pour un système embarqué stable qui transmettra continuellement des informations sans interruption nécessaire.

2.2.1 Principe de la sonde à pointes magnétiques imprimées utilisant l'électronique imprimée

Le concept de la PMNP consiste à dessiner des motifs conducteurs sur un substrat de telle sorte que, lorsqu'ils sont en contact électrique avec le matériau, ils soient équivalents au test MNP. Deux techniques d'impression ont été employé : Impression à l'aide d'un masque, Impression à l'aide d'une machine à jet d'encre

2.3 Validation de la PMNP

L'idée de la PMNP non invasive a été concrétisée. Comme il s'agit d'une nouvelle version de la MNP, sa caractérisation et sa comparaison avec les méthodes ECT déjà existantes sont d'une importance capitale. Le résultat de la comparaison confirmera ou infirmera nos revendications et notre hypothèse.

2.3.1 Configuration expérimentale

Des investigations préliminaires ont été menées sur un matériau ferromagnétique couramment utilisé. L'acier au silicium laminé à grains orientés (GO) a été choisi pour son application historique dans le noyau magnétique des transformateurs et des inducteurs.

L'idée de base est de trier au hasard une tôle magnétique isolée à partir d'une tôle d'acier destinée à être utilisée dans les noyaux magnétiques.

Notre nouveau capteur est censé être capable de transmettre des informations sur la densité du champ magnétique une fois intégré dans le noyau laminé d'une machine électrique. L'intensité du champ magnétique de la surface supérieure et inférieure est mesurée par deux capteurs à effet Hall, l'un placé en bas et l'autre en haut du paquet de feuilles.

L'utilisation du capteur à effet Hall ne garantit pas une mesure locale simultanée de l'intensité du champ magnétique au même endroit où la densité du champ magnétique est mesurée.

2.4 Miniaturisation du système d'acquisition de B_H couplé à la magnétorésistance

La miniaturisation du système de mesure de B_H consiste à disposer de capteurs de taille micro capable d'accéder à l'induction et à l'intensité du champ magnétique local à une position particulière.

L'idée dans cette étude, est de placer le substrat de silicium portant la GMR à côté des points de contact du PMNP. Néanmoins pour une mesure plus optimale, il existe une possibilité de polir le substrat de silicium et d'obtenir une épaisseur d'environ 10µm [87], [88]. Le polissage

permettra de réduire l'entrefer incident créé par l'insertion du capteur dans une pile de laminés. Cependant, une attention et un soin particuliers doivent être apportés à la manipulation de ce capteur très fin.

2.4.2 Magnétorésistances

La magnétorésistance est la capacité d'un matériau à modifier sa résistance en présence d'un champ magnétique. Cet attribut des matériaux magnéto-résistants, leur haute sensibilité et leur précision en font de bons candidats pour être utilisés comme transducteurs de champ magnétique.

Dans notre conception, nous avons opté pour une configuration à deux couches étant donné que notre objectif est d'obtenir la GMR la plus fine possible. La couche dure est fixée dans la direction de la sensibilité.

2.4.3 Montage expérimental

Le dispositif expérimental est observé pour deux régimes différents. Le premier est une évaluation unique d'une feuille instrumentée. Le second est un essai dans un scénario de noyau laminé dans lequel la feuille instrumentée est placée dans une pile de 10 feuilles d'acier.

Une seule tôle d'acier GO est instrumentée avec un PMNP et un GMR. Le PMNP est imprimé en suivant le protocole d'impression de masque décrit dans la section 2.2.2.

En outre, un test sur une pile de tôles est réalisé pour imiter un environnement similaire à celui du noyau magnétique stratifié. Notre idée ici était de créer intentionnellement un gradient d'états magnétiques à travers le noyau laminé et de valider la précision de la méthode de caractérisation non invasive.

Le capteur miniaturisé qui en résulte a montré des résultats impressionnants

2.5 Capteur B_H embarqué portable 2-en-1

L'idée est d'imprimer tous les capteurs sur un seul substrat. Ceci étant, l'épaisseur totale du capteur peut être encore réduite par des techniques de polissage pendant la fabrication [88]. Notre objectif est d'obtenir une épaisseur de substrat inférieure à 1 nm.

2.5.2 Conception du capteur PMNP/GMR

Le cheminement et la disposition de deux capteurs PMNP et de deux GMR sont effectués selon la conception présentée à la figure 2-23. La figure la plus à gauche montre comment les capteurs sont acheminés. La figure la plus à droite montre la disposition de deux GMR. Les deux magnétorésistances ont leur direction de sensibilité décalée de 90° dans le plan vertical. Une fois fabriqué, traité thermiquement et câblé, le capteur subit un test de caractérisation pour évaluer ses paramètres de référence.

2.5.3 Essai sur une seule feuille

Le montage expérimental semble conforme à la norme IEC 60404-3, comme décrit dans les sections 2.4 et 2.3. Avec la feuille instrumentée, des tests de fréquence et de magnitude ont été effectués pour déterminer les fréquences opérationnelles et le seuil de détection de la magnitude. De plus, la capacité 2D a été observée en plaçant le capteur à 45° par rapport à la ligne centrale de la feuille dans le plan de la surface, comme le montre la figure 2-26.

Avec toutes les expérimentations effectuées jusqu'à présent, les résultats obtenus avec le capteur le plus fin seront comparés aux résultats théoriques. Les outils d'analyse numérique " modélisation par éléments finis " et le logiciel " ONELAB " seront utilisés pour résoudre les équations mathématiques décrivant le phénomène d'électromagnétisme dans notre travail.

2.6 Résumé

Utilisé comme capteur magnétique, le capteur PMNP tire également parti de sa géométrie miniaturisée pour étendre son champ d'application à un capteur magnétique intégré à l'intérieur d'une pile de tôles pour le test/évaluation de l'homogénéisation dans les noyaux magnétiques. Les pertes d'énergie dans le noyau magnétique nuisent fortement aux performances des machines électriques.

CHAPITRE 3 :

SIMULATION ET ANALYSE NUMERIQUE DE L'INHOMOGENEITE DE DISTRIBUTION DE CHAMP MAGNETIQUE

Les matériaux ciblés pour ce travail de recherche sont les matériaux ferromagnétiques. L'augmentation de l'efficacité énergétique des matériaux dépend directement des propriétés magnétiques de ces matériaux en termes de pertes de puissance. Pour produire des machines économes en énergie, il est nécessaire de connaître les propriétés magnétiques réelles du matériau utilisé. Ceci peut être obtenu par des mesures et à cette fin, il est préférable d'utiliser la méthode de mesure définie par la norme. Afin d'optimiser le système de contrôle des machines basé sur le contrôle non destructif, l'information locale sur la façon dont les interactions électromagnétiques sont une nécessité. Expérimentalement, nous avons réalisé un capteur embarqué non intrusif pour des mesures locales. De plus, il est nécessaire de savoir comment les choix de paramètres peuvent avoir un impact sur le fonctionnement global du système [92] ; sans avoir à construire de nombreux prototypes, ce qui est très coûteux. Des outils de simulations sont ensuite utilisés pour modéliser le banc expérimental avec différents paramètres associés. A partir de ces modèles, une analyse numérique de l'expression mathématique de divers phénomènes physiques est effectuée pour obtenir des solutions. Sur la base de ces analyses, les chercheurs peuvent ainsi prédire un certain comportement lorsque certains changements particuliers sont apportés [18]. Il existe différents outils de modélisation/simulation en fonction de leurs caractéristiques : moins lourd (convivial), temps de résolution, niveau d'exactitude des solutions, phénomène physique observé, interface graphique d'accommodation pour une observation plus illustrative, pour n'en citer que quelques-uns.

Étant donné que notre objectif principal est de pouvoir prédire la distribution locale du champ magnétique dans un noyau magnétique dans un processus de temps court, nous utilisons le modèle d'hystérésis théorique Jiles-atherthon. De plus, la justification de notre étude a révélé que des modèles numériques d'inhomogénéité dans la distribution magnétique ont déjà été réalisés par des chercheurs et que les pertes par courants de Foucault dans un noyau laminé ont récemment été évaluées numériquement par M. Taghizadeh et al [99],K. Bitsi et al[100] et E.Lamprecht[101] qui n'avaient jamais été confrontés expérimentalement. Il est donc

avantageux et plus logique pour nous d'appliquer la même méthode numérique lors de leur recherche ; c'est-à-dire FEM (méthode des éléments finis).

3.1 Methode éléments finis en utilisant l'interface ONELAB

Pour le développement de notre modèle ferromagnétique, nous avons utilisé la suite logicielle open-source Onelab® avec des modèles mathématiques hystérétiques génériques intégrés : modèles de formulation linéaire, anhystérétique et Jiles-atherton[102]. Les valeurs appropriées des paramètres obtenus empiriquement à partir de l'expérimentation sont saisies dans le programme et les résultats de la simulation sont traités et analysés. Tout au long de notre thèse, l'accent ne sera pas mis sur la modélisation théorique du comportement ferromagnétique.

Le domaine spatial étudié est circonscrit en utilisant le demi-arc de cercle qui tient compte de l'infini. L'âme feuilletée constituée d'une feuille de 10 GO FeSi est représentée par 10 rectangles (280 mm x 0,3 mm) représentant le domaine du fer. Entre deux tôles successives, un rectangle (280x0,03mm) est placé pour rendre compte du revêtement isolant présent sur chaque tôle : c'est le domaine de l'isolation. la bobine d'induction représentée par deux rectangles de couleur bleu ciel (2) ; les deux rectangles représentent la vue de face de la bobine d'excitation lorsqu'elle est coupée suivant le plan (x,y).

Concernant le maillage, chaque tôle d'acier en fer(FeSi) est représentée par un domaine ayant 4 discrétisations dans le plan d'épaisseur à l'aide de mailles triangulaires. Chaque couche isolante constitue le domaine d'isolation qui comporte trois discrétisations utilisant toujours des mailles triangulaires. Les autres domaines constituant le système sont maillés à l'aide de splines.

3.2 model Jiles Atherthon

Nous présentons ici le model de la loi des matériaux choisi. Ainsi que ces paramètres et leurs différents impacts sur un cycle hystérésis.

3.4 le Post-processing

Les valeurs calculées de l'intensité du champ magnétique et de la densité du champ magnétique sont exportées vers MatlabTM pour être tracées. La boucle d'hystérésis est obtenue en traçant B contre H. la boucle B(H) possède des indicateurs qui permettent d'apprécier le comportement

intrinsèque dans le noyau magnétique. Nous distinguons la densité de champ rémanent et l'intensité de champ coercitif et la perte d'hystérésis qui est la zone couverte par l'ensemble de la fonction B(H). La surface est calculée numériquement en intégrant la fonction B(H) par rapport à Hmax et Hmin

3.5 Résumé

La complexité des géométries des noyaux magnétiques est un inconvénient supplémentaire à la simulation du comportement magnétique local dans les dispositifs électromagnétiques. Nous modélisons ainsi notre système électromagnétique en utilisant le FEM auquel la loi modèle JA du matériau a été appliquée telle qu'implémentée dans l'environnement ONELAB. Les résultats de la simulation du modèle de densité de flux magnétique dans un empilement de tôles sont décrits dans ce chapitre. Cependant, l'applicabilité de notre schéma de simulation dans l'étude des modèles de champ magnétique local d'une seule stratification dans une pile a été étudiée. Les solutions numériques une fois obtenues sont traitées à l'aide du logiciel Matlab. La distribution magnétique dérivée attend toujours la validation des mesures expérimentales ; il fait l'objet du chapitre suivant

CHAPITRE 4 :

RESULTATS ET DISCUSSIONS

Avoir accès spontanément à la distribution locale des flux au sein d'un magnétique feuilleté de manière non intrusive constitue le squelette de nos recherches à ce jour. Nous avons affirmé que le capteur PMNP que nous avons fabriqué offre des portes ouvertes pour accéder au flux de la ligne de distribution de flux. En tant que nouveau format de capteur, il est nécessaire de faire au début une série de tests avec d'autres méthodes de détection qui ont été acquises en standard. Ceci constitue notre premier ensemble d'expériences dont l'objectif est de faire une comparaison relative au test standard existant et de valider la fonctionnalité d'intégration/non invasive de notre capteur. les capteurs de caractérisation de base PMNP et GMR pour B et H respectivement, étaient jusqu'à présent éloignés ; mais a été mis à niveau vers un positionnement plus groupé / concentré des deux capteurs. La prochaine série d'expériences a ensuite été orientée vers l'évaluation de la précision de la configuration de détection miniature B_H. De plus, une combinaison de capteurs 2 en 1 du capteur PMNP et GMR pour obtenir une insertion transparente dans le noyau magnétique a été conçue. Ainsi, l'ensemble des résultats obtenus à partir d'expériences utilisant le capteur 2 en 1 a été comparé aux résultats numériques simulés du modèle d'éléments finis.

4.1 Validation du PMNP

Il s'agit de la validation expérimentale du capteur PMNP nouvellement développé en tant que méthode CND magnétique locale et outil d'introduction aux études d'homogénéisation dans un noyau laminé. La configuration expérimentale SST modifiée décrite à la section 2.3.1 a été utilisée pour les deux procédures de validation expérimentale

Ces résultats fournissent la preuve de la faisabilité de la surveillance d'états de laminage magnétique isolés à travers le noyau magnétique laminé. En comparant les surfaces entre les cycles d'hystérésis mesurés et moyens globaux, l'erreur obtenue avec H_{BOT} est de 13,5%, et seulement 2,1% pour H_{TOP}.

En somme, nous avons pu montrer qu'en utilisant les mêmes propriétés d'excitation du circuit magnétique, la tension détectée par la méthode des sondes à pointes magnétiques (MNP et PMNP) est presque équivalente aux valeurs mesurées à l'aide d'une bobine de recherche

classique (un tour) enroulée autour la zone 1–2-3–4 comme le montre la figure 2-1. Des résultats d'induction magnétique et d'hystérésis ont été obtenus à l'aide du capteur imprimé dans des gammes de fréquences de 1 Hz à 200 Hz ; Ainsi, le PMNP est un bon candidat pour la détection en profondeur des défauts dans les matériaux ainsi que la détection des défauts de surface.

4.2 PMNP + GMR regroupés à un point particulier

Dans l'expérience précédente, la taille du capteur à effet hall mesurant l'intensité du champ nous empêche de réaliser une mesure B_H locale simultanément au même endroit. Le capteur à effet Hall est donc remplacé par un capteur GMR qui sera placé à côté du PMNP comme décrit dans la section 2.4.2. une pré-caractérisation des capteurs doubles sera effectuée pour être sûr qu'il se comporte comme prévu. Cela est nécessaire avant de procéder à son intégration sans soudure dans un noyau laminé.

Après le test de pré-caractérisation, nous avons remarqué que les valeurs de coercivité restent inférieures à 30 A/m et la valeur d'induction à saturation proche de 1.8T. Ceci implique qu'il y a un bon lien avec les informations du fabricant (réf. tableau 3-1) concernant la caractéristique magnétique de la tôle d'acier en essai. La cohésion dans les comportements des indicateurs magnétiques révèle une efficacité du capteur GMR utilisé pour mesurer l'intensité du champ magnétique. On peut donc procéder à son utilisation dans un noyau feuilleté.

S’agissant de test sur un empilement de tôles, en vue de la validation de la méthode de caractérisation non invasive, une bobine de détection de 10 tours a été enroulée sur toute la pile de laminage. La force électromotrice mesurée par cette bobine lors du processus d'aimantation a été intégrée et la dérive corrigée en post-traitement comme nous l'avons fait pour le capteur PMNP. Cette mesure a renvoyé l'induction moyenne des empilements de tôles et a été comparée à la somme algébrique obtenue compte tenu des mesures locales et de la conservation du flux magnétique en appliquant l'équation 3-2 et en modifiant le nombre de tôles à 10. Les résultats cohérents et convergents pour les cycles d'hystérésis reconstruits HBOT et HTOP et les cycles expérimentaux de bobine de 10 tours prouvent la validité des capteurs non intrusifs. De plus, des pourcentages d'erreur de 19 % et 8 % (Eq. 5.4) dans la perte d'hystérésis peuvent être calculés entre les cycles d'hystérésis HBOT(B) et HTOP(B) respectivement. Ces résultats fournissent donc des preuves de la faisabilité de la surveillance des états de laminations magnétiques isolés à travers le noyau stratifié ferromagnétique.

Malheureusement, du fait du substrat GMR, le capteur résultant présente une épaisseur encore relativement importante d'environ 500 µm. Cependant, une étape de polissage a été envisagée

pour réduire cette épaisseur à moins de 100 µm. La prochaine série d'expériences sera axée sur le test de la carte de capteur PMNP + GMR intégrée non invasive. Ses résultats seront comparés aux résultats numériques du modèle éléments finis pour validation.

4.3 capteur PMNP + GMR intégrée sur une carte

Apres test de cette carte dans un empilement de tôles, on remarque que les cycles d'hystérésis résultants ne sont pas identiques (probablement à cause d'une estimation imparfaite des paramètres du modèle J-A ou à l'hypothèse de simulation). Néanmoins, l'évolution du gradient magnétique dans les deux cas a presque la même tendance. nous pouvons donc en déduire que la capacité prédictive de la méthode de simulation est évidente ;

De plus, une flexion est observée dans les cycles d'hystérésis des première, deuxième et troisième positions. Un tel comportement a déjà été noté dans la littérature et associé aux pertes dynamiques lors du processus d'aimantation [106], [107].

De plus, des comparaisons approfondies des résultats ont été faites en ce qui concerne la variation d'une série d'indicateurs de cycle d'hystérésis en fonction de la position de la feuille magnétique illustrée à la figure 4-12. Pour une évaluation plus quantitative, le marqueur d'incertitude défini dans l'Eq. 5.5 est appliqué aux cinq indicateurs testés pour vérifier la performance globale de la méthode de simulation proposée. L'erreur est faible pour les premières feuilles (positions 1, 2 et 3). Les grandeurs magnétiques mesurées présentent des valeurs significatives pour ces positions et conduisent à un rapport conséquent entre le signal précieux et le bruit ambiant. À partir des stratifications 4 et plus, les niveaux d'induction sont dans la même plage que l'incertitude PMNP. Pour ces postes, les comparaisons sont imprécises et modifient considérablement l'évaluation quantitative

Ce chapitre était essentiellement axé sur la preuve du concept PMNP, l'évaluation de la précision des différentes versions du système de mesure B_H, à savoir : le PMNP et le GMR regroupés en un point et le PMNP et le GMR intégrés sur un seul patch. Les résultats de la preuve de concept ont révélé une erreur maximale de 5 % par rapport aux capteurs conventionnels (bobine de recherche, capteur de sonde à pointes magnétiques et bobine d'encerclement). L'analyse de la qualité et de la précision du capteur PMNP à différentes fréquences allant de 1 Hz à 200 Hz a montré une bonne adéquation avec les résultats obtenus à l'aide des 3 capteurs conventionnels susmentionnés ; ainsi le PMNP est capable de détecter à la fois les défauts superficiels et en profondeur dans le matériau. Le remplacement du capteur hall par GMR a attribué une valeur ajoutée d'encastrement de nos capteurs B_H de 500µm

d'épaisseur dans une pile de tôles. Une erreur de 19 % et 8 % dans la mesure de la perte d'hystérésis par rapport aux mesures globales de la bobine de 10 tours a été représentée pour la mesure inférieure et supérieure du champ H respectivement. De plus, l'impression des capteurs PMNP et GMR sur le même patch de 30 µm d'épaisseur a réduit l'éventuel espace d'air créé lors de l'introduction du patch entre deux laminations successives. Ce paramètre a ouvert la voie à la caractérisation interne et à la surveillance de la perte de noyau dans un empilement de 10 tôles en configuration SST. La comparaison des résultats de la distribution magnétique avec les données numériques obtenues à partir de la simulation 2D du modèle par éléments finis de notre système électromagnétique a révélé une dérive de 22 %. Cependant, il y avait un bon lien concernant la tendance de la variation des paramètres magnétiques.

CONCLUSIONS ET TRAVAUX FUTURS

Les caractéristiques attrayantes du PMNP incluent la facilité d'utilisation, la sensibilité élevée aux fissures étroites, la polyvalence, le niveau extrêmement élevé de potentiel non invasif, la répétabilité et la fiabilité. La réussite de la fabrication, de la mise en œuvre et des tests de validité a nécessité une sélection rigoureuse de l'instrument et des sondes appropriés, une optimisation de la fréquence des tests et l'utilisation d'étalons de référence. Une norme IEC 60404-3 légèrement modifiée et la norme de mesure de la bobine de recherche / environnante ont été utilisées respectivement pour la configuration de la caractérisation et la validation PMNP. Conformément à nos objectifs, nous les avons atteints avec succès grâce à nos expériences et avons vérifié toutes les hypothèses sauf une énoncées au début de nos recherches ; c'est-à-dire : "Une correspondance entre la caractérisation interne des noyaux magnétiques par rapport aux simulations par éléments finis".

Initialement, le capteur PMNP non invasif a été réalisé en imprimant de l'encre conductrice directement sur le substrat stratifié. Cette méthode réduit considérablement le volume du capteur et les contraintes géométriques. Des résultats d'induction magnétique et d'hystérésis ont été obtenus à l'aide du capteur imprimé dans des gammes de fréquences de 1 Hz à 200 Hz, confirmant que ce type de détection peut fournir des informations sur le comportement magnétique interne d'un empilement de laminage magnétique. En utilisant un modèle d'aimantation uniforme, la tension détectée par la méthode des sondes à pointes magnétiques est presque équivalente aux valeurs mesurées à l'aide d'une bobine de recherche classique (un tour) enroulée autour de la zone 1–2-3–4 comme le montre la figure 3-1. Une erreur moyenne de 0,89 % est obtenue lors de la comparaison du PMNPM avec les mesures de la bobine et les mesures de la bobine de recherche. Ce test initial valide les hypothèses 1 et 2 (réf. section 1.4)

Dans un second temps, toute une méthode de caractérisation non invasive est proposée pour mesurer les cycles d'hystérésis locaux à travers le noyau ferromagnétique feuilleté. Le capteur PMNP a été utilisé pour la caractérisation de l'état magnétique et le GMR miniaturisé pour l'excitation du champ magnétique. Un laminage instrumenté de ces deux capteurs a été posé et déplacé successivement à chaque position de la pile de laminage. Ces résultats fournissent des preuves de la faisabilité de la surveillance des états de lamination magnétique isolés à travers le noyau stratifié ferromagnétique. Par rapport au capteur conventionnel à bobine environnante, un écart relatif de 8% par rapport à la zone de leurs cycles d'hystérésis. Du fait du substrat GMR

qui est en silicium, le capteur résultant présente une épaisseur encore relativement importante d'environ 270 µm. (Objectifs 1,2 et 3 validés)

Enfin, une étape de polissage ou d'amincissement des étapes de fabrication du GMR a été envisagée avant sa mise en œuvre. Un capteur patch de 100 µm d'épaisseur (dont l'épaisseur peut être réduite) combinant des capteurs MNPM et GMR a été proposé pour fournir une caractérisation magnétique en plan à l'intérieur d'un empilement de feuilles laminées ferromagnétiques. Le patch a d'abord été testé sur une seule feuille stratifiée ferromagnétique. Une mesure 2D a été réalisée en comparant les deux paires de capteurs en condition expérimentale (capteur placé à un angle de 45°) ; le capteur a fourni les mêmes informations dans les deux sens. Ensuite, des tests d'empilement ont été effectués en positionnant le patch du capteur entre chaque feuille stratifiée, ce qui a révélé la distribution inhomogène du champ magnétique dans un noyau magnétique. Par la suite, des comparaisons avec des simulations FEM dans le domaine temporel ont été proposées et utilisées comme validation pour les outils expérimentaux et de simulation. Un pourcentage moyen d'erreur relative compris entre 14,5% et 32,7% pour les valeurs d'une série d'indicateurs de cycle d'hystérésis. Ce haut niveau d'erreur ne valide pas d'un coup d'œil l'hypothèse selon laquelle il y a concordance entre les résultats mesurés et simulés. D'autres améliorations sont indispensables pour parvenir à l'adéquation mesure/simulation ; par exemple : les modèles d'hystérésis vectoriels alternatifs, l'étalonnage des capteurs GMR et le traitement du signal des PMNP peuvent être améliorés.

Limites

Malgré le fait que le capteur de patch proposé a fourni des mesures locales précises dans tous les tests effectués, nous avons noté les limitations suivantes :

1) Les contacts électriques PMNP ont été assurés à partir d'une couche supplémentaire d'encre conductrice traitée dans une étape de fabrication ultérieure. Cependant, cette solution n'est pas optimale et des alternatives doivent être déterminées.

2) La fragilité du patch du capteur était la préoccupation la plus critique pour les développements de niveau de maturité technologique (TRL). Le patch aminci doit être manipulé avec soin, en particulier lors des traitements de polissage. L'utilisation de substrats souples est plausible mais constitue des développements chronophages dépassant le cadre de ce projet.

Travaux futurs et perspective

Un substrat flexible est l'objectif à long terme de cette étude. Les perspectives à court terme suivantes existent :

1) Pour tester le patch capteur en situation réelle. Un transformateur de puissance instrumenté a été conçu, comprenant plusieurs patchs de capteurs répartis sur tout le noyau magnétique stratifié du transformateur.

2) Évaluer la détection des ILF ou des bavures de bord avec le capteur patch. Un montage expérimental spécifique comprenant des défauts bien connus doit être conçu à cet effet.

Applications

Cette technique peut détecter l'amincissement des parois, les fissures, les piqûres, la fissuration par corrosion sous contrainte, la fragilisation par l'hydrogène, la carburation, les bosses et les dépôts de saleté, etc. Cette technique trouve de nombreuses applications dans l'industrie mécanique, y compris le tri des matériaux, la détermination de la dureté, l'évaluation de l'adéquation du traitement thermique, le matériau détermination de propriétés, mesures d'épaisseur de revêtement et détection de défauts dans des tubes, des tiges, des barres, des structures multicouches, des disques, des soudures, des lames et d'autres géométries régulières et irrégulières.

REFERENCES

[1] J. D. Ronnie Belmans *et al.*, 'The Potential for Global Energy Savings from High Effciency Distribution Transformers. 50'. http://www.leonardo-energy.org (accessed Nov. 11, 2021).

[2] businessincameroon, '55% less explosions on Eneo Cameroon's transformers during the first semester 2016 - Business in Cameroon'. https://www.businessincameroon.com/electricity/2208-6448-55-less-explosions-on-eneo-cameroon-s-transformers-during-the-first-semester-2016 (accessed Mar. 18, 2022).

[3] R. Mazurek, P. Marketos, A. Moses, and J.-N. Vincent, 'Effect of Artificial Burrs on the Total Power Loss of a Three-Phase Transformer Core', *IEEE Trans. Magn.*, vol. 46, no. 2, pp. 638–641, Feb. 2010, doi: 10.1109/TMAG.2009.2032094.

[4] A. M. Pawlak, 'Magnets in modern rotary actuators', in *IAS '95. Conference Record of the 1995 IEEE Industry Applications Conference Thirtieth IAS Annual Meeting*, Orlando, FL, USA, 1995, vol. 1, pp. 498–504. doi: 10.1109/IAS.1995.530341.

[5] A. Goldman, *Handbook of Modern Ferromagnetic Materials*. Springer Science & Business Media, 2012.

[6] S. Fizek, M. Reisinger, S. Silbers, and W. Amrhein, 'An electromagnet model comprehending eddy current and end effects', in *2015 IEEE 11th International Conference on Power Electronics and Drive Systems*, Sydney, Australia, Jun. 2015, pp. 668–672. doi: 10.1109/PEDS.2015.7203454.

[7] W. S. Jr, 'Induction Coil', 349,611, 1886

[8] D. Jiles, *Introduction to magnetism and magnetic materials*. Chapman and Hall, 1998.

[9] J. Winders, *Power Transformers*, 0 ed. CRC Press, 2002. doi: 10.1201/9780203910474.

[10] K. Yamazaki *et al.*, 'Eddy Current Analysis Considering Lamination for Stator Core Ends of Turbine Generators', *IEEE Transactions on Magnetics*, 2008, doi: 10.1109/TMAG.2007.916246.

[11] K. Muramatsu, T. Okitsu, H. Fujitsu, and F. Shimanoe, 'Method of nonlinear magnetic field analysis taking into account eddy current in laminated core', *IEEE transactions on magnetics*, vol. 40, no. 2, pp. 896–899, 2004.

[12] J. Gyselinck, L. Vandevelde, J. Melkebeek, P. Dular, F. Henrotte, and W. Legros, 'Calculation of eddy currents and associated losses in electrical steel laminations', *IEEE Trans. Magn.*, vol. 35, no. 3, pp. 1191–1194, May 1999, doi: 10.1109/20.767162.

[13] S. Tumanski, 'Induction coil sensors—a review', *Meas. Sci. Technol.*, vol. 18, no. 3, pp. R31–R46, Mar. 2007, doi: 10.1088/0957-0233/18/3/R01.

[14] J. P. A. Bastos and N. Sadowski, *Electromagnetic modeling by finite element methods*. CRC press, 2003.

[15] B. Ducharne, G. Sebald, D. Guyomar, and G. Litak, 'Fractional model of magnetic field penetration into a toroidal soft ferromagnetic sample', *Int. J. Dynam. Control*, vol. 6, no. 1, pp. 89–96, Mar. 2018, doi: 10.1007/s40435-017-0303-0.

[16] M. A. Raulet, B. Ducharne, J. P. Masson, and G. Bayada, 'The magnetic field diffusion equation including dynamic hysteresis: a linear formulation of the problem', *IEEE Transactions on Magnetics*, vol. 40, no. 2, pp. 872–875, Mar. 2004, doi: 10.1109/TMAG.2004.824816.

[17] B. Gupta, B. Ducharne, G. Sebald, and T. Uchimoto, 'A Space Discretized Ferromagnetic Model for Non-Destructive Eddy Current Evaluation', *IEEE Transactions on Magnetics*, vol. 54, no. 3, 2018, doi: 10.1109/TMAG.2017.2773517.

[18] F. Piriou and A. Razek, 'Finite element analysis in electromagnetic systems-accounting for electric circuits', *IEEE Trans. Magn.*, vol. 29, no. 2, pp. 1669–1675, Mar. 1993, doi: 10.1109/20.250727.

[19] J. Yoo and N. Kikuchi, 'Topology optimization in magnetic fields using the homogenization design method', *International Journal for Numerical Methods in Engineering*, vol. 48, Aug. 2000, doi: 10.1002/1097-0207(20000810)48:103.0.CO;2-5.

[20] G. Krismanić, H. Pfützner, and N. Baumgartinger, 'A hand-held sensor for analyses of local distributions of magnetic fields and losses', *Journal of Magnetism and Magnetic Materials*, vol. 215–216, pp. 720–722, Jun. 2000, doi: 10.1016/S0304-8853(00)00269-9.

[21] H. Hamzehbahmani, P. Anderson, J. Hall, and D. Fox, 'Eddy Current Loss Estimation of Edge Burr-Affected Magnetic Laminations Based on Equivalent Electrical Network—Part I: Fundamental Concepts and FEM Modeling', *IEEE Trans. Power Delivery*, vol. 29, no. 2, pp. 642–650, Apr. 2014, doi: 10.1109/TPWRD.2013.2272663.

[22] C. A. Schulz, S. Duchesne, D. Roger, and J.-N. Vincent, 'Short Circuit Current Measurements Between Transformer Sheets', *IEEE Trans. Magn.*, vol. 46, no. 2, pp. 536–539, Feb. 2010, doi: 10.1109/TMAG.2009.2032820.

[23] S. M. Plotnikov, 'Determination of Eddy-Current and Hysteresis Losses in the Magnetic Circuits of Electrical Machines', *Meas Tech*, vol. 63, no. 11, pp. 904–909, Feb. 2021, doi: 10.1007/s11018-021-01866-9.

[24] L. Chmura, P. Morshuis, E. Gulski, J. Smit, and A. Janssen, 'Statistical analysis of subcomponent failures in power transformers', *2011 Electrical Insulation Conference (EIC).*, 2011, doi: 10.1109/EIC.2011.5996149.

[25] Cigré, 'An international survey on failures in large power transformers', *e-cigré ELT_088*.

[26] H. Hamzehbahmani, 'An Experimental Approach for Condition Monitoring of Magnetic Cores With Grain-Oriented Electrical Steels', *IEEE Transactions on Instrumentation and Measurement*, 2020, doi: 10.1109/TIM.2019.2932661.

[27] H. Hamzehbahmani, 'A Phenomenological Approach for Condition Monitoring of Magnetic Cores Based on the Hysteresis Phenomenon', *IEEE Trans. Instrum. Meas.*, vol. 70, pp. 1–9, 2021, doi: 10.1109/TIM.2020.3042314.

[28] J. Sanchez, 'Aide au diagnostic de défauts des transformateurs de puissance', p. 151.

[29] CIGRE, 'Enquête internationale sur les défaillances en service des transformateurs de grande puissance', Electra(88), 1983.

[30] B. Ducharne, G. Sebald, D. Guyomar, and G. Litak, 'Dynamics of magnetic field penetration into soft ferromagnets', *Journal of Applied Physics*, vol. 117, no. 24, p. 243907, Jun. 2015, doi: 10.1063/1.4923162.

[31] R. H. Pry and C. P. Bean, 'Calculation of the Energy Loss in Magnetic Sheet Materials Using a Domain Model', *Journal of Applied Physics*, vol. 29, no. 3, pp. 532–533, Mar. 1958, doi: 10.1063/1.1723212.

[32] J. R. Sheats, 'Manufacturing and commercialization issues in organic electronics', *Journal of Materials Research*, vol. 19, no. 7, pp. 1974–1989, 2004.

[33] J. Dumont-Fillon, 'Contrôle non destructif (CND)', *Contrôle non destructif*, Jan. 1996, doi: 10.51257/a-v1-r1400.

[34] Jun Yamauchi, ‘Fundamentals of Magnetism’, Weinheim: WILEY-VCH Verlag GmbH & Co, 2008.

[35] I. R. Harris and A. J. Williams, ‘Magnetic Materials’, *Material Science and Engineering*, p. 11.

[36] C. F., ‘Materials handbook : a concise desktop reference’, Springer, 2008.

[37] florin Ciuprina and N. Petru, ‘science des materiaux de l`electrotechnique’. Universitatea Politehnica Bucureşti, 2021. Accessed: May 08, 2022. [Online]. Available: https://studylibfr.com/doc/2641217/science-des-materiaux-de-l-electrotechnique

[38] P. Weiss, ‘L’hypothèse du champ moléculaire et la propriété ferromagnétique’, *J. Phys. Theor. Appl.*, vol. 6, no. 1, pp. 661–690, 1907, doi: 10.1051/jphystap:019070060066100.

[39] P. Brissonneau, *Magnétisme et matériaux magnétiques pour l’électrotechnique*, Edition.

[40] N. Sommer, ‘Critical domain wall behavior in chiral magnetic nanowires induced by spin polarized currents’, p. 65.

[41] C. Zorni, ‘Contrôle non destructif par courants de Foucault de milieux ferromagnétiques: de l’expérience au modèle d’interaction’, p. 120.

[42] S. Huang, X. Wu, X. Liu, J. Gao, and Y. He, ‘Overview of condition monitoring and operation control of electric power conversion systems in direct-drive wind turbines under faults’, *Front. Mech. Eng.*, vol. 12, no. 3, pp. 281–302, Sep. 2017, doi: 10.1007/s11465-017-0442-1.

[43] N. Domingues, ‘Industry 4.0 in maintenance: Using condition monitoring in electric machines’, in *2021 International Conference on Decision Aid Sciences and Application (DASA)*, Sakheer, Bahrain, Dec. 2021, pp. 456–462. doi: 10.1109/DASA53625.2021.9682254.

[44] Z. Tian, T. Jin, B. Wu, and F. Ding, ‘Condition based maintenance optimization for wind power generation systems under continuous monitoring’, *Renewable Energy*, vol. 36, no. 5, pp. 1502–1509, May 2011, doi: 10.1016/j.renene.2010.10.028.

[45] CIGRE, WG A2.37, ‘transformer reliability survey’, Paris, France, Brochure 642, 2015.

[46] C. A. Schulz, S. Duchesne, D. Roger, and J.-N. Vincent, ‘Capacitive short circuit detection in transformer core laminations’, *Journal of Magnetism and Magnetic Materials*, vol. 320, no. 20, pp. e911–e914, Oct. 2008, doi: 10.1016/j.jmmm.2008.04.090.

[47] D. B. Paley, ‘Current low power core testing using EL CID’, in *IEE Colloquium Understanding Your Condition Monitoring*, Chester, UK, 1999, vol. 1999, pp. 7–7. doi: 10.1049/ic:19990657.

[48] Q. Fu, J. Zhu, Z.-H. Mao, G. Zhang, and T. Chen, ‘Online Condition Monitoring of Onboard Traction Transformer Core Based on Core-Loss Calculation Model’, *IEEE Trans. Ind. Electron.*, vol. 65, no. 4, pp. 3499–3508, Apr. 2018, doi: 10.1109/TIE.2017.2758721.

[49] K. Lee, J. Hong, K. Lee, S. B. Lee, and E. J. Wiedenbrug, ‘A Stator Core Quality Assessment Technique for Inverter-Fed Induction Machines’, in *2008 IEEE Industry Applications Society Annual Meeting*, Edmonton, Alberta, Canada, Oct. 2008, pp. 1–8. doi: 10.1109/08IAS.2008.21.

[50] R. Romary, S. Jelassi, and J. F. Brudny, ‘Stator-Interlaminar-Fault Detection Using an External-Flux-Density Sensor’, *IEEE Trans. Ind. Electron.*, vol. 57, no. 1, pp. 237–243, Jan. 2010, doi: 10.1109/TIE.2009.2029525.

[51] D. Lin and E. F. Fuchs, 'Real-Time Monitoring of Iron-Core and Copper Losses of Transformers Under (Non)Sinusoidal Operation', *IEEE Trans. Power Delivery*, vol. 21, no. 3, pp. 1333–1341, Jul. 2006, doi: 10.1109/TPWRD.2006.874118.

[52] A. Lotfi, H. Kr. Hoidalen, E. Agheb, and A. Nysveen, 'Characterization of Magnetic Losses in the Transformer Tank Steel', *IEEE Trans. Magn.*, vol. 52, no. 5, pp. 1–4, May 2016, doi: 10.1109/TMAG.2015.2512929.

[53] 'Comparison of Non-Destructive Testing Methods | NDT | The Modal Shop, Inc.' https://www.modalshop.com/ndt/Comparison-of-Non-Destructive-Methods?ID=256#VISUAL%20INSPECTION (accessed May 13, 2022).

[54] B. Ducharne, 'Micromagnetic nondestructive testing Barkhausen noise vs other techniques', in *Barkhausen Noise for Non-Destructive Testing and Materials Characterization in Low Carbon Steels*, Elsevier, 2020, pp. 223–238. doi: 10.1016/B978-0-08-102800-1.00008-3.

[55] J. García-Martín, J. Gómez-Gil, and E. Vázquez-Sánchez, 'Non-Destructive Techniques Based on Eddy Current Testing', *Sensors*, vol. 11, no. 3, pp. 2525–2565, Feb. 2011, doi: 10.3390/s110302525.

[56] '1348828761350-NDT.pdf'. Accessed: May 12, 2022. [Online]. Available: https://ncr.indianrailways.gov.in/cris/uploads/files/1348828761350-NDT.pdf

[57] P. C. Bhagi, 'Eddy Current Testing: Basics', *Journal of Non-Destructive Testing & Evaluation*, vol. 10, pp. 7–16, Mar. 2011.

[58] H.L. Libby, 'Introduction to Electromagnetic Non-destructive Test Methods', New York: Wiley-Interscience, 1971.

[59] 'Nondestructive Evaluation Physics : Electricity'. https://www.nde-ed.org/Physics/Electricity/depthcurrentdensity.xhtml (accessed Apr. 30, 2022).

[60] A. Skarlatos, G. Pichenot, D. Lesselier, M. Lambert, and B. Duchene, 'Electromagnetic Modeling of a Damaged Ferromagnetic Metal Tube by a Volume Integral Equation Formulation', *IEEE Trans. Magn.*, vol. 44, no. 5, pp. 623–632, May 2008, doi: 10.1109/TMAG.2008.918206.

[61] C. Ravat *et al.*, 'Study for the Design of Eddy Current Microsensor Arrays for Non Destructive Testing Applications', in *TRANSDUCERS 2007 - 2007 International Solid-State Sensors, Actuators and Microsystems Conference*, Lyon, France, 2007, pp. 583–586. doi: 10.1109/SENSOR.2007.4300197.

[62] K. Senda, M. Kurosawa, M. Ishida, M. Komatsubara, and T. Yamaguchi, 'Local magnetic properties in grain-oriented electrical steel measured by the modified needle probe method', *Journal of Magnetism and Magnetic Materials*, vol. 215–216, pp. 136–139, Jun. 2000, doi: 10.1016/S0304-8853(00)00096-2.

[63] S. Zurek, 'Systematic measurement errors of local B-coils due to holes', *Electrotachnical Review*, vol. 1, no. 3, pp. 8–14, Mar. 2018, doi: 10.15199/48.2018.03.02.

[64] E. Werner, 'Einrichtung zur Messung magnetischer Eigenschaften von Blechen bei Wechselstrom magnetisierung (The device for testing of electrical steel magnetized by AC field)', 191 015

[65] L. H. Stauffer, U.S.A , Pattern N°: 2 828 467, 1952

[66] T. Yamaguchi, K. Senda, M. Ishida, K. Sato, A. Honda, and T. Yamamoto, 'Theoretical analysis of localized magnetic flux measurement by needle probe', *J. Phys. IV France*, vol. 08, no. PR2, pp. Pr2-717-Pr2-720, Jun. 1998, doi: 10.1051/jp4:19982167.

[67] R. E. Tompkins, L. H. Stauffer, and A. Kaplan, ‘New Magnetic Core Loss Comparator’, *Journal of Applied Physics*, vol. 29, no. 3, pp. 502–503, Mar. 1958, doi: 10.1063/1.1723199.

[68] M. De Wulf, L. Dupré, D. Makaveev, and J. Melkebeek, ‘Needle-probe techniques for local magnetic flux measurements’, *Journal of Applied Physics*, vol. 93, no. 10, pp. 8271–8273, May 2003, doi: 10.1063/1.1544485.

[69] K. Matsubara, T. Nakata, and Y. Kadota, ‘A novel method of measurements of magnetic flux in silicon steel sheet with magnetic flux leakage’, presented at the National Conf IEE, Japan, 1988.

[70] N. J. Lewis, P. I. Anderson, Y. Gao, and F. Robinson, ‘Development and application of measurement techniques for evaluating localised magnetic properties in electrical steel’, *Journal of Magnetism and Magnetic Materials*, vol. 452, pp. 495–501, Apr. 2018, doi: 10.1016/j.jmmm.2017.11.036.

[71] K. Senda, M. Ishida, K. Sato, M. Komatsubara, and T. Yamaguchi, ‘Localized magnetic properties in grain-oriented electrical steel measured by needle probe method’, *Elect. Eng. Jpn.*, vol. 126, no. 4, pp. 1–11, Mar. 1999, doi: 10.1002/(SICI)1520-6416(199903)126:4<1::AID-EEJ1>3.0.CO;2-7.

[72] H. Pfutzner and G. Krismanic, ‘The Needle Method for Induction Tests: Sources of Error’, *IEEE Trans. Magn.*, vol. 40, no. 3, pp. 1610–1616, May 2004, doi: 10.1109/TMAG.2004.826617.

[73] G. Crevecoeur, L. Dupre, L. Vandenbossche, and R. Van de Walle, ‘Local Identification of Magnetic Hysteresis Properties Near Cutting Edges of Electrical Steel Sheets’, *IEEE Trans. Magn.*, vol. 44, no. 6, pp. 1010–1013, Jun. 2008, doi: 10.1109/TMAG.2007.915298.

[74] G. Crevecoeur, L. Dupre, L. Vandenbossche, and R. Van de Walle, ‘Reconstruction of local magnetic properties of steel sheets by needle probe methods using space mapping techniques’, *Journal of Applied Physics*, vol. 99, no. 8, p. 08H905, Apr. 2006, doi: 10.1063/1.2176321.

[75] F. J. Wilkins and A. E. Drake, ‘Measurement and interpretation of power losses in electrical sheet steel’, *Proc. Inst. Electr. Eng. UK*, vol. 112, no. 4, p. 771, 1965, doi: 10.1049/piee.1965.0133.

[76] G. Loisos and A. J. Moses, ‘Critical evaluation and limitations of localized flux density measurements in electrical steels’, *IEEE Trans. Magn.*, vol. 37, no. 4, pp. 2755–2757, Jul. 2001, doi: 10.1109/20.951297.

[77] A. A.-E. Abdallh, P. Sergeant, G. Crevecoeur, L. Vandenbossche, L. Dupre, and M. Sablik, ‘Magnetic Material Identification in Geometries With Non-Uniform Electromagnetic Fields Using Global and Local Magnetic Measurements’, *IEEE Trans. Magn.*, vol. 45, no. 10, pp. 4157–4160, Oct. 2009, doi: 10.1109/TMAG.2009.2022021.

[78] S. Zurek and T. Meydan, ‘A novel capacitive flux density sensor’, *Sensors and Actuators A: Physical*, vol. 129, no. 1–2, pp. 121–125, May 2006, doi: 10.1016/j.sna.2005.11.027.

[79] R. Mazurek, ‘Effects of burrs on a three phase transformer core including local loss, total loss and flux distribution’, 2012.

[80] B. Park, D. Kim, S. Jeong, J. Moon, and J. S. Kim, ‘Direct Writing of Copper Conductive Patterns by Ink-Jet Printing’, *Thin Solid Films*, vol. 515, pp. 7706–7711, Jul. 2007, doi: 10.1016/j.tsf.2006.11.142.

[81] S. H. Nguedjang Kouakeuo *et al.*, 'Embedded printed magnetic needle probes sensor for the real-time control of the local induction state through a laminated magnetic core', *Journal of Magnetism and Magnetic Materials*, vol. 505, p. 166767, Jul. 2020, doi: 10.1016/j.jmmm.2020.166767.

[82] 'Methods of measurement of the magnetic properties of electrical steel strip and sheet by means of a single sheet tester', IEC 60404–3,

[83] D. Miyagi, T. Yamazaki, D. Otome, M. Nakano, and N. Takahashi, 'Development of Measurement System of Magnetic Properties at High Flux Density Using Novel Single-Sheet Tester', *IEEE Trans. Magn.*, vol. 45, no. 10, pp. 3889–3892, Oct. 2009, doi: 10.1109/TMAG.2009.2022332.

[84] Y. A. Tene Deffo, P. Tsafack, B. Ducharne, B. Gupta, A. Chazotte-Leconte, and L. Morel, 'Local Measurement of Peening-Induced Residual Stresses on Iron Nickel Material Using Needle Probes Technique', *IEEE Trans. Magn.*, vol. 55, no. 7, pp. 1–8, Jul. 2019, doi: 10.1109/TMAG.2019.2894977.

[85] J. Torrejon *et al.*, 'Multiple Giant-Magnetoresistance Sensors Controlled by Additive Dipolar Coupling', *Phys. Rev. Applied*, vol. 13, no. 3, p. 034031, Mar. 2020, doi: 10.1103/PhysRevApplied.13.034031.

[86] J. Moulin *et al.*, 'Optimizing magnetoresistive sensor signal-to-noise via pinning field tuning', *Appl. Phys. Lett.*, vol. 115, no. 12, p. 122406, Sep. 2019, doi: 10.1063/1.5108604.

[87] M. Gerken *et al.*, 'Traceably calibrated scanning Hall probe microscopy at room temperature', *J. Sens. Sens. Syst.*, vol. 9, no. 2, pp. 391–399, Nov. 2020, doi: 10.5194/jsss-9-391-2020.

[88] C. Chopin *et al.*, 'Magnetoresistive Sensor in Two-Dimension on a 25 μm Thick Silicon Substrate for In Vivo Neuronal Measurements', *ACS Sens.*, vol. 5, no. 11, pp. 3493–3500, Nov. 2020, doi: 10.1021/acssensors.0c01578.

[89] A. Jander, C. Smith, and R. Schneider, 'Magnetoresistive sensors for nondestructive evaluation (Invited Paper)', presented at the Nondestructive Evaulation for Health Monitoring and Diagnostics, San Diego, CA, May 2005, p. 1. doi: 10.1117/12.601826.

[90] S. H. Nguedjang Kouakeuo *et al.*, 'Non-invasive local magnetic hysteresis characterization of a ferromagnetic laminated core', *Journal of Magnetism and Magnetic Materials*, vol. 527, p. 167783, Jun. 2021, doi: 10.1016/j.jmmm.2021.167783.

[91] B. Gupta, T. Uchimoto, B. Ducharne, G. Sebald, T. Miyazaki, and T. Takagi, 'Magnetic incremental permeability non-destructive evaluation of 12 Cr-Mo-W-V steel creep test samples with varied ageing levels and thermal treatments', *NDT & E International*, vol. 104, pp. 42–50, Jun. 2019, doi: 10.1016/j.ndteint.2019.03.006.

[92] U. D. Annakkage, P. G. McLaren, E. Dirks, R. P. Jayasinghe, and A. D. Parker, 'A current transformer model based on the Jiles-Atherton theory of ferromagnetic hysteresis', *IEEE Trans. Power Delivery*, vol. 15, no. 1, pp. 57–61, Jan. 2000, doi: 10.1109/61.847229.

[93] A. Iványi, 'Hysteresis Models in Electromagnatic Computation'. 2017.

[94] L. Li, 'Stress effects on ferromagnetic materials: investigation of stainless steel and nickel', Doctor of Philosophy, Iowa State University, Digital Repository, Ames, 2004. doi: 10.31274/rtd-180813-8795.

[95] N. Prabhu Gaunkar, 'Magnetic hysteresis and Barkhausen noise emission analysis of magnetic materials and composites', Master of Science, Iowa State University, Digital Repository, Ames, 2014. doi: 10.31274/etd-180810-3823.

[96] A. Raghunathan, ‘Growth,Characterization and Modelling of Novel Magnetic Thin Films for Engineering Applications’, Cardiff University, UK, 2010.

[97] Tene Deffo Yves Armand, ‘NON-DESTRUCTIVE TESTING AND CONTROL FOR LOCAL MAGNETIC CHARACTERIZATION OF MATERIAL STEEL BY THE NEEDLE PROBE TECHNIQUE’, University of Buea, BUEA, 2019.

[98] Y. Bernard, E. Mendes, and F. Bouillault, ‘Dynamic hysteresis modeling based on Preisach model’, *IEEE Trans. Magn.*, vol. 38, no. 2, pp. 885–888, Mar. 2002, doi: 10.1109/20.996228.

[99] M. Taghizadeh Kakhki, J. Cros, and P. Viarouge, ‘New Approach for Accurate Prediction of Eddy Current Losses in Laminated Material in the Presence of Skin Effect With 2-D FEA’, *IEEE Trans. Magn.*, vol. 52, no. 3, pp. 1–4, Mar. 2016, doi: 10.1109/TMAG.2015.2481924.

[100] K. Bitsi, D. Kowal, and R.-R. Moghaddam, ‘3-D FEM Investigation of Eddy Current Losses in Rotor Lamination Steel Sheets’, in *2018 XIII International Conference on Electrical Machines (ICEM)*, Alexandroupoli, Sep. 2018, pp. 1047–1053. doi: 10.1109/ICELMACH.2018.8507048.

[101] E. Lamprecht, M. Homme, and T. Albrecht, ‘Investigations of eddy current losses in laminated cores due to the impact of various stacking processes’, in *2012 2nd International Electric Drives Production Conference (EDPC)*, Nuremberg, Germany, Oct. 2012, pp. 1–8. doi: 10.1109/EDPC.2012.6425097.

[102] C. Geuzaine, F. Henrotte, J.-F. Remacle, E. Marchandise, and R. V. Sabariego, ‘ONELAB: Open Numerical Engineering LABoratory’, presented at the 11e Colloque National en Calcul des Structures (CSMA 2013), Giens, France, 2013. Accessed: Jun. 27, 2022. [Online]. Available: https://orbi.uliege.be/handle/2268/171456

[103] D. C. Jiles and D. L. Atherton, ‘Theory of ferromagnetic hysteresis (invited)’, *Journal of Applied Physics*, vol. 55, no. 6, pp. 2115–2120, Mar. 1984, doi: 10.1063/1.333582.

[104] N. Sadowski, N. J. Batistela, J. P. A. Bastos, and M. Lajoie-Mazenc, ‘An inverse Jiles-Atherton model to take into account hysteresis in time-stepping finite-element calculations’, *IEEE Trans. Magn.*, vol. 38, no. 2, pp. 797–800, Mar. 2002, doi: 10.1109/20.996206.

[105] A. Benabou, ‘Contribution à la caractérisation et à la modélisation de matériaux magnétiques en vue d’une implantation dans un code de calcul de champ’, These de doctorat, Lille 1, 2002. Accessed: May 09, 2022. [Online]. Available: http://www.theses.fr/2002LIL10135

[106] S. E. Zirka, Y. I. Moroz, N. Chiesa, R. G. Harrison, and H. Kr. Hoidalen, ‘Implementation of Inverse Hysteresis Model Into EMTP—Part I: Static Model’, *IEEE Trans. Power Delivery*, vol. 30, no. 5, pp. 2224–2232, Oct. 2015, doi: 10.1109/TPWRD.2015.2416201.

[107] S. E. Zirka, Y. I. Moroz, N. Chiesa, R. G. Harrison, and H. Kr. Hoidalen, ‘Implementation of Inverse Hysteresis Model Into EMTP—Part II: Dynamic Model’, *IEEE Trans. Power Delivery*, vol. 30, no. 5, pp. 2233–2241, Oct. 2015, doi: 10.1109/TPWRD.2015.2416199.

[108] B. Ducharne, S. Zurek, and G. Sebald, ‘A universal method based on fractional derivatives for modeling magnetic losses under alternating and rotational magnetization conditions’, *Journal of Magnetism and Magnetic Materials*, vol. 550, p. 169071, May 2022, doi: 10.1016/j.jmmm.2022.169071.

[109] S. Yue, P. I. Anderson, Y. Li, Q. Yang, and A. Moses, ‘A Modified Inverse Vector Hysteresis Model for Nonoriented Electrical Steels Considering Anisotropy for FEA’, *IEEE Trans. Energy Convers.*, vol. 36, no. 4, pp. 3251–3260, Dec. 2021, doi: 10.1109/TEC.2021.3073349.

[110] B. Ducharne, S. Zurek, L. Daniel, and G. Sebald, ‘An anisotropic vector hysteresis model of ferromagnetic behavior under alternating and rotational magnetic field’, *Journal of Magnetism and Magnetic Materials*, vol. 549, p. 169045, May 2022, doi: 10.1016/j.jmmm.2022.169045.

PUBLICATIONS

S. H. Nguedjang Kouakeuo et al., ‘Embedded printed magnetic needle probes sensor for the real-time control of the local induction state through a laminated magnetic core’, Journal of Magnetism and Magnetic Materials, vol. 505, p. 166767, Jul. 2020, doi: 10.1016/j.jmmm.2020.166767.

B. Ducharne, Y.A. Tene Deffo, P. Tsafack, **S.H. Nguedjang Kouakeuo**, Directional magnetic Barkhausen noise measurement using the magnetic needle probe method, Journal of Magnetism and Magnetic Materials, Volume 519, 2021, 167453, ISSN 0304-8853, https://doi.org/10.1016/j.jmmm.2020.167453.

S. H. Nguedjang Kouakeuo et al., ‘Non-invasive local magnetic hysteresis characterization of a ferromagnetic laminated core’, Journal of Magnetism and Magnetic Materials, vol. 527, p. 167783, Jun. 2021, doi: 10.1016/j.jmmm.2021.167783.

S. H. Nguedjang Kouakeuo et al., "Internal Characterization of Magnetic Cores, Comparison to Finite Element Simulations: A Route for Dimensioning and Condition Monitoring," in IEEE Transactions on Instrumentation and Measurement, vol. 71, pp. 1-10, 2022, Art no. 6005310, doi: 10.1109/TIM.2022.3194905.